Faculty of Engineering
Department of Civil Engineering

A BAYESIAN APPROACH TO THE GROUNDWATER INVERSE PROBLEM FOR STEADY STATE FLOW AND HEAT TRANSPORT

by

Yefang JIANG

A Thesis
Submitted to the Faculty of Graduate Studies
in partial fulfillment of the requirement for the Degree of

Master of Science in Civil Engineering

Department of Civil Engineering
University of Manitoba
Winnipeg, Manitoba, Canada
April 2002

UNIVERSITY OF MANITOBA

0-612-76969-0

THE UNIVERSITY OF MANITOBA

FACULTY OF GRADUATE STUDIES

*****

COPYRIGHT PERMISSION PAGE

A BAYESIAN APPROACH TO THE GROUNDWATER INVERSE PROBLEM FOR STEADY STATE FLOW AND HEAT TRANSPORT

BY

YEFANG JIANG

A Thesis/Practicum submitted to the Faculty of Graduate Studies of The University

of Manitoba in partial fulfillment of the requirements of the degree

of

Master of Science

Abstract

In this thesis the Bayesian approach proposed by Woodbury and Ulrych (2000) is extended to estimate transmissivity field of highly heterogeneous aquifers for two-dimensional steady state groundwater flow. Boundary conditions are Dirichlet and Neumann type, and sink and source terms are included.

This new algorithm is examined against a fictitious aquifer with both "high" and "extremely high" variations of ln (T). The addition of the hydraulic head data is shown to improve the ln (T) estimates, in comparison to simply interpolating the sparse ln (T) data alone. Forward solutions with the conditional-expected ln (T) field indicate that the conditional heads match the true heads better than the unconditional linearized approximation. This finding suggests that the Bayesian approach can be applied not only to the groundwater inverse problems for which linearized approximation is valid, but also to cases where linearized approximation may not be satisfactory due to high heterogeneity.

The new Bayesian code is employed to calibrate a high-resolution finite difference model of the Edwards Aquifer, Taxes. The posterior ln (T) fields from this application yield better fits when compared to the prior ln (T) determined from upscaling and co-kriging.

The methodology for the spatial inversion of transmissivity for two-dimensional steady state groundwater heat transport is developed based on the full-Bayesian approach. This new algorithm is examined against a generic example. It is found that the use of temperature data is showed to improve the ln (T) estimates, when compared to the updated ln (T) field conditioned on sparse ln (T) and head data. Also the addition of temperature data without head data to the update aids refinement of the ln (T) field compared to simply interpolating the sparse ln (T) data alone.

Acknowledgements

This research work was performed under the guidance of Dr. Allan D. Woodbury. I would like to thank Dr. Woodbury for all the help, advice, support and funding that he provided during the course of this study. His encouragement, constant enthusiasm and patience were deeply appreciated. I have benefited in many ways from working with him. I acknowledge with thanks Dr. Scott Painter from the Southwest Research Institute in the United States. He provided the data set of the Edwards Aquifer and his suggestions on the simulations of the Edwards Aquifer were greatly appreciated. I am also grateful to Dr. G. Naterer for his help on my convective heat transfer study. I wish to thank Dr. Jim Graham, Dr. Marolo Alfaro and Dr. James Blatz, Kerry Lynch and Travor Mazak for their support and assistance during my study in the Geotechnical Group. I would like to thank Mr. Marvin Eyolfson from Manitoba Hydro for serving as my advisory committee member.

Special thanks are extended to Dr. Keni Zhang from Laurence Berkley Laboratory in the United States for providing valuable assistance on my study. Thanks are also extended to the fellow graduate students for their friendship and support during my program. In particular I would like to express my appreciation to Rebecca Mcmillan and Grant Ferguson. I benefited greatly from studying with them.

Financial support was provided by a research grant from Manitoba Hydro. Funding was also partially provided by the Edwards Aquifer Authority. They were highly appreciated.

Finally, and most importantly, I thank my wife Jian Huang and my son Eddie Jiang for their tremendous support and sacrifices during the course of my study. I am grateful to my parents and parents-in-law for their continuous support as well as the support of my brothers'.

Table of Contents

List of Figures and Tables

List of Abbreviations

CNWRA	Center for Nuclear Waste Regulatory Analyses
FD	finite difference
FE	finite element
FEM	finite element method
LHS	left hand side
MRE	minimum relative entropy
pdf	probability density function
RHS	right hand side
RMS	root mean squared
S solution	symmetrical solution
USGS	United States Geological Survey
U solution	unsymmetrical solution

List of Notations

$\mathbf{A}$	global stiffness matrix
A	amplitude
$\mathbf{B}$	constant matrix
B	aquifer thickness
b	Box-car pdf
C_d	covariance of observed data
c_f	specific heat of water
C_p	covariance of prior pdf
C_q	covariance of posterior pdf
$\mathbf{D}$	Boolean matrix
d	spatial distance
$\mathbf{d}^*$	vector of observed data
$\mathbf{F}$	vector of conditional-expected ln (T)
F	conditional-expected ln (T)
$\mathbf{f}$	vector of zero-mean ln (T) perturbation
f	zero-mean ln (T) perturbation
f_1	known hydraulic head
f_2	known flux
$\mathbf{G}$	linear transformation, matrix of kernels
$\mathbf{H}$	vector of conditional-expected hydraulic head
H	conditional-expected hydraulic head
$\mathbf{h}$	vector of zero-mean hydraulic head perturbation
h	zero-mean hydraulic head perturbation
$\mathbf{I}$	unit matrix
L^*	length of flow field

$\mathbf{L}$	lower triangular matrix
L	lower bound to a parameter
ln (k)	natural logarithm hydraulic conductivity
ln (T)	natural logarithm transmissivity
$\mathbf{M}$	constant matrices
$\mathbf{m}$	vector of model
$\mathbf{m}_0$	minimum length solution to the inverse problem
$\langle \mathbf{m} \rangle$	vector of posterior mean values
$\mathbf{N}$	constant matrix
nm	length of model vector
np	length of observed data
$\mathbf{O}$	constant matrix
p	probability
Pe	Pelect number
q	source or sink of flow
q^*	flow rate per unit aquifer width
q_x and q_y	specific discharges
$\mathbf{S}$	constant matrix
$\mathbf{s}$	vector of prior mean values
T	transmissivity
U	upper bound to a parameter
x and y	Cartesian coordinates
Y	natural logarithm transmissivity
$\mathbf{Y}$	vector of natural logarithm transmissivity
$\mathbf{Z}$	random variable vector of standard Gaussian distribution
$\boldsymbol{\nu}$	vector of noise (residuals between true and observed data)
σ_d^2	variance of d^*
σ_Y^2	variance of Y
λ_x	integral scale in x direction
λ_y	integral scale in y direction
Ω	minimum relative entropy
β	Lagrange multipliers
$\mathbf{\Phi}$	vector of total hydraulic head
Φ	total hydraulic head
Γ_1	Dirichlet boundary
Γ_2	Neumann boundary
δ	Kronecker number
λ_e	effective thermal conductivity
λ_f	thermal conductivity of water
λ_s	thermal conductivity of solid of porous medium
ω	porosity
ρ_f	density of water
θ	groundwater temperature

$\boldsymbol{\eta}$	vector of conditional-expected temperature
η	conditional-expected temperature
$\boldsymbol{\varsigma}$	vector of zero-mean temperature perturbation
ς	zero-mean temperature perturbation

Chapter 1

Introduction

1.1 Groundwater Inverse Problem

Numerical models are widely employed to simulate the responses of groundwater systems. One well-recognized difficulty for groundwater model applications is to obtain sufficient and reliable hydrogeological parameters for model input. Groundwater systems are often highly heterogeneous and the large spatial variability of a groundwater system predominantly controls the flow field and hence the distributions of contaminants and heat. In practice, there may not be sufficient measurements of hydraulic parameters for a comprehensive, detailed characterization. A large portion of the model input has to be determined through estimation, which is referred to as 'parameter estimation', 'parameter identification' or the 'inverse problem' (Neuman et al., 1979).

The full inverse problem is ill-posed, and this is characterized by instability and non-uniqueness. The instability of the inverse solution stems from the fact that small errors in observed data, such as hydraulic heads, concentrations or temperatures, can cause serious errors in the identified parameters. If the number of estimated parameters is larger than known variables, the problem is under-determined. An under-determined nature of the inverse problem leads to non-uniqueness.

Carrera and Neuman (1986) demonstrated that the instability and nonuniqueness of solutions to the inverse problems can only be eliminated through introducing additional measurements and information. This implies that regularization is also essential for the groundwater inverse problem. What and how information should be added remains an open question.

1.2 Approaches to the Inverse Problem

The difficulty of solving the ill-posed groundwater inverse problem is well recognized and has attracted a remarkable research effort (see reviews by Woodbury, 1987; Yeh, 1987; McLaughlin and Townley, 1996; Kitanidis, 1996). Various techniques have been developed to solve the groundwater inverse problem.

The manual trial and error calibration procedure is a classical approach for modeling. It is accomplished through the selection of a set of parameters in such a way that measurements of the water table, the concentration of solutes and other variables describing the system can be reproduced through the model. This method is time consuming and the usual over-parameterization practice may not well reflect the variation of estimated parameters.

Non-linear regression (Cooley, 1977; Yeh and Yoon, 1981) can be used to automatically estimate hydrogeological parameters. The underlying theory is based on weighted least squares minimization or the maximum likelihood framework. The trend surface and zones derived from regression, although useful in representing large-scale variability, cannot account for short-distance variability of hydrogeological parameters.

If hydraulic heads (concentrations or temperatures) are known, a direct solution to the groundwater inverse problem for unknown parameters may be possible. This can be formulated as an optimal problem by minimizing an objective function based on solution error. Linear programming (Kleinecke, 1971), multi-objective decision process (Neuman, 1971) and quadratic programming (Hefez, 1975) can be employed to solve this problem. To build the optimal model, missing data (heads, concentrations, or temperatures) have to be estimated by interpolation. Regularity conditions, such as bounds, are required to achieve a solution. An objective function of an inverse problem can be formed through minimizing a "norm", or the difference between observed and calculated heads (concentrations or temperatures) at specified observation points. As a result the interpolation of measured data can be avoided. In general, a set of initial estimations of the parameters is used and the solutions are sought in an iterative manner until the system model response is sufficiently close to the measured observations. Neuman and Yakowitz (1979) introduced a nonlinear optimal approach to solve the inverse problem. Woodbury and Smith et al. (1987) extended the optimization approach by constructing a variety of models under different norms, which generate a set of solutions to the inverse problem. The consistency between the solutions suggests correct model structure. The main advantage of this approach is that the formulation of the inverse problem is applicable to the situation where number of observations is limited, and it does not require computation of a Jacobian. A disadvantage of this approach is that the minimization is usually nonlinear and often non-convex. The algorithm is inefficient, because it requires repeated forward modeling.

Alternate methods of inversion are Kriging and Cokriging. De Marsily (1984) detailed the principles of Kriging application in groundwater hydrology. Kriging is posed as: given a set of measurements of unknown parameters over the domain, estimate the values at other locations. The estimation is determined by a linear combination of the measurements using interpolation weights, which must be determined, and the problem is sought by minimizing the objective function (mean square error) subjective to a constraint that the weights sum to one. This results in a constrained optimization problem that can be solved using Lagrange multipliers. The approach requires a database sufficient to estimate variograms and covariograms. In practice, this requirement may be difficult to achieve. Kriging and Cokriging are widely used in groundwater hydrology (Hoeksema and Kitanidis, 1986; Roth and Chiles et al., 1998; Yeh et al., 1996; Zhang and Yeh, 1997). Clifton and Neuman (1983) used Kriging to estimate the hydraulic conductivity of the Avra Valley aquifer in Southern Arizona. Kitanidis and Vomvoris (1983) developed an approach to the groundwater inversion problem based on Kriging and they used both hydraulic conductivity and hydraulic head measurements. Hoeksema and Kitanidis (1986) applied the geostatistical approach to the case of two-dimensional steady state flow. A finite difference numerical model of groundwater flow was used to relate the head and transmissivity variability and Cokriging was used to estimate the unknown transmissivity field. A linear relationship between hydraulic parameters and hydraulic head perturbations is required to develop cross-covariance in the inversion, and variogram function must be evaluated based on the measurements.

Bayesian updating methods provide an alternate philosophy to Kriging to solving the groundwater inverse problem. In this approach, hydrogeological parameters are considered as stochastic variables and the prior statistical values (for instance, mean and covariance) of the variables can be defined subjectively. The posterior values can be obtained by using Bayes' Theorem. The updated estimates can be used as input variables in further conditional simulations such as hydraulic head, contaminant concentration and temperature. Kitanidis (1986) showed that Kriging is a special case of Bayesian estimation. Massmann and Freeze (1989) also compared Kriging and Bayesian estimators. Bayesian updating has been implemented in site characterization (Hachich and Vanmarck, 1983; Kitanidis, 1986). Woodbury (1989) detailed Bayesian Updating procedure of the groundwater inversion problem. Woodbury and Ulrych (1993; 1998; 2000) introduced the theory for estimating pdf of a stochastic variable in groundwater hydrology based on maximum entropy and minimum relative entropy (MRE) principles. The procedure is to minimize the entropy of the estimated pdf to the prior pdf of the property concerned, and yields an equation for posterior pdf. For the inverse problem, expected values of posterior pdf can be used.

Woodbury and Ulrych (2000) proposed full-Bayesian approach to steady state groundwater inversion. First, transmissivity measurements were used to update prior estimations and then hydraulic head measurements were incorporated into the updating procedure by using a linearized steady state groundwater flow equation. They showed that the resolution of aquifer parameters is gradually improved. The full-Bayesian approach applies to the estimation of aquifer parameters with limited measurements and appears promising for practical use. The Woodbury and Ulrych algorithm only deals with the aquifers with Dirichlet conditions and needed to be modified for more realistic hydrogeological conditions, such as Neumann conditions and sinks or sources. If, and how well, the full-Bayesian approach works on a high variance ln (T) aquifer remains an open question. Woodbury and Rubin (2000) also used the measurements of tracer transport to infer medium parameters by full-Bayesian approach and presented encouraging results. These findings imply that more knowledge about the system is added in the solution to the inversion problem, the resolution of aquifer parameters is further improved. The full-Bayesian approach allows various sources of information related to the inverse problem, especially those uncertain data, to be incorporated in the form of probability distribution into the estimation process.

1.3 Groundwater/Heat Transport and the Inverse Problem

Woodbury and Rubin (2000) stated "The conjunctive use of temperature and hydrogeological data for site characterization has the potential to reduce the concern of nonuniqueness of solution to an inverse problem. This potential is evident from published works relating heat transport to the aquifer's hydrogeological features and from the studies that attempted using temperature data for site characterization."

Groundwater motion may redistribute heat in subsurface environment in an otherwise conductive geothermal regime. The disturbance primarily depends on groundwater velocity, which is dominated by hydraulic parameters. Research efforts have been directed toward how groundwater flow influences the regional geothermal regime (Parsons, 1970; Smith et al., 1983; Woodbury et al., 1987; Forster et al. 1988). Smith et al. (1983) and Woodbury et al. (1985) presented detailed reviews on the effects of groundwater flow on subsurface thermal regime. The theory of heat transfer in porous media is of interest because of its many applications. Bredehoeft and Papadopulos (1965) developed an analytical solution to the one dimensional heat transport problem for determining groundwater velocity from temperature profiles. Kukkonen et al. (1994) described a procedure of using geothermal temperature measurement to infer pale-climatic change. Groundwater temperature measurement has been used to identify potential geotechnical problems (Smith, 1989). Another important concern regarding groundwater heat transfer is thermal energy storage and recovery from aquifer (Tsang et al., 1981; Sykes et al., 1982; Xue et al., 1990; Molson et al., 1992). Coupled modeling groundwater flow and heat transport is a key tool to evaluate the geothermal regime. Bear (1972; 1981) gave a detailed description on governing equations of heat transport in porous medium.

Subsurface temperature distributions may carry direct information on groundwater movement due to advective heat transport, and subsurface temperature information can be used in the groundwater inverse problem. Woodbury and Smith (1988) used a joint inverse of both hydrogeological data and temperature measurements to characterize site hydraulic parameters. They introduced an objective function, which explicitly includes hydraulic conductivity, hydraulic head and temperature, and used the constrained simplex technique to solve the optimal problem.

Wang et al. (1989) proposed another approach of solving the groundwater inverse problem using both hydraulic parameters and thermal parameters. A Bayesian maximum technique was adopted in their work. Unknown hydraulic heads, temperatures, hydraulic *a posterior* parameters and thermal parameters were simultaneously treated as random variables, which were related through finite element formulations to the nonlinear two-dimensional steady state coupled governing equations. They treated the inversion as a stochastic optimal problem (maximum likelihood estimation), whose optimal solution was obtained by maximizing the posterior pdf, and a gradient method was adopted to solve the optimal problem. Parameter zoning had to be introduced into their approach due to large number of unknowns involved.

1.4 Objective and Research Methodology

It can be concluded from above review that geological materials are often highly heterogeneous and a stochastic approach may be more applicable to the spatial variations over short distances. The groundwater inverse problem is born with instability and non-uniqueness, which can only be eliminated through introducing additional measurements and information. Data for hydrogeological parameter estimation are multi-source, such as the estimated parameter, hydraulic head, contaminant concentration and temperature measurements and subjective information etc. The information available is limited for a single source, but diversified and uncertain. With such a problem on hand using a Bayesian approach appears beneficial for several reasons. First, the estimated parameter distribution is handled as a stochastic field, and this may better address the spatial variations over short distance compared with the conceptual models based on large zones. Second, allowing addition of information from many different sources may further constraint the inverse problem. Additionally, the available information is incorporated as probabilistic distribution into the estimation. Such treatment may reduce the concern about uncertainty with the data.

This study will focus on extending the Bayesian approach to the groundwater inverse problem to real world settings. Combining hydrologic and thermal data in a full-Bayesian approach to the groundwater inverse problem will be investigated.

First, it will be showed whether the linearization solution adequately approximates well the traditional numerical solution to a steady state groundwater flow problem with high-variance ln (T), and Dirichlet and Neumann conditions and sources or sinks. If and how well the Bayesian approach works for such settings will be assessed. The algorithm and code will be developed.

Second, the new algorithm will be extended to calibrate a high-resolution mathematical model of the Edwards aquifer, Texas. Such application will further examine if and how well the Bayesian approach works for a real world system with high-variance ln (T) and complicated boundary configuration.

Finally, this work will show whether the linearization approach applied to two-dimensional steady state groundwater heat transport and groundwater temperature measurement can be used to condition hydraulic parameters based on the full-Bayesian methodology. An algorithm of combining both hydrologic and thermal data into the groundwater inverse problem by Bayesian approach will be developed.

These studies will then extend the findings of Woodbury and Ulrych (2000). The final results of this study will include a thesis, publications, data sets and the inversion codes.

In order to accomplish the objectives, following methodology will be adopted:

First, a synthetic groundwater system will be designed and a natural logarithm transmissivity field [denoted as ln (T)] along with its associated hydraulic head field will be generated. This will be accomplished by using a multivariate random number generator with known statistical parameters. High and extremely high variances of ln (T), which are similar to that of the Edwards aquifer, will be used. The hydraulic heads will be solved by the finite element method. The generated fields will act as a known parameter and data set. Then the linearized equations for the system will be solved. Comparison of the 'true' finite element (FE) solution and the linearized solution will illustrate how well the linear approach works for the high-variance system with complicated boundary configuration. Following this step, random samples of ln (T) values and the computed hydraulic heads will be taken from the fictitious system. The sampling data are analogous to field or laboratory measurements.

Second, the Bayesian Updating procedure will be performed. Bayesian interpolation will be implemented based on the point sample of ln (T). Then the interpolated ln (T) field will be updated by incorporating the head measurements. The combined Bayesian updates will produce conditional-expected ln (T) fields and estimated errors. Such tests will illustrate if the addition of the hydraulic head data is shown to improve the ln (T) estimates, in comparison to simply interpolating the sparse ln (T) data alone.

Third, this new algorithm will then be applied to calibration of the high-resolution numerical model of the Edwards aquifer, which is being developed by the United States Geological Survey (USGS). To use the algorithm a finite element model, which is compatible to the finite different model, will be developed. The data for the finite different model will be transferred into the finite element model. The upscaled ln (T) field and the associated statistics provided by the Center for Nuclear Waste Regulatory Analyses (CNWRA) at the Southwest Research Institute in the United States will act as prior input. This thesis will produce a posterior ln (T) field conditioned on the hydraulic head measurements. Comparison of the computed heads with the posterior ln (T) and the measured heads will show the performance of the Bayesian approach to this real world case.

Finally, the Bayesian approach will be extended to the groundwater inverse problem for steady state heat transport. Again a fictitious aquifer will be designed and a ln (T) field along with its associated hydraulic head field and temperature field will be generated. The hydraulic heads and temperatures will be solved by the finite element method (FEM). Appropriate boundary conditions will be assigned to the system. The generated fields will act as known parameter and data set. The first test of the numerical procedure is to check if the linearized solution to the heat transport equation produces a reasonably accurate temperature field. Random samples of ln (T), the computed hydraulic heads and temperatures will be taken from the fictitious system. The sampling data analogous to field or laboratory measurements will be used to reconstruct the known ln (T) field through Bayesian updating. The first two steps Bayesian updating as discussed above will be repeated. Following each step of the update, temperature data will be incorporated respectively and this will check whether temperature incorporation improves the parameter resolution, especially in the cases with sparse observations and absence of head measurements. Noisy simulations with uncertain hyperparameters will be carried out. The pdfs for these hyperparameters will be determined from minimum relative entropy consideration and the effects of the hyperparameters will be removed through marginalization, which can be accomplished through Monte Carlo modeling. In total, three steps will be needed for the Bayesian updating procedure.

Chapter 2

Full-Bayesian Approach to Linear Inversion

2.1 Bayesian Solution to the Linear Inverse Problem

In this chapter the Bayesian solution to the linear inverse problem will be reviewed. The reader is referred to Woodbury (1989) and Woodbury and Ulrych (1998; 2000) for details. One of the most common tasks for the groundwater inversion is to map a ln (T) field (nm values) given observations at np locations in a discretized flow domain. The measurements can be ln (T), hydraulic head and temperature over the domain. Usually np is much smaller than nm-np. This problem can be formulated as the following linear inversion problem,

$$\mathbf{d}^* = \mathbf{Gm} + \nu \qquad (2\text{-}1)$$

where $\mathbf{d}^*$ is an observed data vector (np×1), **m** is a model vector (nm×1), **G** is the kernel (np×nm), which transforms model from model space into data space and $\mathbf{v}$ is a noise vector (np×1).

The direct solution to equation (2-1) is,

$$\mathbf{m}_0 = \mathbf{G}^T \left(\mathbf{G}\mathbf{G}^T\right)^{-1} \mathbf{d}^* \qquad (2\text{-}2)$$

This solution is non-unique because there are fewer equations than unknown model parameters. To obtain a unique solution to the inverse problem, one must have some means of singling out one solution from the infinite number of solutions with zero prediction error. Some information not contained in the equation must be added to the problem. The Bayesian solution is one way to accomplish this task. The solution is a model, which is in some sense 'small' in length away from a preconceived notion or behavior of the field.

Bayesian inference supposes that an observer can define a prior probability density function of a model (**m**), [denoted as $p(\mathbf{m}|\mathbf{I})$]. This pdf can be defined on the basis of observations, personal experience or judgment. It can be updated as new information, such as measurements, become available.

If $\mathbf{v}$ is assumed a zero-mean vector, then

$$E(\nu) = 0 \tag{2-3}$$

$$\mathbf{C}_d = E\left(\nu\nu^T\right) \tag{2-4}$$

where $\mathbf{C}_d$ is the covariance of the noise $\mathbf{v}$.

If $\mathbf{v}$ is independent and identically distributed (iid), (2-4) reduces to,

$$\mathbf{C}_d = \sigma_d^2\mathbf{I} \tag{2-5}$$

where σ_d^2 is the variance of $\mathbf{v}$ and $\mathbf{I}$ is a unit matrix.

The prior unconditional mean and covariance of **m** are expressed as,

$$E(\mathbf{m}) = \mathbf{s} \tag{2-6}$$

$$E[(\mathbf{m}-\mathbf{s})(\mathbf{m}-\mathbf{s})^T] = \mathbf{C}_p \tag{2-7}$$

If $\mathbf{C}_p$ is represented by an exponential correlation structure, it is in the following form,

$$C_p(k,l) = \sigma_Y^2 \exp\left\{-\left[\frac{(x_k - x_l)^2}{\lambda_x^2} + \frac{(y_k - y_l)^2}{\lambda_y^2}\right]^{\frac{1}{2}}\right\} \tag{2-8}$$

where σ_Y^2 is the variance of ln (T), λ is the integral scale and k and l refer to any two points in question. Note that the spatial correlation structure may take other forms rather than an exponential one.

If the combination of forward modeling and measurement errors is assumed Gaussian, then the likelihood function $p(\mathbf{d}^*|\mathbf{m},\mathbf{I})$ can be defined as (Woodbury and Ulrych, 200),

$$p(\mathbf{d}^*|\mathbf{m},\mathbf{I}) = \left[(2\pi)^{np}|\mathbf{C}_d|\right]^{-\frac{1}{2}} \exp\left[-\frac{1}{2}(\mathbf{d}^* - \mathbf{Gm})^T \mathbf{C}_d^{-1}(\mathbf{d}^* - \mathbf{Gm})\right] \tag{2-9}$$

where np is the length of $\mathbf{d}^*$.

If the ln (T) distribution can be assumed multivariate Gaussian (Freeze, 1975), its pdf is expressed as,

$$p(\mathbf{m}|\mathbf{I}) = \left[(2\pi)^{nm}|\mathbf{C}_p|\right]^{-\frac{1}{2}} \exp\left[-\frac{1}{2}(\mathbf{m} - \mathbf{s})^T \mathbf{C}_p^{-1}(\mathbf{m} - \mathbf{s})\right] \tag{2-10}$$

where nm is the length of $\mathbf{m}$.

The posterior conditional pdf from Bayes' Theorem is (see Ulrych et al., 2000),

$$p(\mathbf{m}|\mathbf{d}^*,\mathbf{I}) = \frac{p(\mathbf{d}^*|\mathbf{m},\mathbf{I})p(\mathbf{m}|\mathbf{I})}{\int(\mathbf{d}^*|\mathbf{m},\mathbf{I})p(\mathbf{m}|\mathbf{I})d\mathbf{m}} \tag{2-11}$$

Inserting both likelihood and prior pdf into Bayes' Theorem and performing the integration, the conditional posterior pdf can be obtained,

$$p(\mathbf{m}|\mathbf{d}^*,\mathbf{I}) = \left[(2\pi)^{nm}|\mathbf{C}_q|\right]^{-\frac{1}{2}} \exp\left[-\frac{1}{2}(\mathbf{m}-\langle\mathbf{m}\rangle)^T \mathbf{C}_q^{-1}(\mathbf{m}-\langle\mathbf{m}\rangle)\right] \tag{2-12}$$

The first two conditional moments of this pdf are given (Tarantola 1987),

$$\langle\mathbf{m}\rangle = \mathbf{s} + \mathbf{C}_p\mathbf{G}^T\left(\mathbf{G}\mathbf{C}_p\mathbf{G}^T + \mathbf{C}_d\right)^{-1}\left(\mathbf{d}^* - \mathbf{G}\mathbf{s}\right) \tag{2-13}$$

$$\mathbf{C}_q = \mathbf{C}_p - \mathbf{C}_p\mathbf{G}^T\left(\mathbf{G}\mathbf{C}_p\mathbf{G}^T + \mathbf{C}_d\right)^{-1}\mathbf{G}\mathbf{C}_p \tag{2-14}$$

where $\langle\mathbf{m}\rangle$ and $\mathbf{C}_q$ are the posterior conditional mean and covariance, respectively. The expected value $\langle\mathbf{m}\rangle$ is viewed as the Bayesian solution of the inverse problem. Note that the solution corresponds to the conditional expectation. $\mathbf{C}_p$ physically represents the correlation or spatial variability of the model **m**.

Note that the forms of $\mathbf{C}_p$ and $\mathbf{C}_d$ may be known or assumed (say exponential correlation structure for $\mathbf{C}_p$), and the associated statistic properties, such as integral scale λ and standard deviations σ_Y in $\mathbf{C}_p$ and σ_d in $\mathbf{C}_d$, and the prior mean **s,** may not be known. If unknown, these parameters are termed hyperparameters and the prior pdf for each of them can be determined from minimum relative entropy theory (Woodbury and Ulrych, 2000). Their effects on the estimation can be removed through marginalization, which can be accomplished by Monte Carlo sampling. This will be discussed in the following sections. Although it is not necessary to evaluate a variogram for the Bayesian framework as required for Kriging, a spatial structure of the estimated parameter has to be known. In addition, the covariance matrix must be positive-definite symmetric. If the prior pdf and likelihood are not Gaussian, the analytical formulation of the posterior pdf may not be available. Also, explicit expressions like equations (2-13) and (2-14) are not available for nonlinear data-model transformation. These belong to nonlinear inversion and will not be discussed here.

Given np observed ln (T) values as $\mathbf{d}^*$, a simple linear interpolation technique follows naturally from the above theoretical discussion. Where the i'th measurement point corresponds to an interpolated point, $G_{ij} = 1$, otherwise G_{ij} is zero. If hydraulic head or groundwater temperature measurements represent data and ln (T) is the model, the inverse kernel should take different form rather than simply setting the elements in G as one or zero. These will be detailed in Chapter 3 and Chapter 5.

2.2 Full-Bayesian Approach to Linear Inversion

2.2.1 Marginalization/Monte Carlo Sampling

As noted in the above section the Bayesian solution of the inverse problem could involve a set of hyperparameters. The exact values of these hyperparameters may not be known in practice. Woodbury and Ulrych (2000) treated them as random variables and termed such methodology "full-Bayesian" approach to signify that that the inference problem will consist of both primary parameter and hyperparameter estimation. Suppose that the form of the pdf is known, but the values of the 'hyperparameters' are not. Their effects on the primary parameter estimation can be removed through marginalization.

Recall the solution to Bayes' theorem for the case of Gaussian priors and a linear functional transformation (2-12), using the definition of expectation,

$$\langle \mathbf{m} \rangle = \int p\left(\mathbf{m} \middle| \mathbf{d}^*, \mathbf{I}\right) \mathbf{m}\, d\mathbf{m} \tag{2-15}$$

Assuming the joint pdf, $p(\mathbf{u})$, of the hyperparameters $\mathbf{u} = \left(\mathbf{s}, \sigma_Y^2, \lambda, \sigma_d^2\right)$ known, the marginalization can be described as,

$$\langle \mathbf{m} \rangle = \int_m \int_u p(\mathbf{m}|\mathbf{d}^*, \mathbf{I}, \mathbf{u}) p(\mathbf{u}) \mathbf{m} d\mathbf{u} d\mathbf{m} \tag{2-16}$$

Inserting equation (2-13) into (2-16) and changing the order of integration results in,

$$\langle \mathbf{m} \rangle = \int_u \left\{ \mathbf{s} + \mathbf{C}_p \mathbf{G}^T \left(\mathbf{G} \mathbf{C}_p \mathbf{G}^T + \mathbf{C}_d \right)^{-1} \left(\mathbf{d}^* - \mathbf{G} \mathbf{s} \right) \right\} p(\mathbf{u}) d\mathbf{u} \tag{2-17}$$

Similarly the covariance, $\mathbf{C}_p$ is

$$\mathbf{C}_q = \int_u \left\{ \mathbf{C}_p - \mathbf{C}_p \mathbf{G}^T \left(\mathbf{G} \mathbf{C}_p \mathbf{G}^T + \mathbf{C}_d \right)^{-1} \mathbf{G} \mathbf{C}_p \right\} p(\mathbf{u}) d\mathbf{u} \tag{2-18}$$

The integration of equations (2-16) and (2-17) can be carried out through numerical integration, which can be accomplished using the Monte Carlo sampling. The integrals are evaluated by generating a series of random model vectors using a multivariate random number generator with $p(\mathbf{u})$ as the pdf (Woodbury and Ulrych, 2000).

2.2.2 Determination of Prior pdfs of Hyperparameters

An immediate question arises as to how to determine the prior pdfs for these hyperparameters. Woodbury and Ulrych (1993; 1995; 2000) deal with the estimation of appropriate prior pdf's for hydrogeologic applications and the essence of their results is briefly repeated here. Woodbury and Ulrych (1993) stated, "It is acknowledged that hydrogeologic databases are such that the reasonable upper and lower bounds are obtainable on virtually all model parameters. This information implies that our base level of knowledge is a joint box-car pdf (uniform distribution between an upper and lower bound). The box-car pdf, $b(\mathbf{m})$, is

$$b(\mathbf{m}) = \begin{cases} \dfrac{1}{U_i - L_i} & \text{for } L_i \le m_i \le U_i \\ \\ 0 & \text{otherwise} \end{cases} \tag{2-19}$$

where $i = 0,\ldots,N$ is the number of parameters, and L_i and U_i are the individual lower and upper bounds. $b(\mathbf{m})$ is a joint pdf for all the parameters. Suppose additional information such as an informed guess, limited tests, or calibration becomes available. This 'new' prior estimate of the model is defined here as **s**. Assume **s** is the expected value vector of a pdf $p(\mathbf{m})$ which is chosen so it has minimum relative entropy (MRE) to a box-car pdf, subject to the expected value constraints, s_i". Woodbury and Ulrych (1993) presented that the entropy of $p(\mathbf{m})$ relative to the box-car distribution $b(\mathbf{m})$ is,

$$\Omega(p,b) = \int_M p(\mathbf{m}) \ln\left[\frac{p(\mathbf{m})}{b(\mathbf{m})}\right] d\mathbf{m} \tag{2-20}$$

The range of integration of all the variables m is (L_i, U_i), so the above integral over M implies a multiple integral over all the lower and upper bounds. As shown by Woodbury and Ulrych (1993), $p(\mathbf{m})$ has the following form,

$$p(\mathbf{m}) = \prod_{i=0}^{N} \begin{cases} \dfrac{\beta_i \exp(-\beta_i m_i)}{-\exp(-U_i\beta_i) + \exp(-L_i\beta_i)} & \text{for } s_i \ne \dfrac{U}{2} \\ \\ \dfrac{1}{U_i - L_i} & \text{for } s_i = \dfrac{U}{2} \end{cases} \tag{2-21}$$

"which is a multivariate truncated exponential. The β_i terms are Lagrange multipliers, which must be determined from the upper and lower bounds and the expected value constraints. The pdf preserves the statistical independence of the parameters. That is, if no correlation is known *a priori*, MRE does not inject any correlation into the posterior. In this manner $p(\mathbf{m})$ has the most freedom in assigning realization of the process." The distribution is not symmetric. As $U \rightarrow \infty$ and $L \rightarrow \infty$, $p(\mathbf{m})$ reduces to a multivariate exponential distribution. It is important to note that the above approach of determining is the one, which is the most uncommitted about unknown information.

The process of determining the pdfs for the hyperparameters can be summarized as two steps. First, identify the appropriate upper and lower bounds for each parameter as well as expected values. Second, compute the Lagrange multipliers (β_i, see Woodbury and Ulrych, 1993) based on the upper and lower bounds and the expected value constraints.

2.2.3 Multivariate Random Number Generator

The multivariate random number generator, which will be used to generate the realization of a given Gaussian pdf in next chapter, is discussed here. The generator is built according to the following theory (Mao and Wang, 1998). Recall that $Y = \ln(T)$ $(\mathbf{Y} = \mathbf{m})$ is assumed multivariate Gaussian and its pdf is as follows,

$$p(\mathbf{m}) = \left[(2\pi)^{nm}\left|\mathbf{C}_p\right|\right]^{-\frac{1}{2}} \exp\left[-\frac{1}{2}(\mathbf{m}-\mathbf{s})^T \mathbf{C}_p^{-1}(\mathbf{m}-\mathbf{s})\right] \qquad (2\text{-}22)$$

Here $\mathbf{C}_p$ is the covariance matrix, $\mathbf{s}$ is a vector of mean values, $\left|\mathbf{C}_p\right|$ is the determinant of $\mathbf{C}_p$ and nm is the length of $\mathbf{m}$.

If ln (T) is assumed to have an exponential spatial correlation structure, $\mathbf{C}_p$ can be evaluated through (2-8). Because $\mathbf{C}_p$ is symmetric and definite, it can be factorized through Cholesky Decomposition, namely

$$\mathbf{C}_p = \mathbf{L}\mathbf{L}^T \tag{2-23}$$

If $\mathbf{Z} = (Z_1, Z_2, \cdots, Z_k) \sim N(0, \mathbf{I})$, then $\mathbf{m} = \mathbf{LZ} + \mathbf{s} \sim N(\mathbf{s}, \mathbf{C}_p)$.

Following this procedure a realization of $\mathbf{m}$ can be generated by calling a standard normal random number generator.

2.3 Summary

In this chapter the Bayesian approach to the linear inverse problem proposed by Woodbury and Ulrych (1993; 1995 and 2000) is reviewed. The objective of the parameter estimation is to map a ln (T) field with a dimension of nm given measurements at np points (nm>>np). This exercise is formulated as a general linear inversion problem. Both the ln (T) field and the combination of forward modeling and measurement errors are assumed Gaussian. With the Gaussian prior pdf and likelihood function, one can obtain a Gaussian posterior pdf from Bayes Theorem. The first central moment associated with the posterior pdf is taken as the Bayesian solution of the inverse problem. Prior pdfs of any hyperparameters associated with the two central moments are determined from consistent considerations and any uncertainties in hyperparameters are removed by marginalization.

Chapter 3

Bayesian Approach to the Inverse Problem for Steady state Groundwater Flow

In Chapter 2 it is showed that the unconditional ln (T) field can be updated from ln (T) measurements following the Bayesian methodology. This update can be considered as a typical spatial interpolation. Woodbury and Ulrych (2000) showed that this updated ln (T) field can be further conditioned on hydraulic head measurements through adopting a linearized aquifer equation. This can be accomplished following an updating procedure similar to the interpolation scheme based on a linear formulation between head and ln (T) perturbations. Their algorithm was originally applied to aquifers with Dirichlet conditions and low-variance ln (T). In this chapter the algorithm is extended to highly heterogeneous aquifers with Dirichlet and Neumann conditions and sources and sinks. Theoretical examples are designed to examine the new algorithm.

3.1 Updating ln (T) Field by Hydraulic Head Measurements

This discussion will focus on two-dimensional, steady state, heterogeneous, isotropic groundwater flow systems, which can be a confined aquifer or a linearized unconfined aquifer. The system has Dirichlet and Neumann conditions and sources and sinks. Because an equivalent formulation can be derived for sink or source, flux boundary and pumping wells when the finite element method is applied to the governing equation, only sources or sinks appear in the governing equation for simplicity. The theory below can be easily extended to a cross-section flow system because its governing equation is similar to that of the plane flow problem. For plane two-dimensional, steady state, heterogeneous, isotropic and linear groundwater flow, the governing equation can be written as,

$$\frac{\partial}{\partial x}\left(T\frac{\partial \Phi}{\partial x}\right)+\frac{\partial}{\partial y}\left(T\frac{\partial \Phi}{\partial y}\right)+q=0 \tag{3-1}$$

where T is the transmissivity, Φ is the hydraulic head, q is a source or sink, and x and y are Cartesian coordinates.

The boundary conditions are as follows,

$$\Phi(x,y)\big|_{\Gamma_1}=f_1(x,y),\ (x,y)\in\Gamma_1 \tag{3-2}$$

$$T\frac{\partial \Phi}{\partial \mathbf{n}}\Big|_{\Gamma_2}=f_2(x,y),\ \ (x,y)\in\Gamma_2 \tag{3-3}$$

where f_1 is the known hydraulic head, Γ_1 represents first kind boundary, f_2 is the known flux, Γ_2 is second type boundary, and **n** is an unit vector normal to second type boundary.

Application of FEM to equation (3-1) will generate a non-linear equation in terms of head and transmissivity. Note that a linear relationship between data and model is required for the Bayesian updating procedure [refer to equation (2-1)]. To obtain a linear relationship between the head and ln (T), a linearized approximation to the governing equation is adopted (Hoekesema et al., 1984; Dagan 1985).

Let $Y=\ln(T)$ and replace T with $\exp(Y)$, (3-1) reduces to,

$$\frac{\partial^2 \Phi}{\partial x^2}+\frac{\partial^2 \Phi}{\partial y^2}+\frac{\partial Y}{\partial x}\frac{\partial \Phi}{\partial x}+\frac{\partial Y}{\partial y}\frac{\partial \Phi}{\partial y}+\frac{q}{\exp(Y)}=0 \tag{3-4}$$

Let

$$\Phi=H+h \tag{3-5}$$

$$Y = F + f \tag{3-6}$$

where H is the conditional-expected hydraulic head, h is the zero-mean head perturbation, F is the conditional-expected ln (T) (prior) and f is the zero-mean ln (T) perturbation.

Inserting equations (3-5) and (3-6), (3-4) reduces to,

$$\frac{\partial^2(H+h)}{\partial x^2}+\frac{\partial^2(H+h)}{\partial y^2}+\frac{\partial(F+f)}{\partial x}\frac{\partial(H+h)}{\partial x}+\frac{\partial(F+f)}{\partial y}\frac{\partial(H+h)}{\partial y}+\frac{q}{\exp(F+f)}=0 \tag{3-7}$$

Taking expected values of both sides of (3-7) and dropping out the products of perturbations produces,

$$\frac{\partial^2 H}{\partial x^2}+\frac{\partial^2 H}{\partial y^2}+\frac{\partial F}{\partial x}\frac{\partial H}{\partial x}+\frac{\partial F}{\partial y}\frac{\partial H}{\partial y}+\frac{q}{\exp(F)}=0 \tag{3-8}$$

Subtracting (3-8) from (3-7) yields,

$$\frac{\partial^2 h}{\partial x^2}+\frac{\partial^2 h}{\partial y^2}+\frac{\partial F}{\partial x}\frac{\partial h}{\partial x}+\frac{\partial F}{\partial y}\frac{\partial h}{\partial y}=-\frac{\partial f}{\partial x}\frac{\partial H}{\partial x}-\frac{\partial f}{\partial y}\frac{\partial H}{\partial y}+\frac{q}{\exp(F)}f \tag{3-9}$$

Note that a first-order approximation of Taylor's series for the exponential term is adopted.

It is straightforward to solve for conditional-expected head from equation (3-8) by FEM. Given the conditional-expected head the following formulation can obtained by applying FEM to equation (3-9),

$$\mathbf{Ah} = (\mathbf{B} + \mathbf{S})\mathbf{f} \tag{3-10}$$

where **A**, **B** and **S** are constant matrices, **A** represents a global stiffness matrix, **B** and **S** represent finite element formulations to the right hand side terms, **h** is a vector of non-boundary head perturbations, and **f** is a vector of ln (T) perturbations at the nodes.

Rearranging equation (3-10) and performing some simple matrix operations leads to,

$$\mathbf{D}[\mathbf{\Phi} - \mathbf{H} + \mathbf{A}^{-1}(\mathbf{B}+\mathbf{S})\mathbf{F}] = \mathbf{D}[\mathbf{A}^{-1}(\mathbf{B}+\mathbf{S})]\mathbf{Y} \tag{3-11}$$

D is a Boolean matrix that filters out the computed values of head perturbations at nodes other than measurement points. Here **F**, is a vector of prior conditional-expected ln (T), and is known, **H** is the conditional-expected hydraulic head vector and **F** is the conditional-expected vector of ln (T) (prior). $\mathbf{G} = \mathbf{D}[\mathbf{A}^{-1}(\mathbf{B}+\mathbf{S})]$ is the kernel. Equation (3-11) takes the form of $\mathbf{d}^* = \mathbf{Gm} + \nu$. The LHS is replaced with the known data and RHS is the product of the kernel and model. This linear formulation can be readily used to update the prior ln (T) field conditioned on head measurements following the Bayesian framework detailed in Chapter 2.

3.2 High-variance ln (T) Example

In this section the new algorithm will be examined against a fictitious aquifer with high variance ln (T), and Dirichlet and Neumann conditions and sources or sinks. First it will be showed how well the linearization solution approximates the traditional numerical solution to this system. Then, if and how well the full-Bayesian approach works for such realistic settings will be demonstrated.

3.2.1 Fictitious Aquifer

The fictitious system is a 30 by 30 km rectangular confined aquifer and it is discretized into 1809 nodes and 2048 triangle elements with spatial size equal to 937.5 m.

A multivariate random number generator (see 2.2.3) is then employed to generate an ln (T) field for the system (Figure 3-1). The ln (T) field is assumed Gaussian and has an exponential correlation structure. The statistical properties for such a generation include unconditional mean s=9.4, σ_Y=1.5, and λ =5,000 m. The generated ln (T) field with a statistics of mean=8.87 and standard deviation=1.3 from 100 samples is analogous to a true ln (T) field. Note that the standard deviation of ln (T) is 1.5, which is moderately high.

The north, south and east sides of the aquifer are specified as Dirichlet boundaries. The heads at northeast corner and southwest corner are assigned 616 and 600 m respectively. The heads at the boundaries between these two points are determined following a mean gradient at (616-600)/42426=0.0004. The west side is set as a prescribed flux boundary and the flux at each node on this boundary is so determined that the above hydraulic gradient can be maintained across the domain. Finally the finite element system has 994 degrees of freedom. Seven pumping wells with pumping rates ranging from 1500 to 15,000 m^3/d are assigned at the nodes with larger ln (T) values.

3.2.2 True Solution and Linearized Solution to Hydraulic Head

How well the linearized solution approximates the true solution with high-variance ln (T) and sink/source terms will be assessed next. Applying FEM to (3-4) yields the 'true' head field. FEM is employed to solve the equation (3-8) and (3-9) for the unconditional-expected head and perturbation head fields respectively. Note that the unconditional value of ln (T) is constant (flat), i.e. $\frac{\partial F}{\partial x} = \frac{\partial F}{\partial y} = 0$. Figure 3-2 and Figure 3-3 illustrate that the linearized solution approximates the true solution very well for the standard deviation of ln (T) up to 1.5. The linear fit gives R^2 coefficient=0.995, which is close to 1. The standard deviation error RMS (Root Mean Square) of the true field against the linearized solution is 0.24 m, which is less than 1.5% of the maximum head difference across the aquifer. The larger errors occur in the areas with pumping wells or Neumann boundary conditions.

3.2.3 Bayesian Updating

Random samples of the computed head field and true ln (T) field are taken from the aquifer. These samples are analogous to field measurements. The locations of sampled heads coincide with that of the ln (T). Thus at every measured head location there also exists a transmissivity measurement. The numbers of samples are initially 20, then 50 and finally 100. These measurements are used to reconstruct the true ln (T) field through the Bayesian approach. For the three cases above this gives 974, 944 and 894 unknown ln (T) values to be solved for in the FE grid. The hyperparameters are assumed known in the simulations. The samples of ln (T) are used to evaluate the prior mean and variance. The integral scale and data noise are fixed at 5,000 m and 0.1 m respectively.

Bayesian updating is carried out for cases of 20-point, 50-point and 100-point samples respectively. First Bayesian interpolation is performed based on the point sample of ln (T). Then the interpolated ln (T) field is updated by incorporating the head measurements. The updated ln (T) fields and the estimated errors are contoured. Comparing the interpolated ln (T) fields (Figures 3-4, 3-14 and 3-24) and hydraulic head conditioned ln (T) fields (Figures 3-5, 3-15 and 3-25) with the true ln (T) field (Figure 3-1), one can see that the resolution of the reconstructed ln (T) field gradually improves as the incorporations of ln (T) and head measurements into the updating procedure. The results of the simulations can be illustrated in tabular form (Table 3-1). As showed, in every case the addition of head data aids considerable in the refinement of the estimated ln (T) field. At a glance one can see the conditioning effects of ln (T) and head data as illustrated in Figures 3-6, 3-7, 3-16, 3-17, 3-26 and 3-27, in which the standard deviations in ln (T) are plotted. The more data are incorporated the better the reconstructed ln (T) fields approximate the true ln (T) field and the more the estimated errors reduce. Carefully examining Table 3-1 one can see that RMS (B50) and RMS (B100) are close to RMS

(H20) and RMS (H50) respectively. This suggests that joint use of sparse ln (T) and head measurements may yield equivalent estimations from large number of ln (T) measurements and application of Bayesian approach for site characterization may potentially reduce cost.

Table 3-1 Square root of the mean squared difference between the conditional field and the 'true' field

	B20	H20	B50	H50	B100	H100
RMS	1.0773	0.9345	0.9265	0.7949	0.7978	0.7214

Note: RMS refers to the square root of the mean squared difference between the conditional ln (T) field and the 'true' ln (T) field. B20, B50 and B100 refer to a Bayesian update for the 20, 50 and 100 point sample, respectively; H20 and so on refer to the ln (T) field updated from the hydraulic head and ln (T) interpolated fields.

The forward problems with the interpolated ln (T) fields and head-conditioned ln (T) fields are solved respectively. The computed heads are plotted against the true heads at the sampled locations (see Figures 3-8, 3-9, 3-18, 3-19, 3-28 and 3-29). These Figures indicate that the computed heads based on the updated ln (T) from head and ln (T) measurements approximate the true heads very well. For verification all the computed heads are plotted against the true heads together with the linear fits. Figures 3-11, 3-21 and 3-31 show that not only do the conditional heads match the true heads at sampled locations well but also the remaining heads across the domain. This can also be confirmed by comparing the contours of true head field against the conditioned head field (Figures 3-12, 3-13, 3-22, 3-23, 3-32 and 3-33). Again the updates from combination of ln (T) and head measurements yield better head fits than those from simply interpolated ln (T) fields.

Carefully reexamining the inverse results of the 20-point sample case gives us more information on the performance of the Bayesian approach with sparse measurements. One may not visibly see much refinement on the updated ln (T) field (Figure 3-25) from 20-point ln (T) and head measurements compared to the true field (Figure 3-1).

Comparisons of Figure 3-30 and Figure 3-31, and Figure 3-32 and Figure 3-33 indicate that the flow model is fully calibrated with only 20 ln (T) and 20 head measurements for such high variation aquifer. It can be concluded from the findings that the Bayesian approach can be applied to the estimation of high-variance ln (T) fields given sparse measurements.

3.3 Extremely High-variance ln (T) Example

The new inverse algorithm is further examined against a case of an extremely high-variance ln (T). The fictitious aquifer discussed above is redesigned into an 'Edwards-Aquifer-like' system in terms of extremely high heterogeneity. The finite element grid, first type boundaries and pumping wells are the same to those of the high-variance case. The ln (T) field is regenerated with the statistics from the Edwards aquifer (unconditional mean s=9.4, standard deviation σ_Y=3.0 and integral scale λ=5,000 m) and the flow rates at the second type boundary are accordingly adjusted so that a mean smooth hydraulic gradient (=0.0004) can be achieved. The generated ln (T) field (Figure 3-34) with a statistics of mean=8.35 and standard deviation=2.6 from 100 samples simulates a true ln (T) field.

Note that equation (3-4) is of a similar form to the standard advection-dispersion equation, which suffers from numerical error for coarse grids. Given the generated high-variance ln (T) field and finite element grid accurate head fields cannot be found by solving (3-4) due to numerical error. Therefore, the 'true' head field is obtained by solving equation (3-1) instead of (3-4). Ln (T) within each element is evaluated by averaging the values at the three nodes of the element.

Figure 3-35 and Figure 3-36 illustrate the comparisons between the linearized solution and the 'true' solutions. The RMS of the true field against the linearized solution is 0.83 m, which is still less than 5% of the maximum head difference across the aquifer, for the standard deviation of ln (T) up to 3. The linear approximation, though poorer than that of the previous case, is acceptable.

Bayesian updating is performed for a series of tests. Again, random samples of the computed head field and true ln (T) field are taken from the aquifer. The numbers of samples are initially 20, then 50 and finally 100. These measurements are used to recover the true ln (T) field through the Bayesian approach. The hyperparameters are assumed known in the simulations. The samples of ln (T) are used to evaluate the prior mean and variance. The integral scale and data noise are fixed at 5,000 m and 0.1 m respectively. Bayesian interpolation is performed based on the point sample of ln (T). Then, the interpolated ln (T) field is updated by incorporating the head measurements. The results of the ln (T) update for 100-point samples are showed on Figure 3-37 to Figure 3-40. Comparing Figure 3-37 and Figure 3-38 with Figure 3-34, one can observe that the resolution of the reconstructed ln (T) field gradually improves as the incorporations of ln (T) and head measurements into the updating procedure. The results of the simulations can be illustrated in tabular form (Table 3-2), including runs that are not presented graphically. As showed, in every case the addition of head data aids considerable in the refinement of the estimated ln (T) field. The more data are incorporated the better the reconstructed ln (T) approximates the true ln (T) field. This is especially true for this extremely high variance case. At a glance one can see the conditioning effects of ln (T) and head data as illustrated in Figure 3-39 and Figure 3-40 in which the standard deviations in ln (T) are plotted.

The forward problems with the posterior ln (T) fields are solved respectively. The computed heads are plotted against the true heads at the sampled locations (see Figure 3-41 and Figure 3-42). Figure 41 shows that the computed heads based the updated ln (T) from head and ln (T) measurements approximate the true heads very well. From Figure 3-44 one can see that not only do the conditional heads match the true heads at sampled locations well but also the remaining heads across the domain. This verifies that the full-Bayesian approach can be applied to the estimation of extremely high-variance ln (T) fields. Comparison of Figure 3-43 and Figure 3-44 shows that the head field obtained from the combination-conditional ln (T) approximates the true head field better than the one from interpolated ln (T) field. Figures 3-47 to Figure 3-52, which present the comparisons between the conditional heads and true heads for the case of 50 sample points, shows that the full-Bayesian approach works well for the cases of high-variance ln (T) and sparse data.

Comparing Figure 3-44 with Figure 3-35, and Figure 3-46 with Figure 3-37 one can see that the conditional heads match the true heads much better than the unconditional linearized approximation does. This finding implies that Bayesian approach can be applied to the groundwater inverse problems for which the linearized approximation is strictly valid as well as to the cases of high heterogeneity. Analyzing equation (3-7) and (3-8) one can see the reason behind this fact. Recall that the unconditional mean F is constant, i.e. $\frac{\partial F}{\partial x} = \frac{\partial F}{\partial y} = 0$, when the linearized equations are solved. For the second step Bayesian updating F is the prior conditional-expected ln (T) from interpolation, which is not constant. This conditional-expected ln (T) field is closer to the true field, and reduces the perturbation terms. The prior ln (T) plays a non-negligible role in the second step updating. From this point one can argue that the Bayesian estimation is superior to the classical geostatistical approach in dealing with prior information.

Table 3-2 Square root of the mean squared difference between the conditional field and the 'true' field

	B20	H20	B50	H50	B100	H100
RMS	2.1549	1.9386	1.8524	1.6476	1.5951	1.4740

Note: RMS refers to the square root of the mean squared difference between the conditional ln (T) field and the 'true' ln (T) field. B20, B50 and B100 refer to a Bayesian update for the 20, 50 and 100 point sample, respectively; H20 and so on refer to the ln (T) field updated from the hydraulic head and ln (T) interpolated fields.

The findings from this example as well as many other simulations, although not showed here, suggest that the Bayesian methodology can be applied to the estimation of hydrogeological parameters and automatic calibration of two-dimensional steady state groundwater flow model involved in extremely high variance of ln (T) with both Dirichlet and Neumann conditions and sinks or sources.

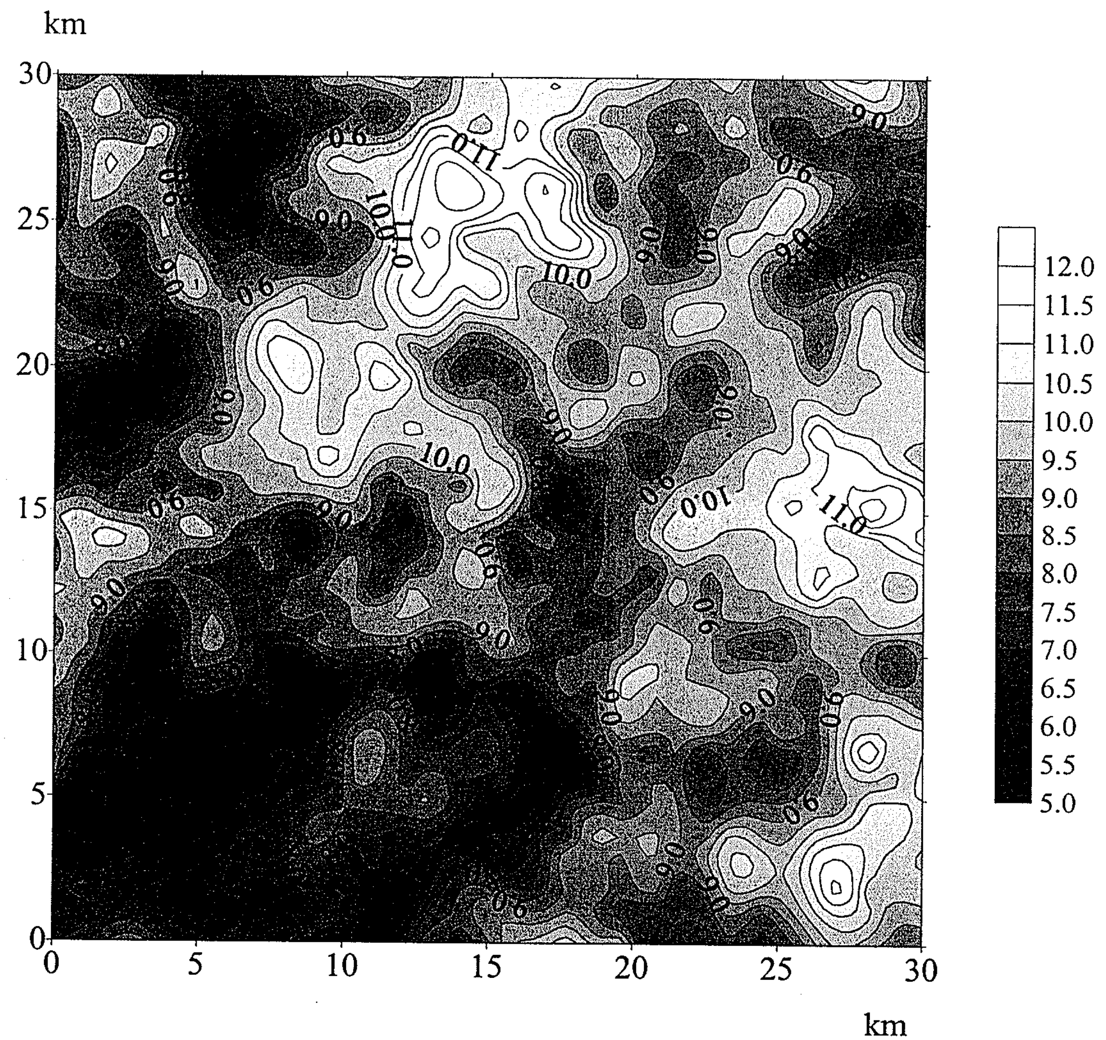

Figure 3-1 ln (T) field generated by a multivariate random number generator (actual statistics: mean=9.4, standard deviation=1.5, integral scale=5000 m)

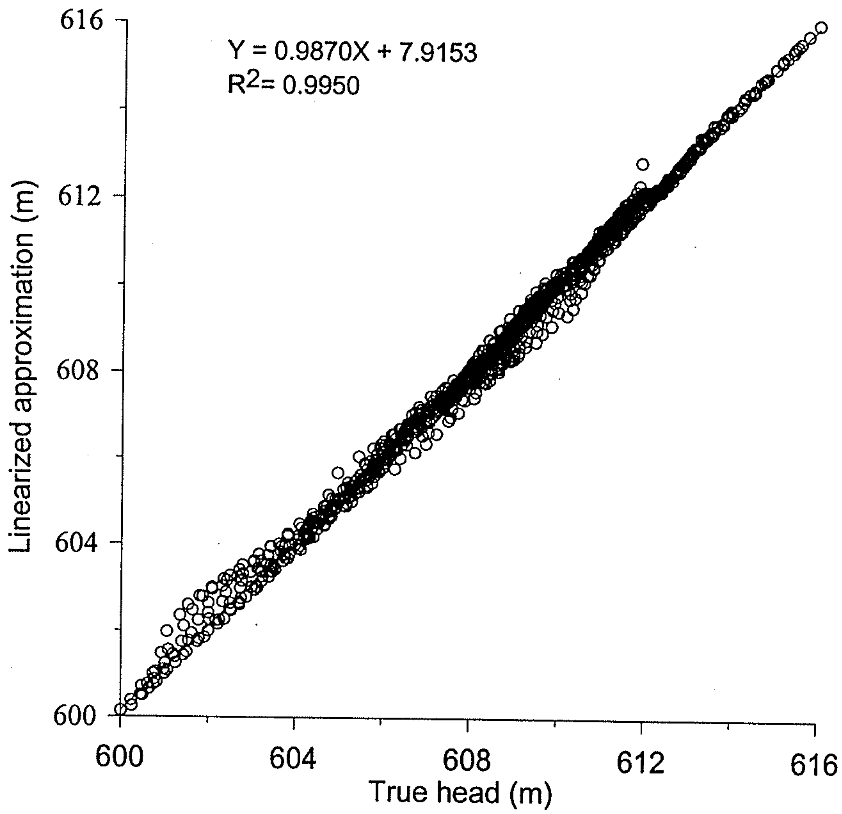

Figure 3-2 True head versus linearized approximation for ln (T) variance=2.25

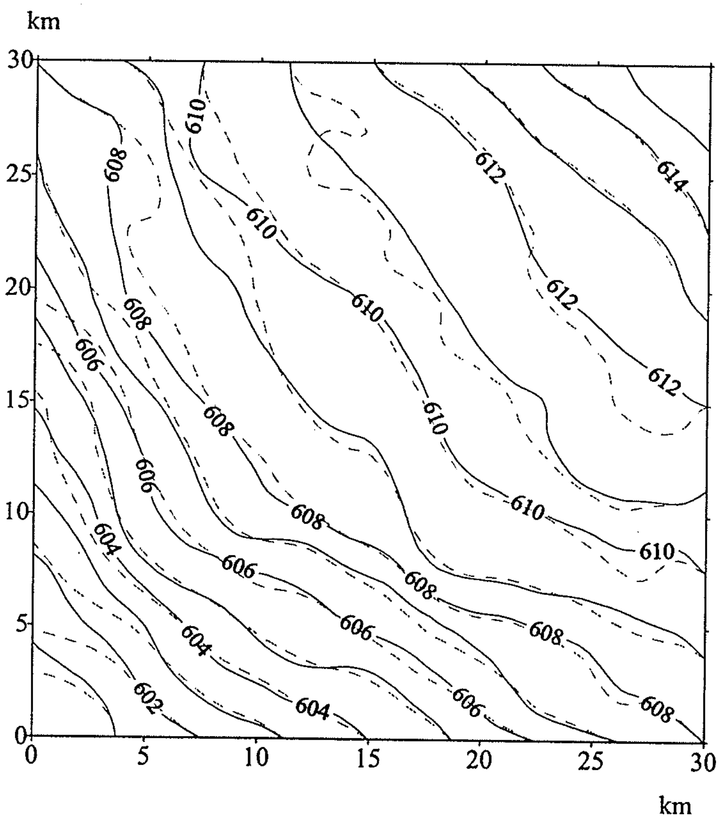

Figure 3-3 True head field (solid) versus linearized head field (dash) for ln (T) variance=2.25

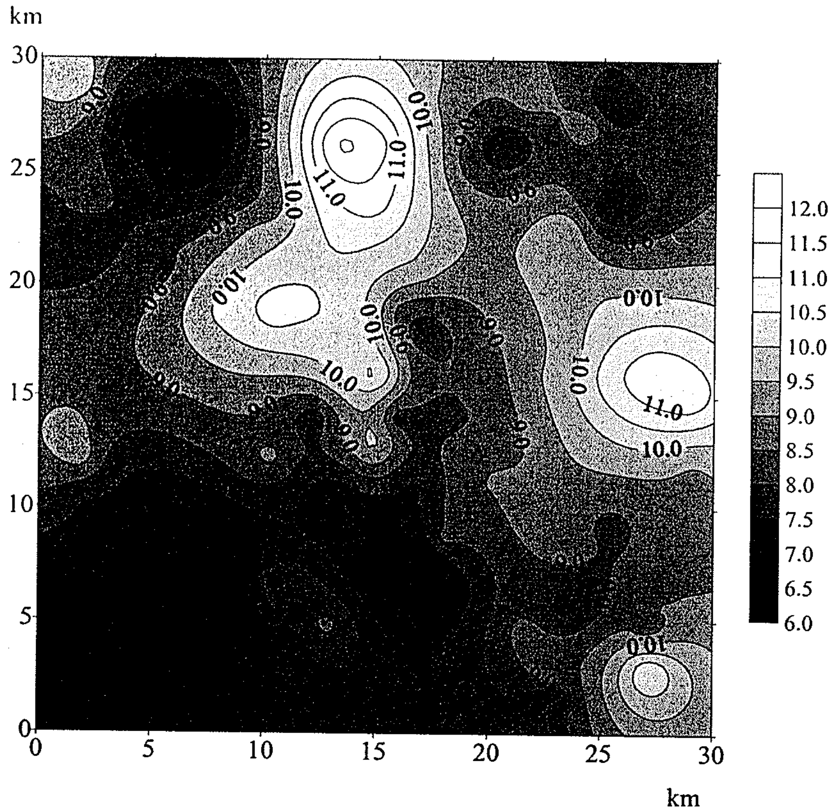

Figure 3-4 Bayesian updated ln (T) field from 100 points of ln (T)

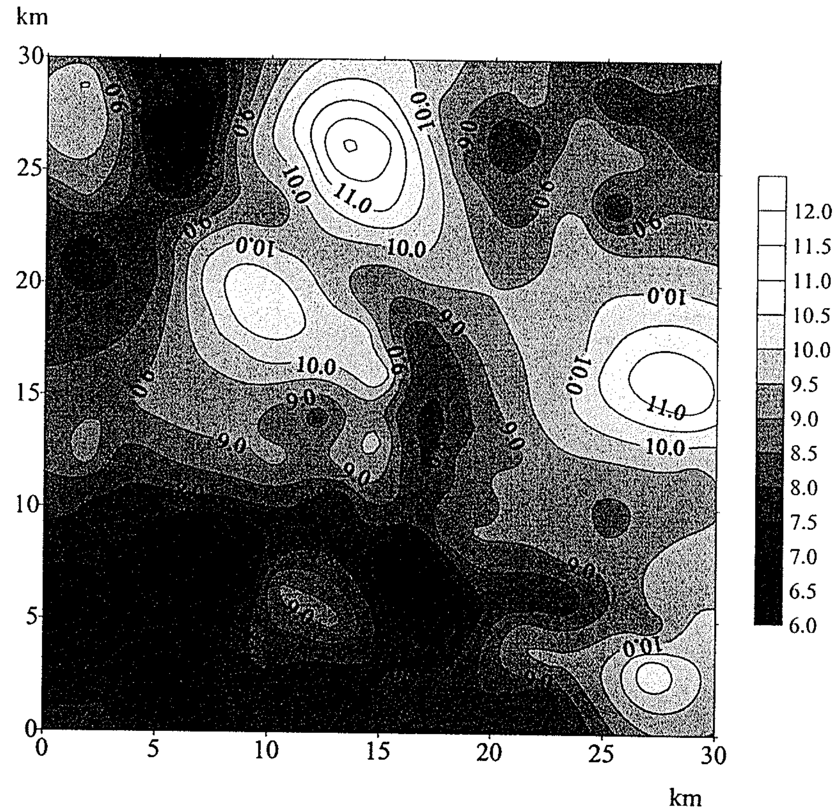

Figure 3-5 Bayesian updated ln (T) field from 100 points of ln (T) and heads

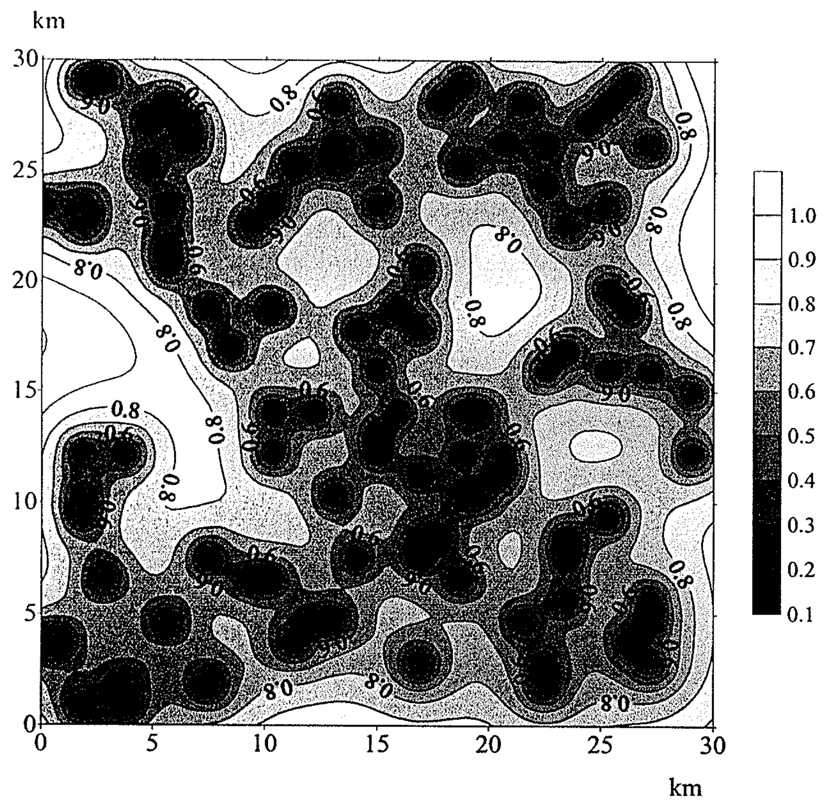

Figure 3-6 Standard deviation of updated ln (T) field from 100 points of ln (T)

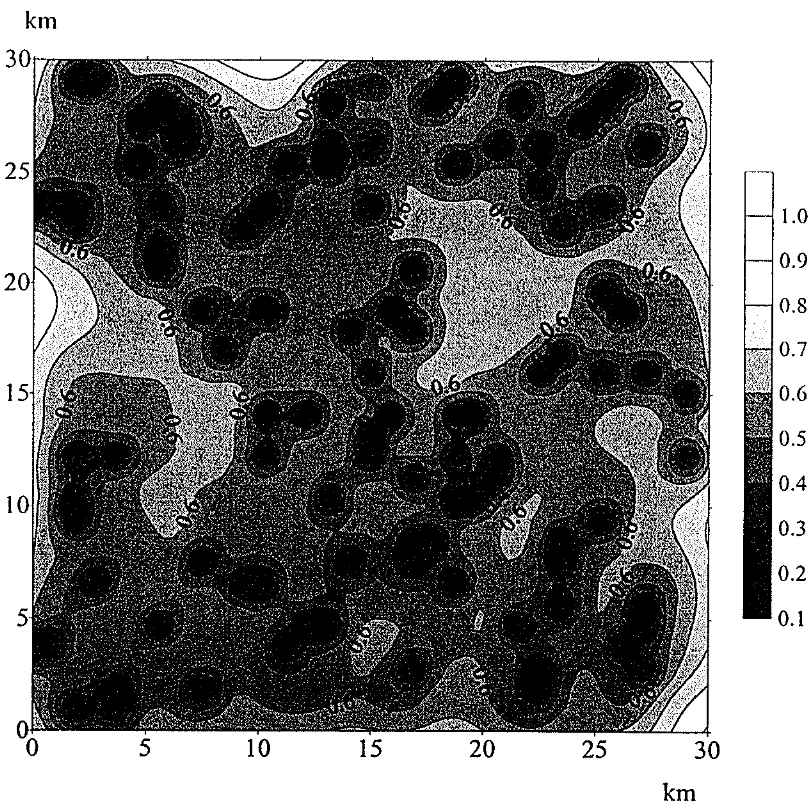

Figure 3-7 Standard deviation of updated ln (T) field from 100 points of ln (T) and heads

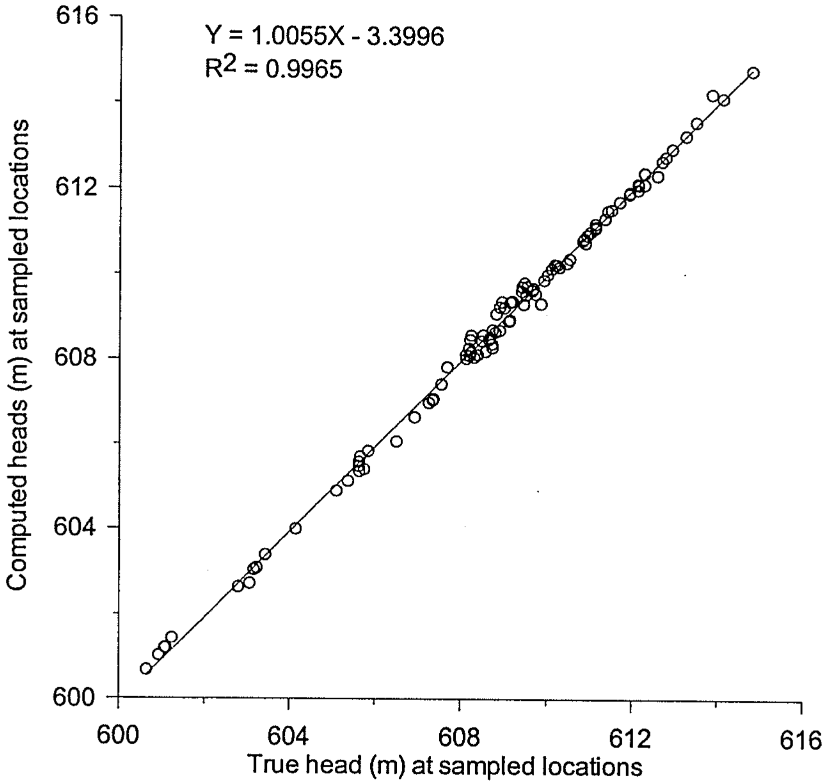

Figure 3-8 True heads versus computed heads based on updated ln (T) from 100 points of ln (T)

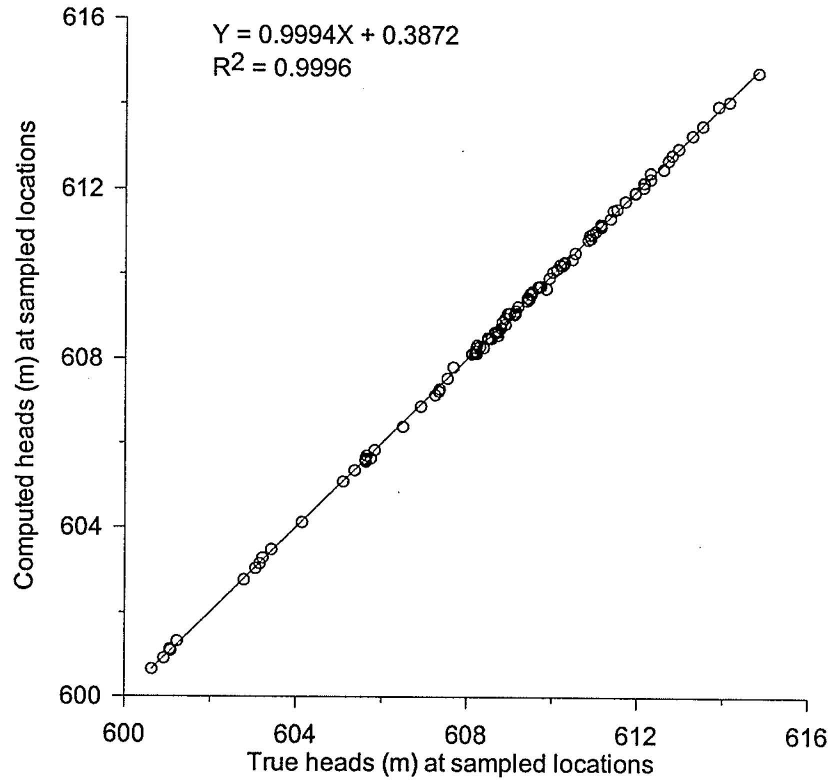

Figure 3-9 True heads versus computed heads based on ln (T) from 100 points of ln (T) and heads

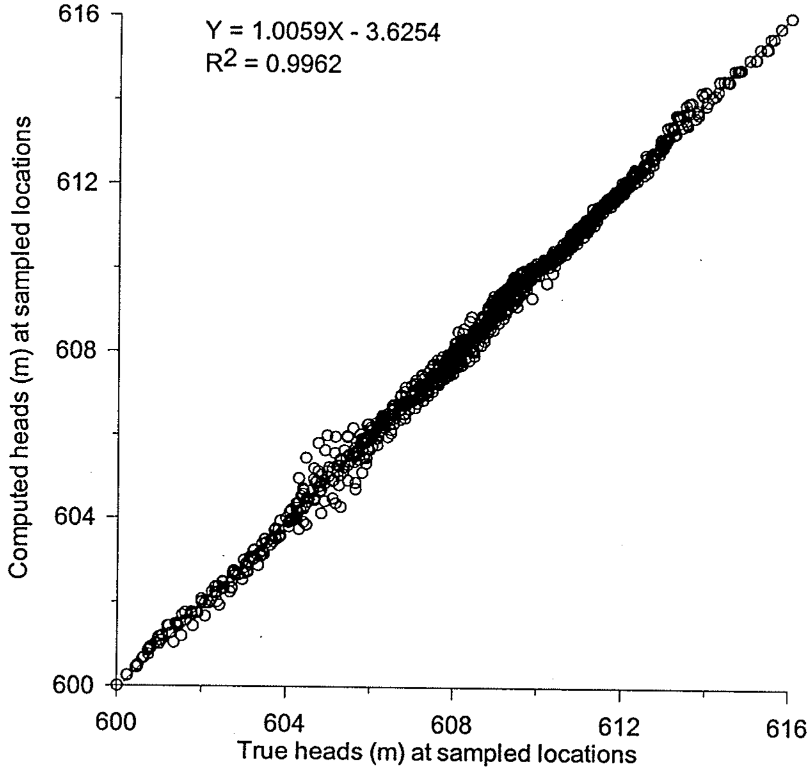

Figure 3-10 True heads versus computed heads based on updated ln (T) from 100 points of ln (T) (verification)

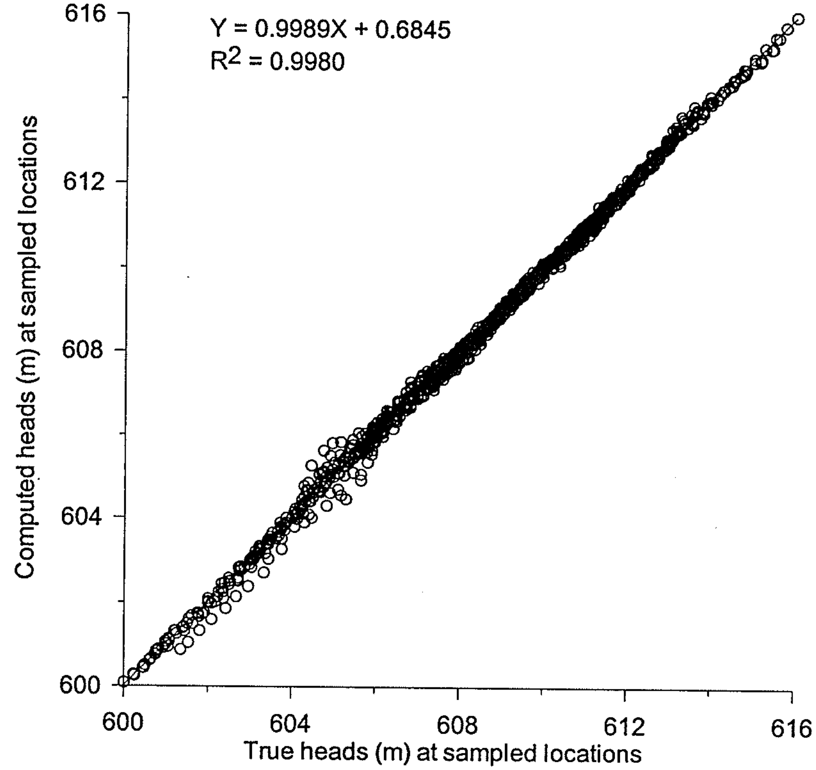

Figure 3-11 True heads versus computed heads based on updated ln (T) from 100 points of ln (T) and heads (verification)

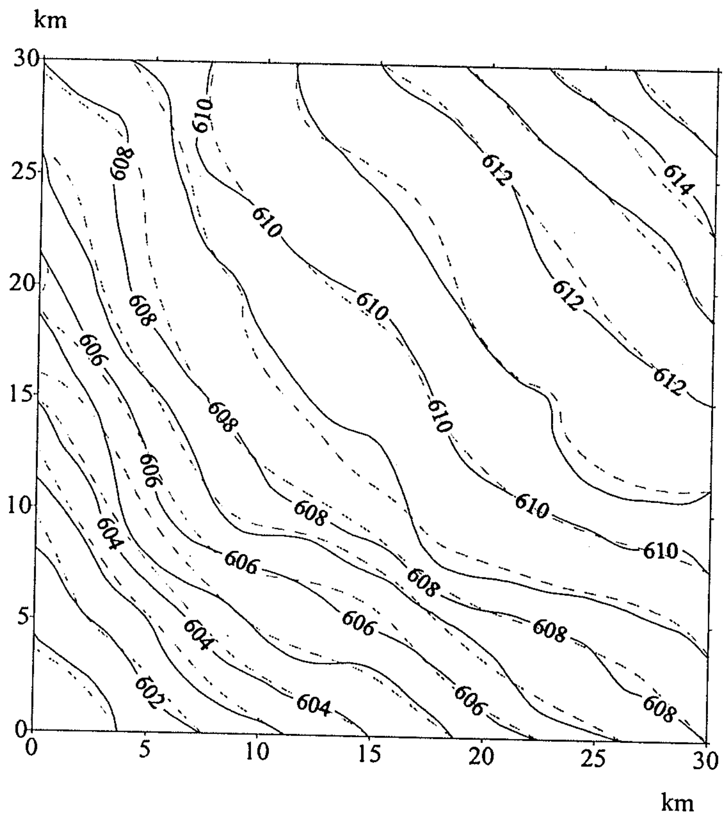

Figure 3-12 True head (solid) field versus computed head field (dash) based on updated ln (T) from 100 points of ln (T)

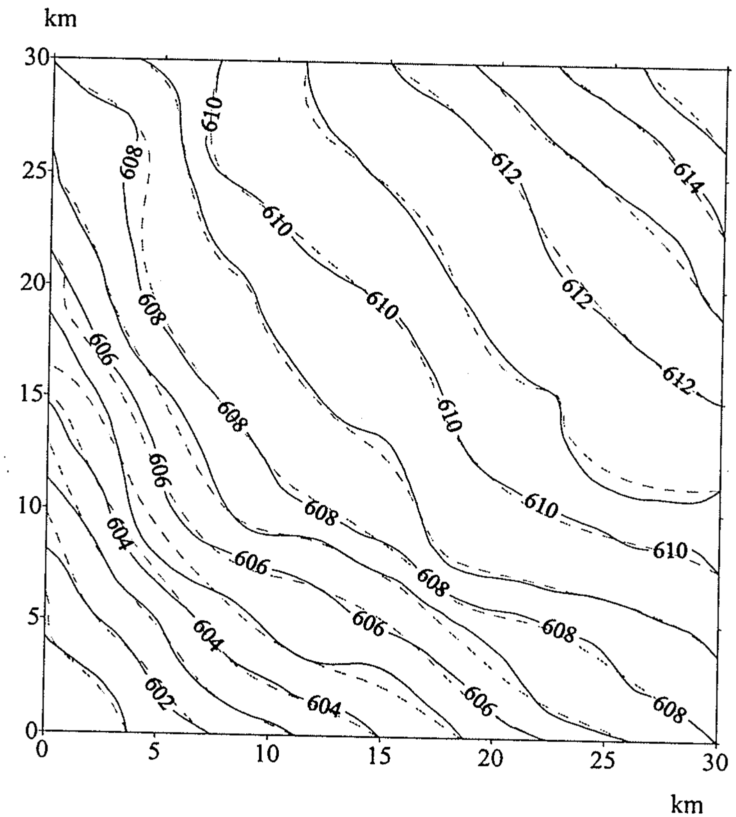

Figure 3-13 True head (solid) field versus computed head (dash) field based on updated ln (T) from 100 points of ln (T) and heads

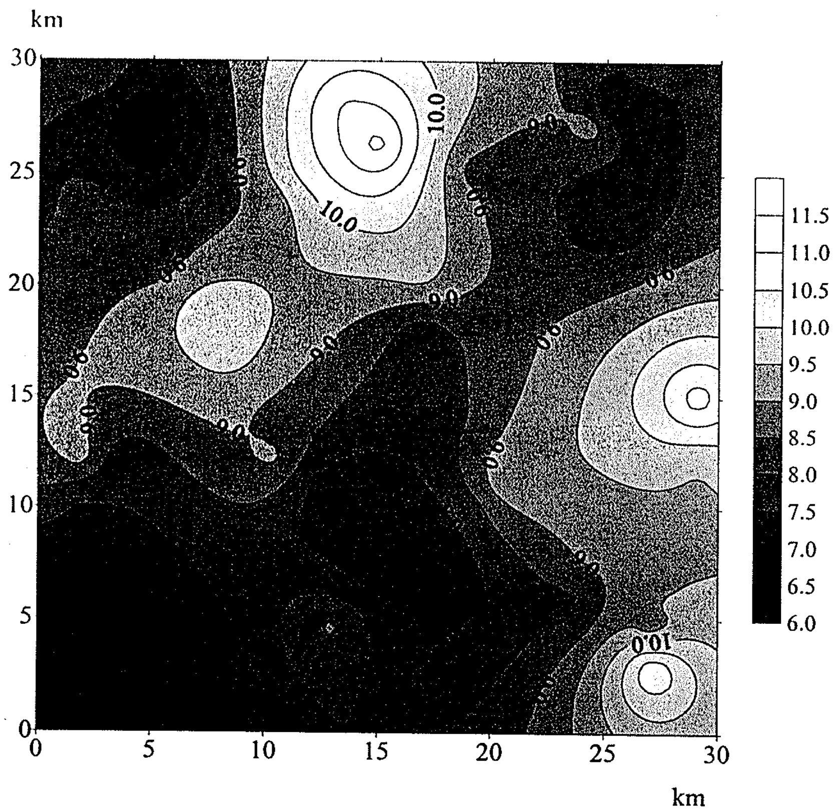

Figure 3-14 Bayesian updated ln (T) field from 50 points of ln (T)

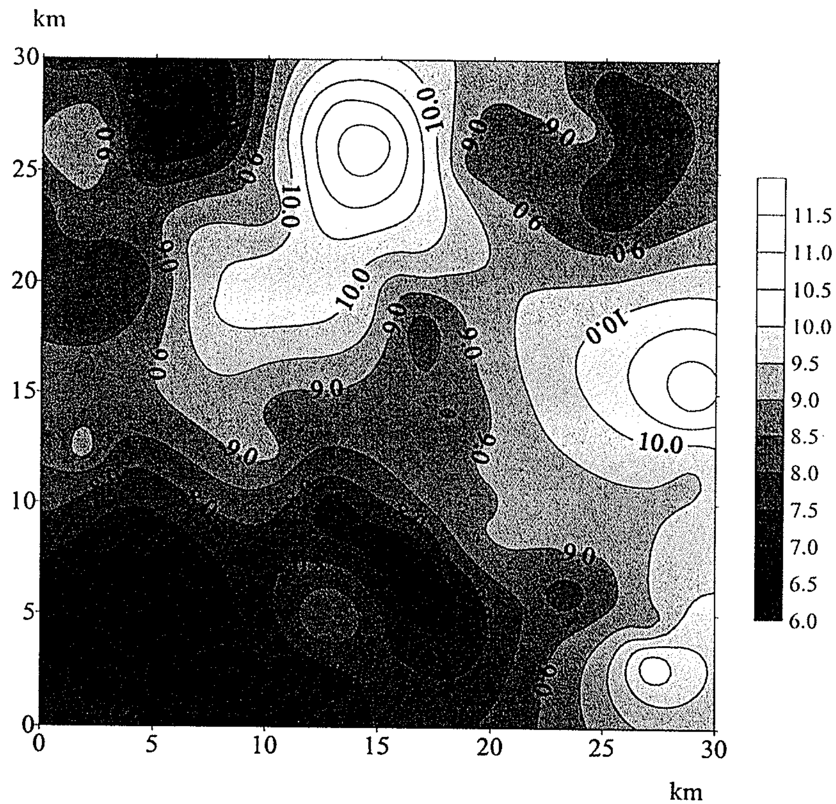

Figure 3-15 Bayesian updated ln (T) field from 50 points of ln (T) and heads

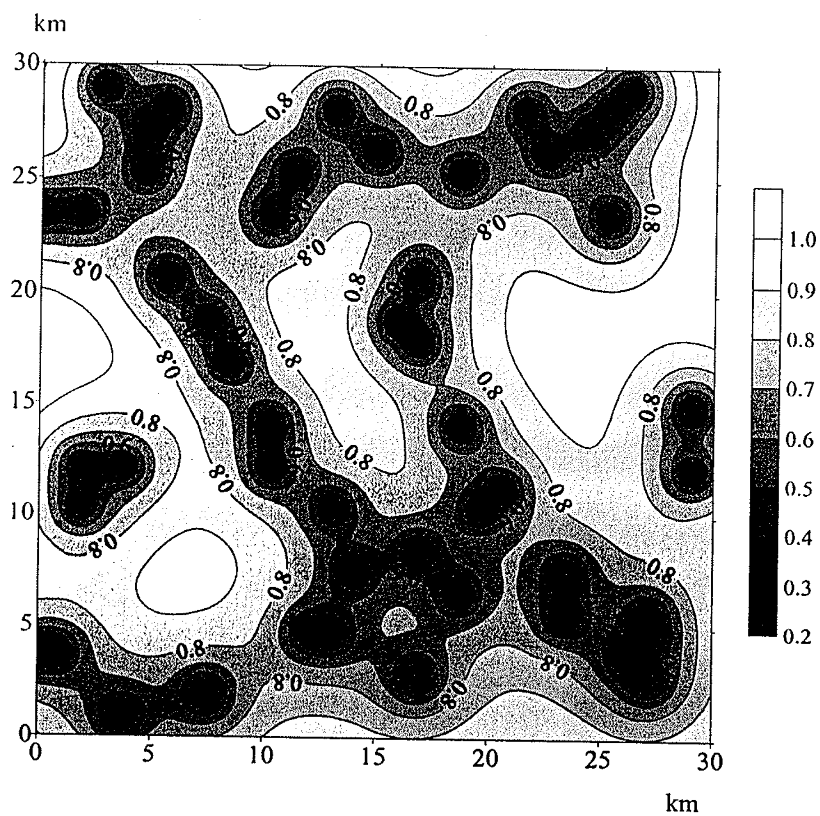

Figure 3-16 Standard deviation of updated ln (T) field from 50 points of ln (T)

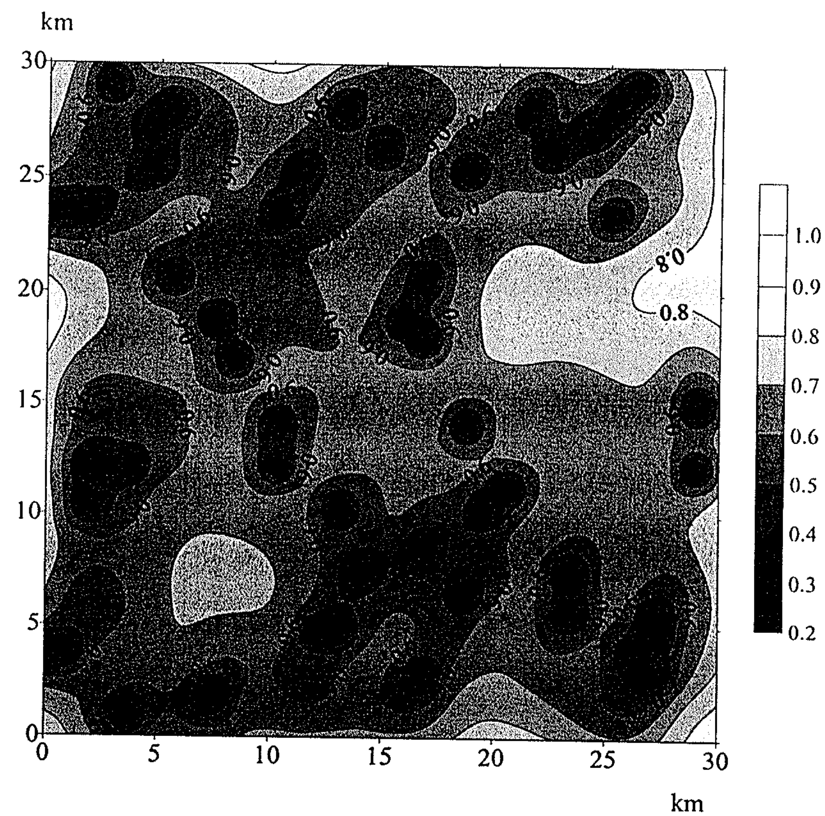

Figure 3-17 Standard deviation of updated ln (T) field from 50 points of heads and ln (T)

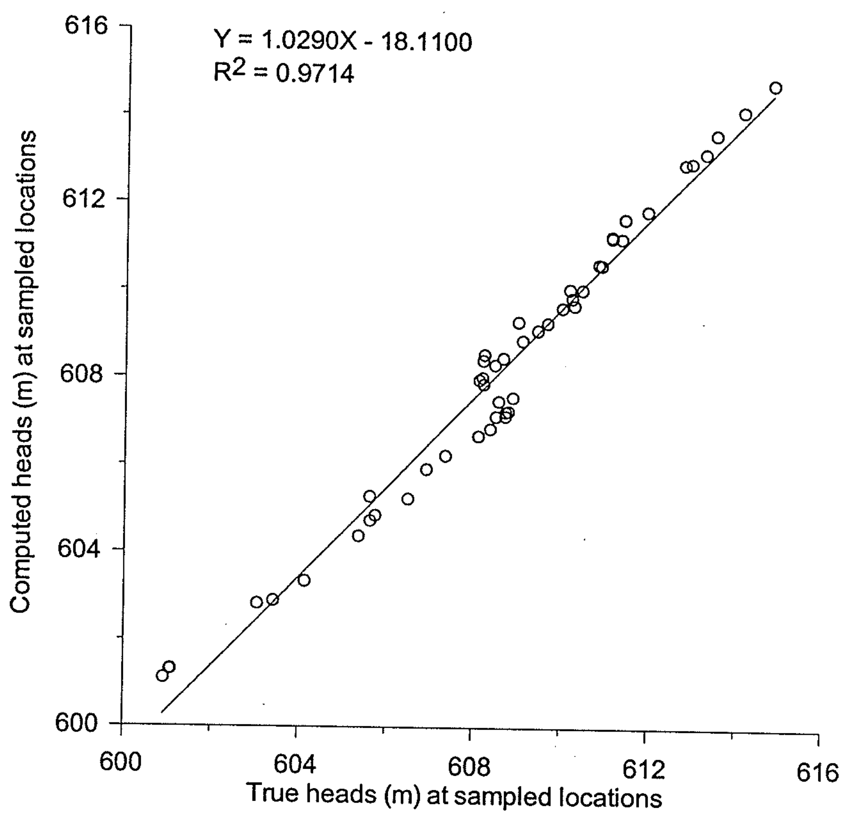

Figure 3-18 True heads versus computed heads based on updated ln (T) from 50 points of ln (T)

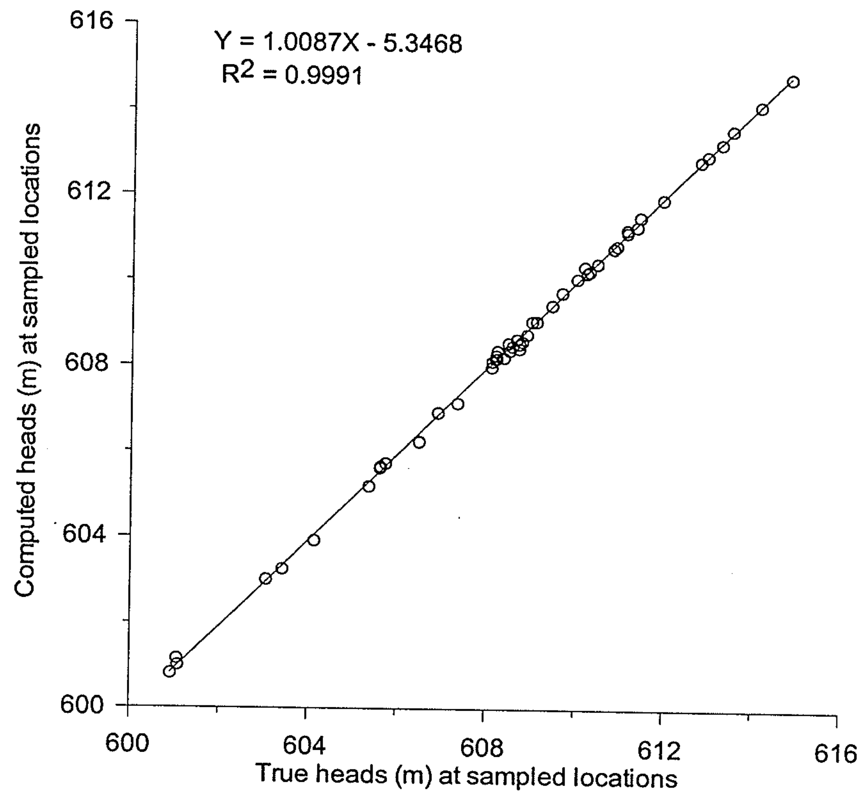

Figure 3-19 True heads versus computed heads based on updated ln (T) from 50 points of ln (T) and heads

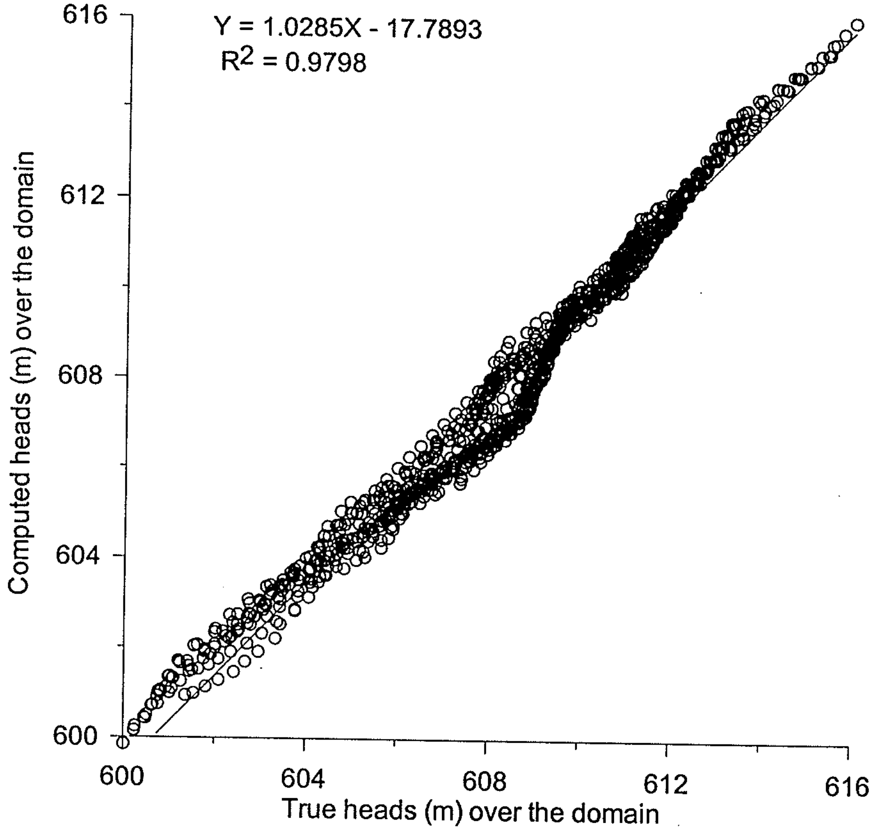

Figure 3-20 True heads versus computed heads based on updated ln (T) from 50 points of ln (T) (verification)

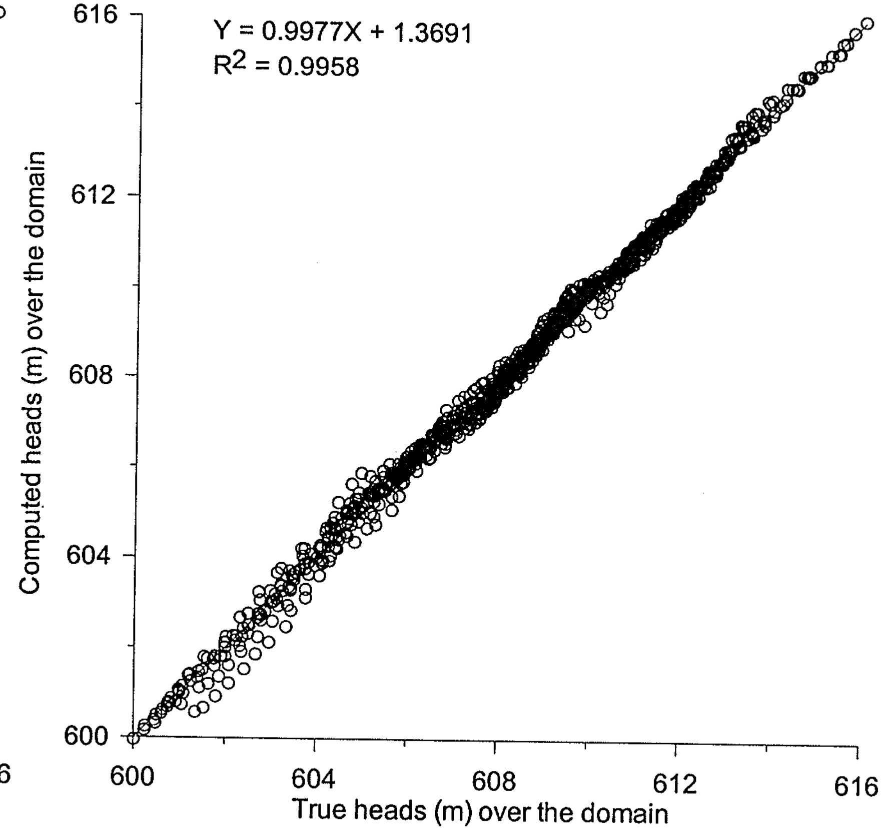

Figure 3-21 True heads versus computed heads based on updated ln (T) from 50 points of ln (T) and heads (verification)

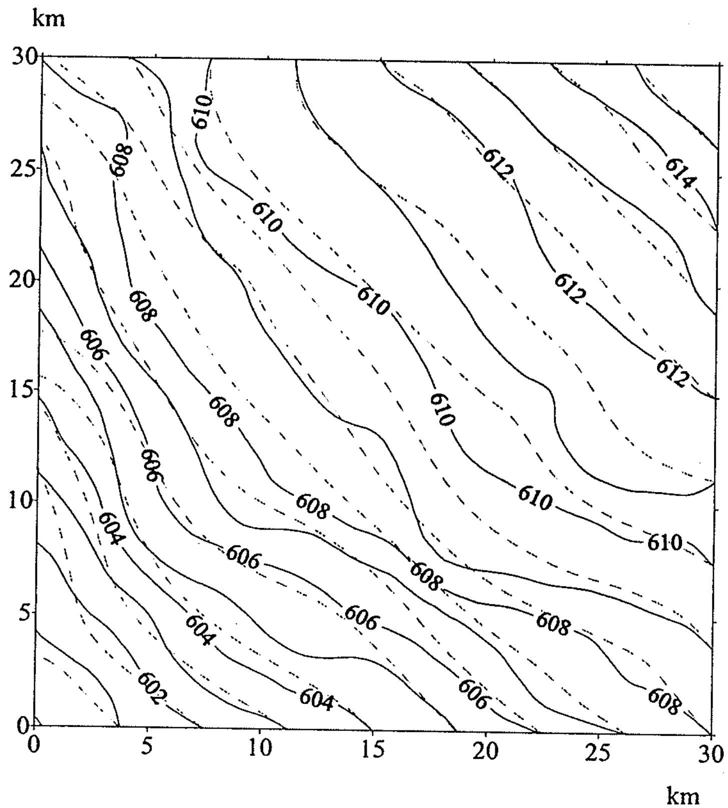

Figure 3-22 True head (solid) field versus computed head (dash) field based on updated ln (T) from 50 points of ln (T)

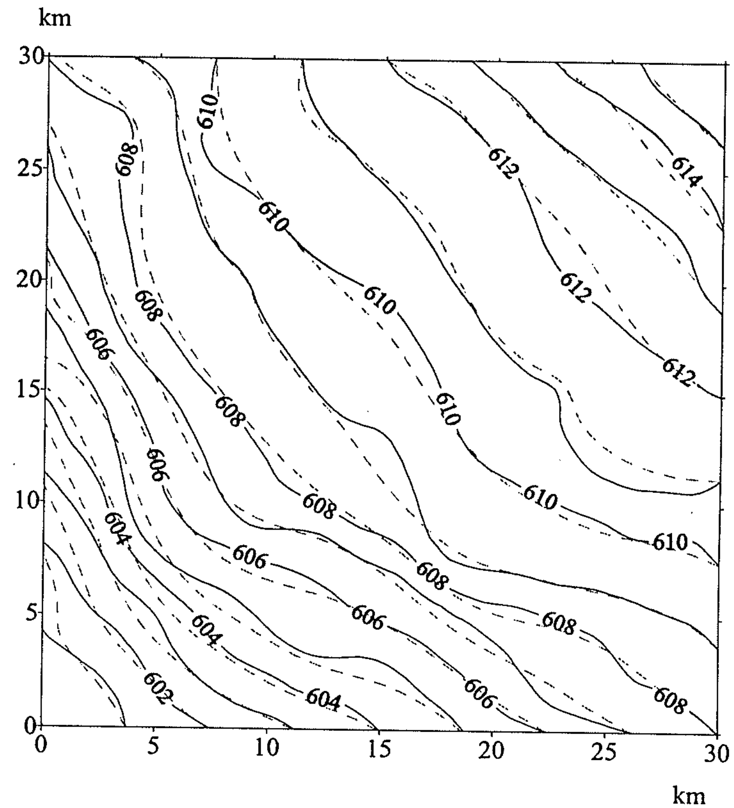

Figure 3-23 True head (solid) field versus computed head (dash) field based on updated ln (T) from 50 points of ln (T) and heads

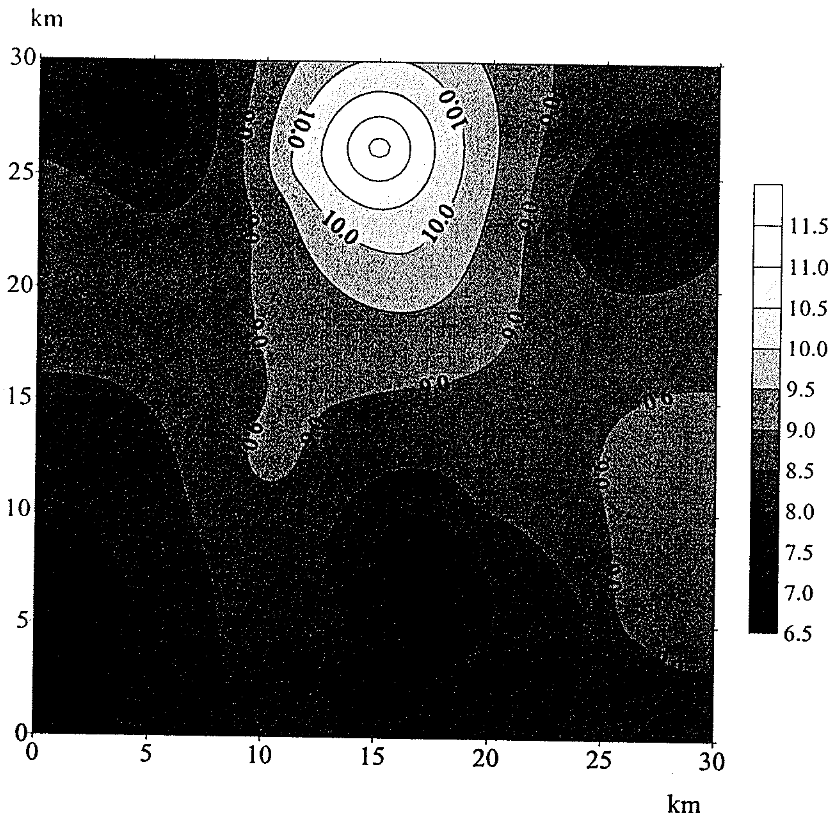

Figure 3-24 Bayesian updated ln (T) field from 20 points of ln (T)

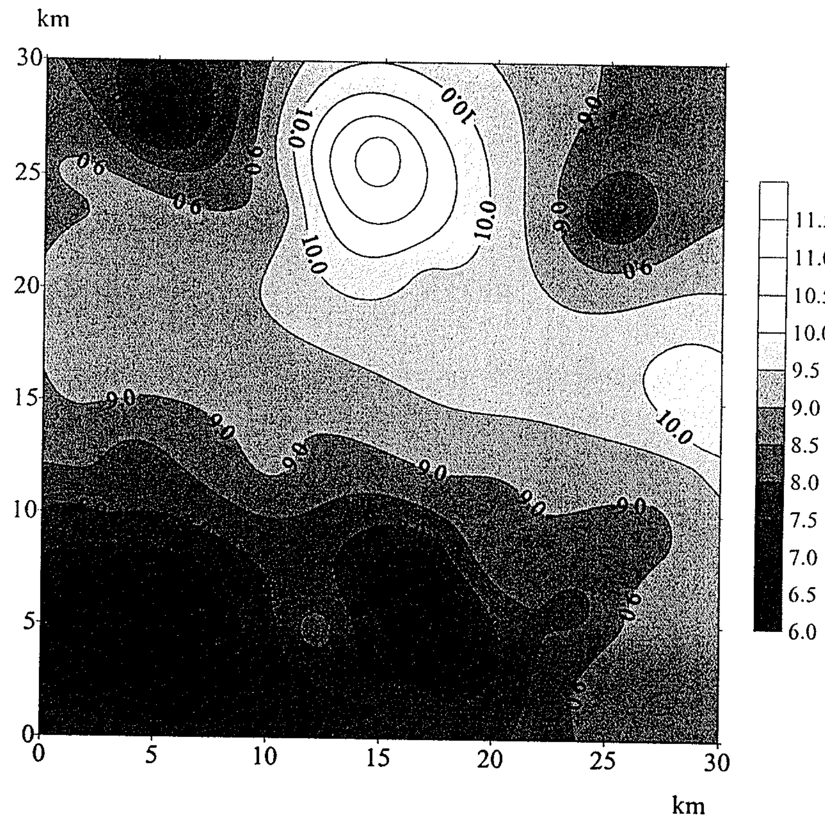

Figure 3-25 Bayesian updated ln (T) field from 20 points of ln (T) and heads

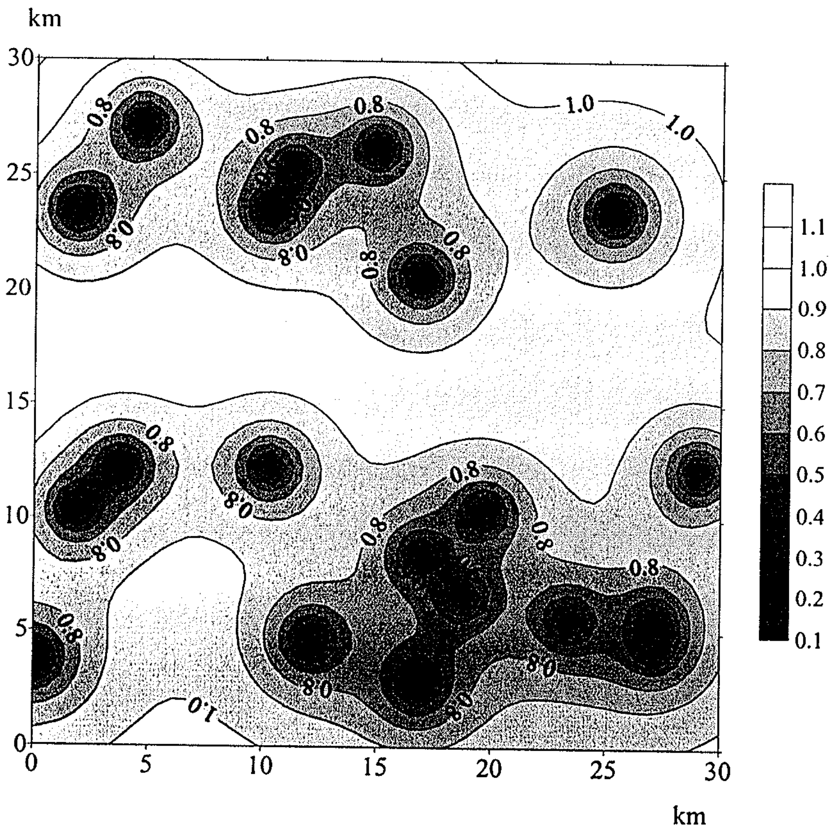

Figure 3-26 Standard deviation of updated ln (T) field from 20 points of ln (T)

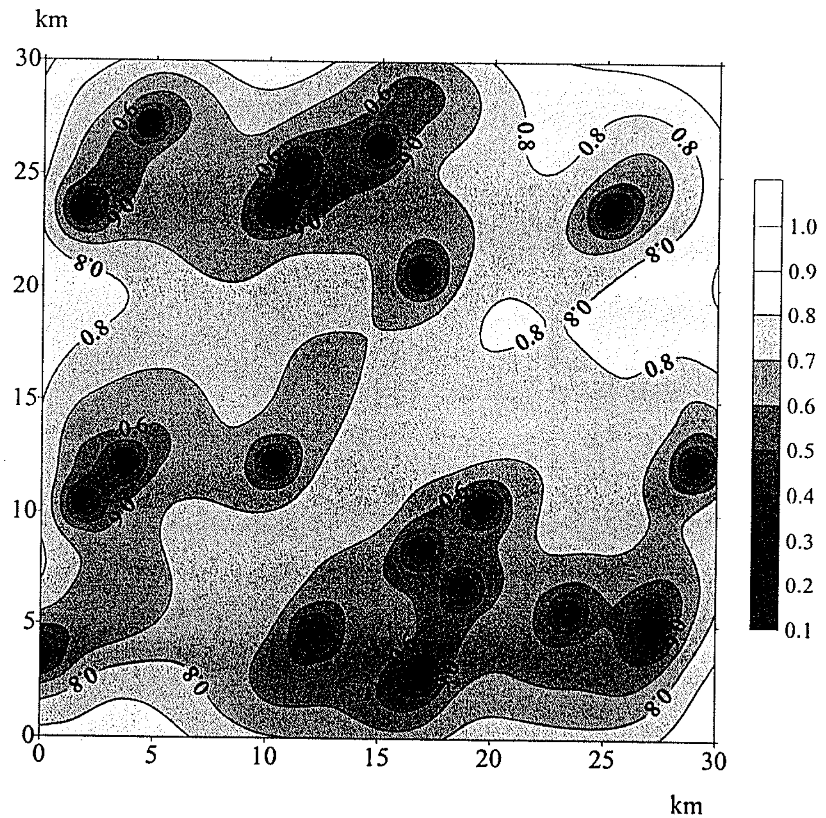

Figure 3-27 Standard deviation of updated ln (T) field from 20 points of ln (T) and heads

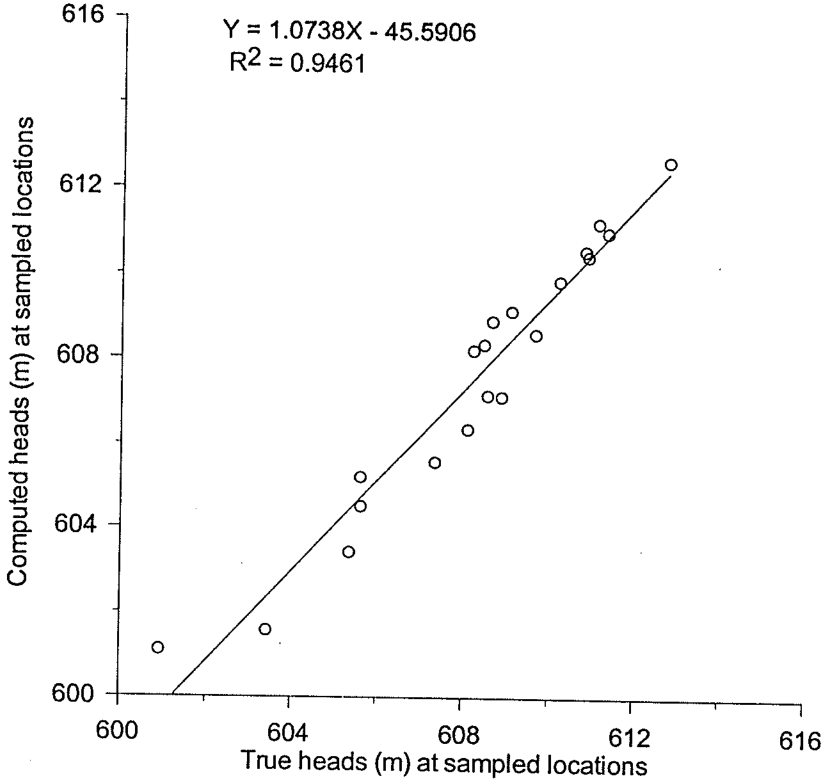

Figure 3-28 True heads versus computed heads based on updated ln (T) from 20 points of ln (T)

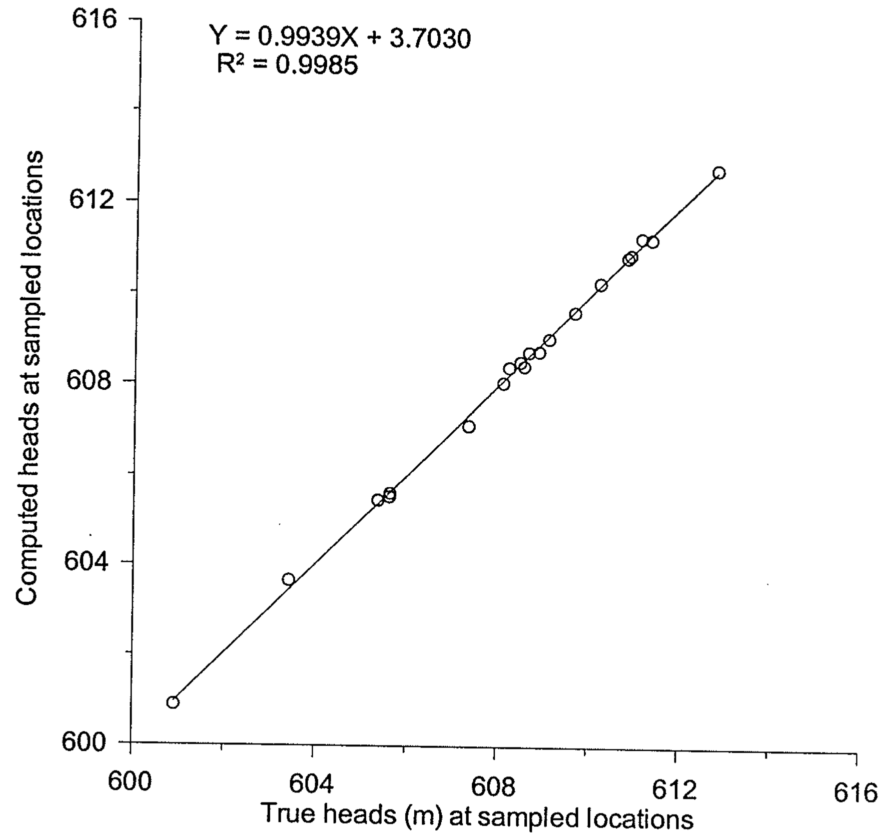

Figure 3-29 True heads versus computed heads based on updated ln (T) from 20 points of ln (T) and heads

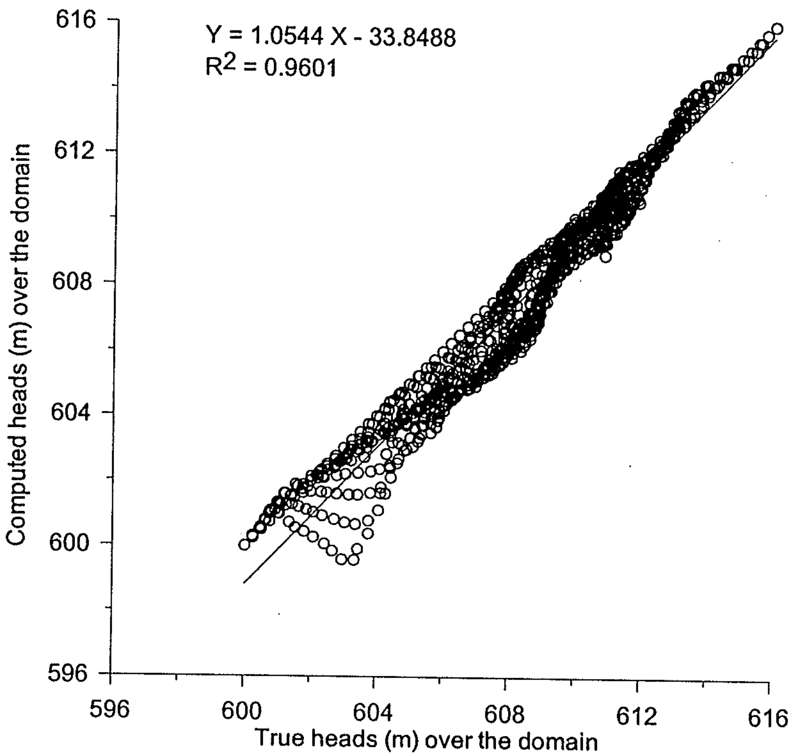

Figure 3-30 True heads versus computed heads based on updated ln (T) from 20 points of ln (T) (verification)

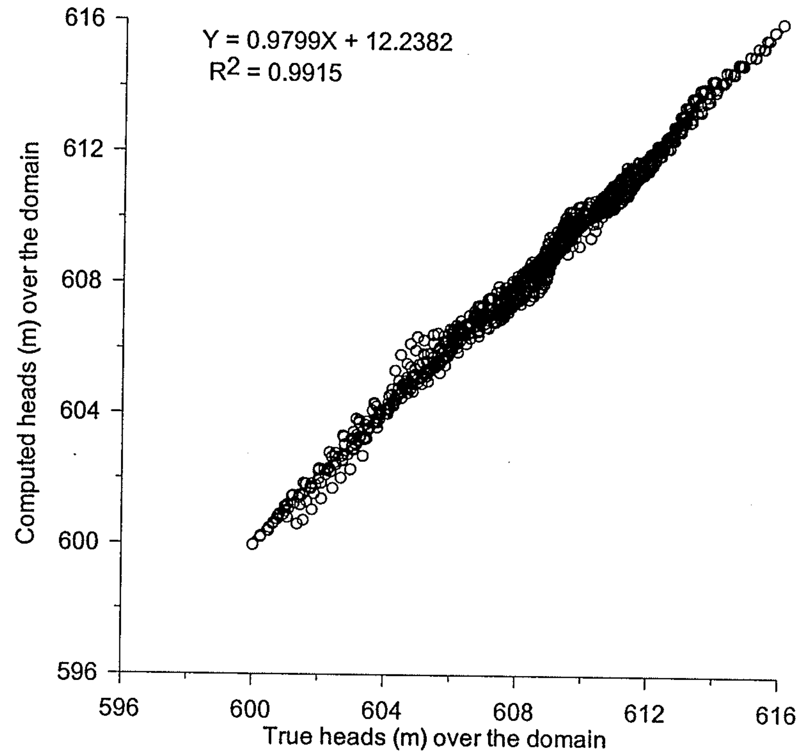

Figure 3-31 True heads versus computed heads based on updated ln (T) from 20 points of ln (T) and heads (verification)

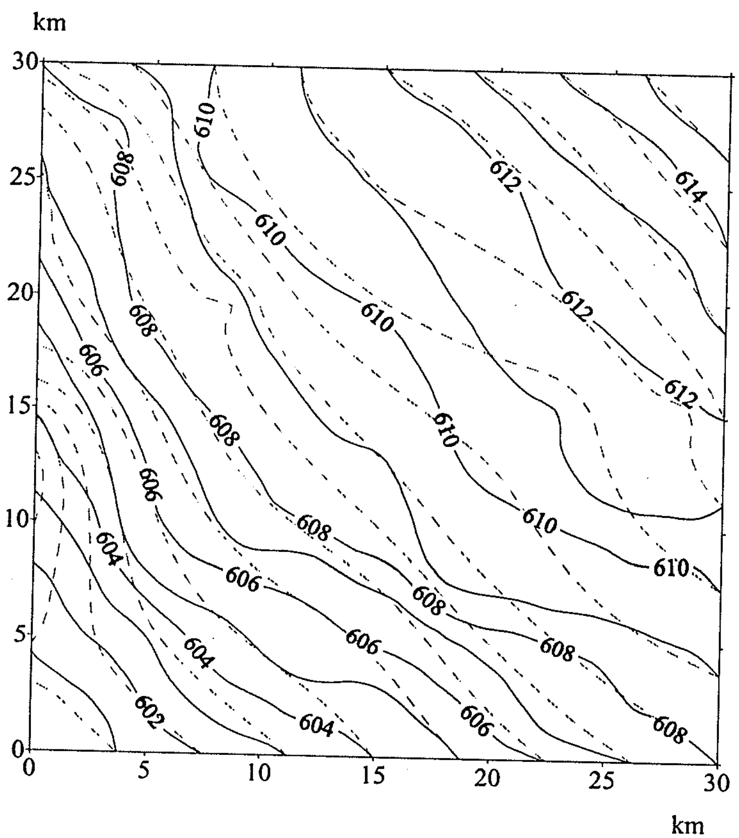

Figure 3-32 True head (solid) field versus computed head (dash) field based on updated ln (T) from 20 points of ln (T)

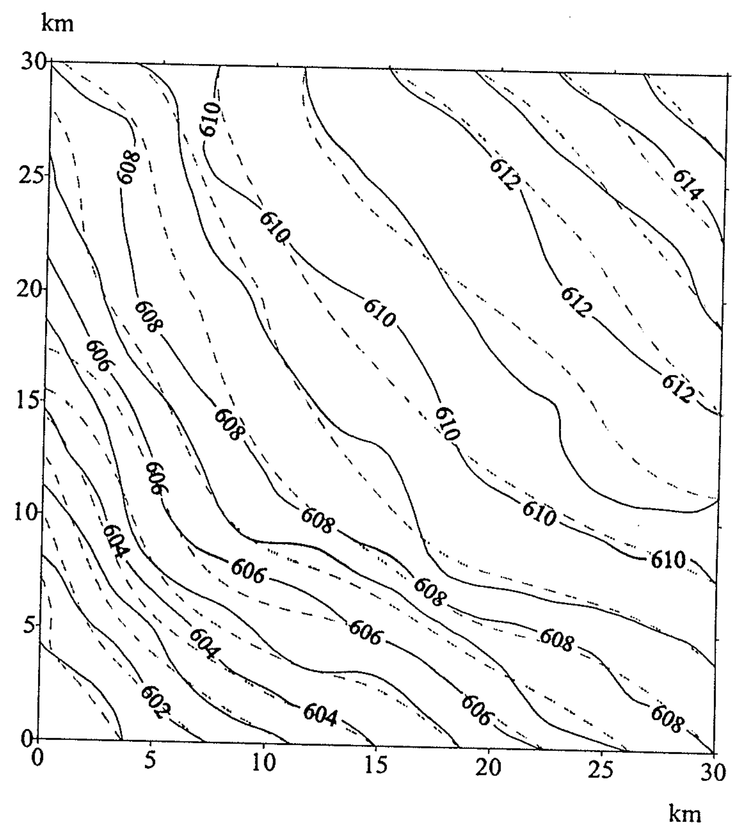

Figure 3-33 True head (solid) field versus computed head (dash) field based on updated ln (T) from 20 points of ln (T) and heads

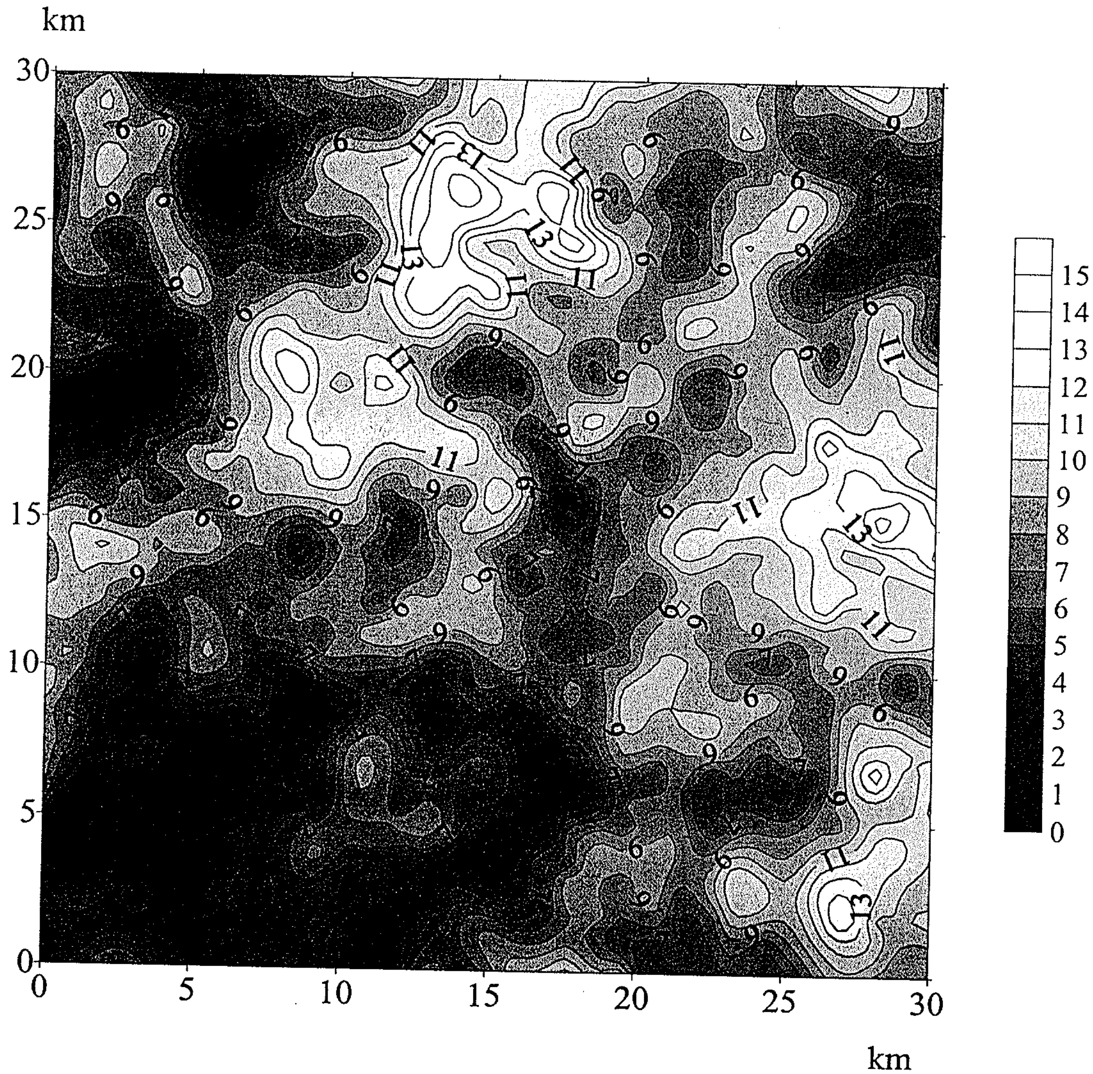

Figure 3-34 ln (T) field generated by multivariate random number generator (actual statistics: mean=9.4, standard deviation=3.0, integral scale=5000 m)

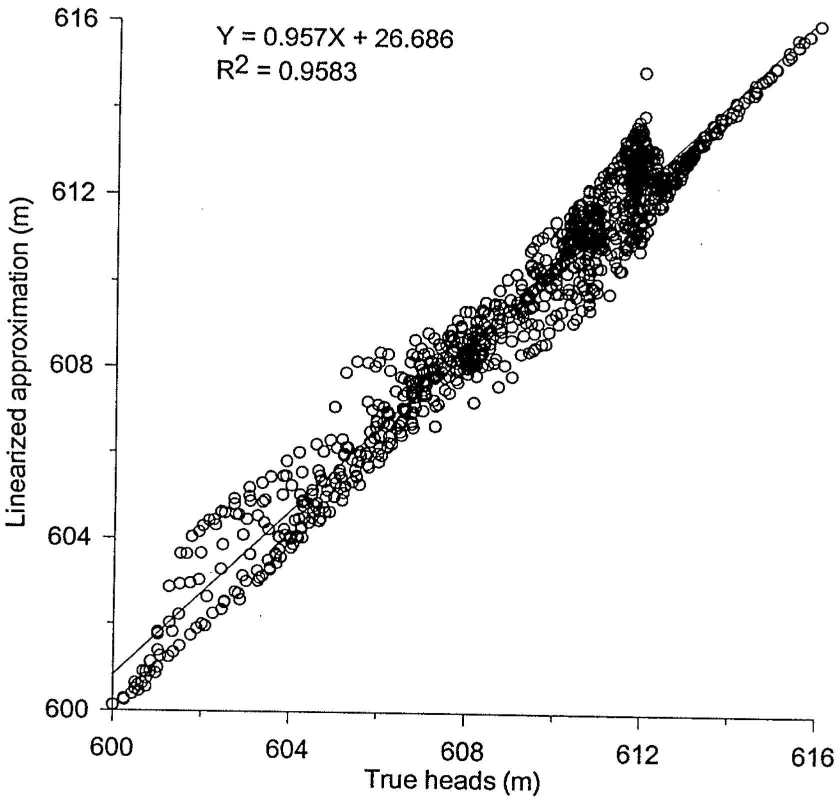

Figure 3-35 True head versus linearized approximation for ln (T) variance up to 9

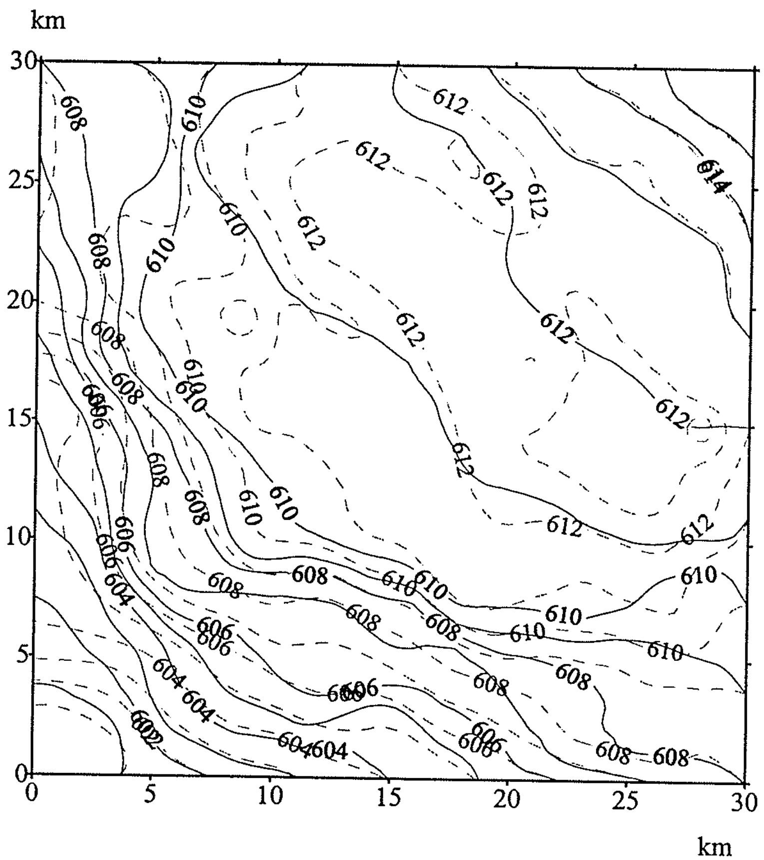

Figure 3-36 True head field (solid) versus linearized head field (dash) for ln (T) variance up to 9

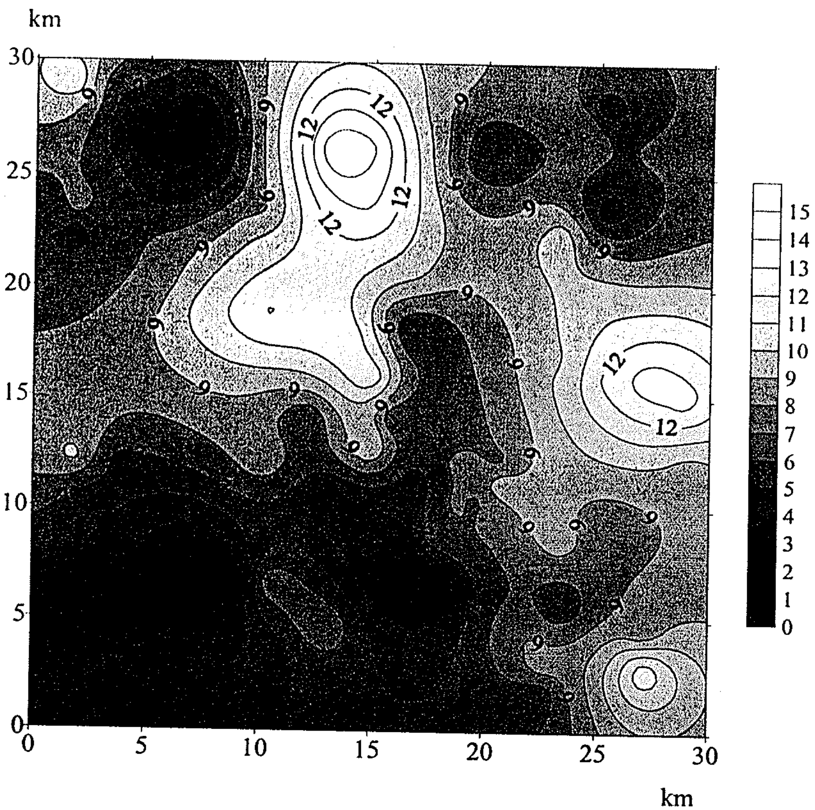

Figure 3-37 Bayesian updated ln (T) field from 100 points of ln (T)

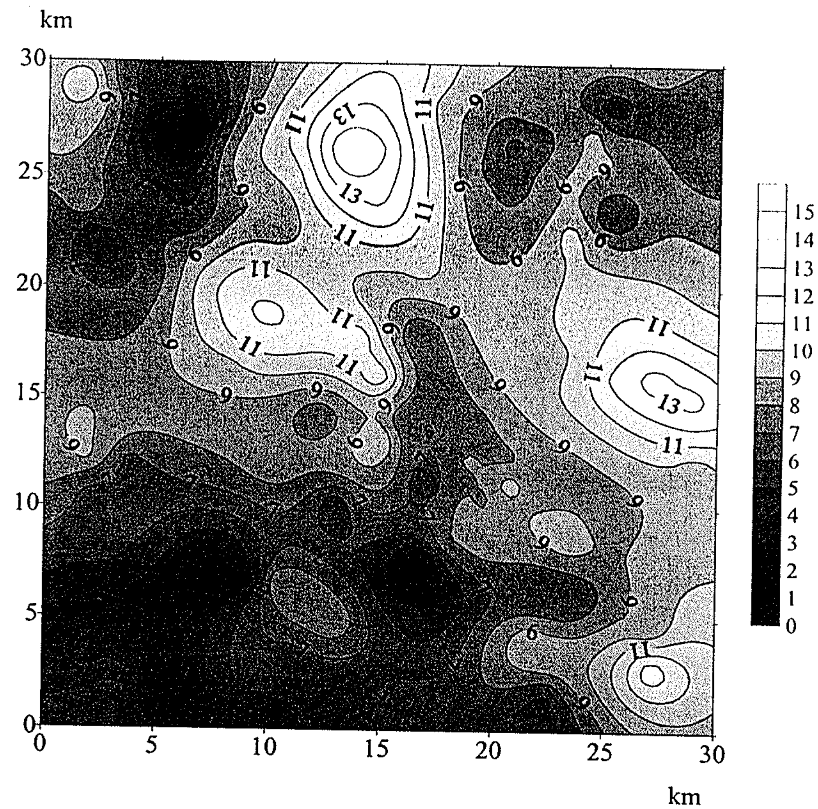

Figure 3-38 Bayesian updated ln (T) field from 100 points of ln (T) and heads

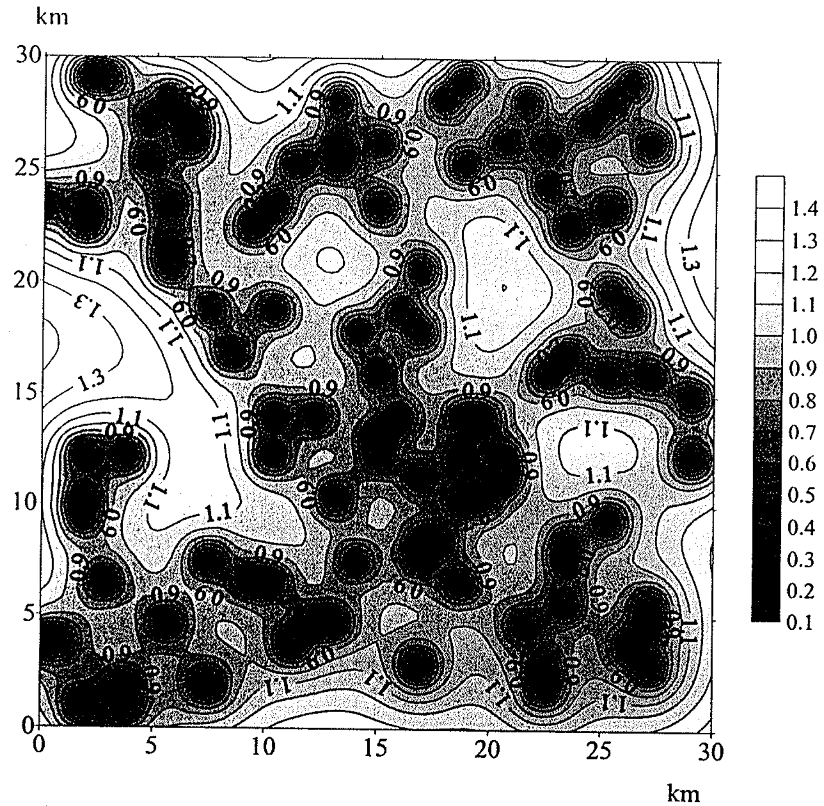

Figure 3-39 Standard deviation of updated ln (T) field from 100 points of ln (T)

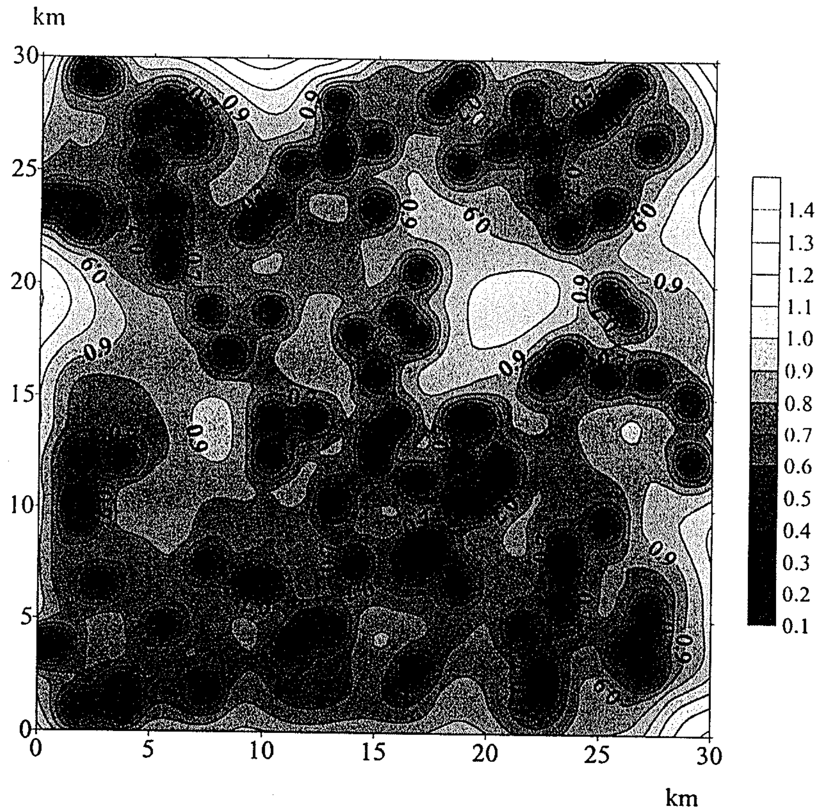

Figure 3-40 Standard deviation of updated ln (T) field from 100 points of ln (T) and heads

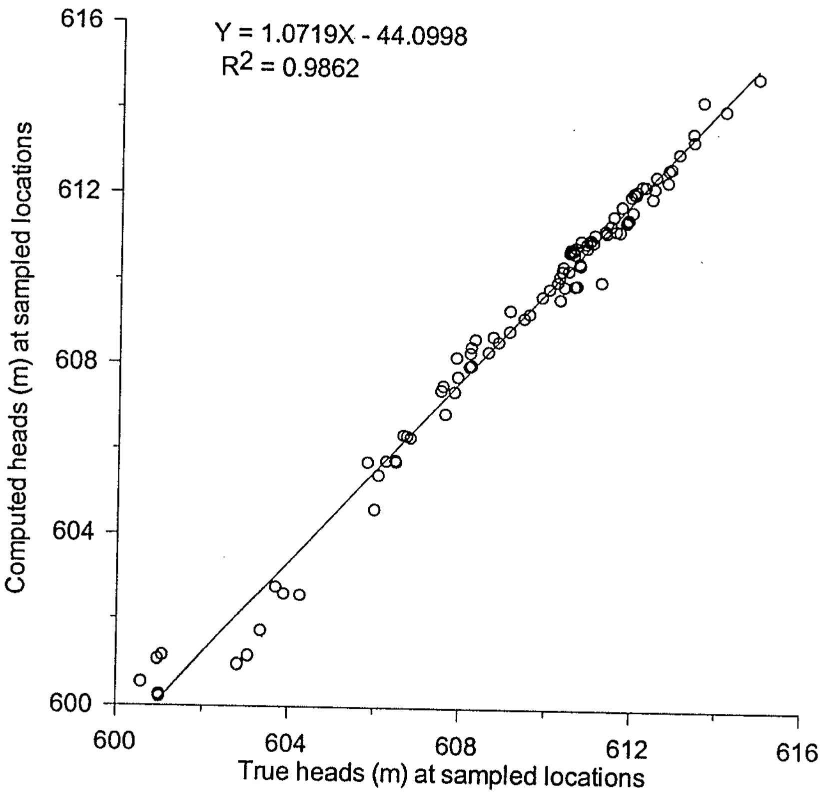

Figure 3-41 True heads versus computed heads based on updated ln (T) from 100 points of ln (T)

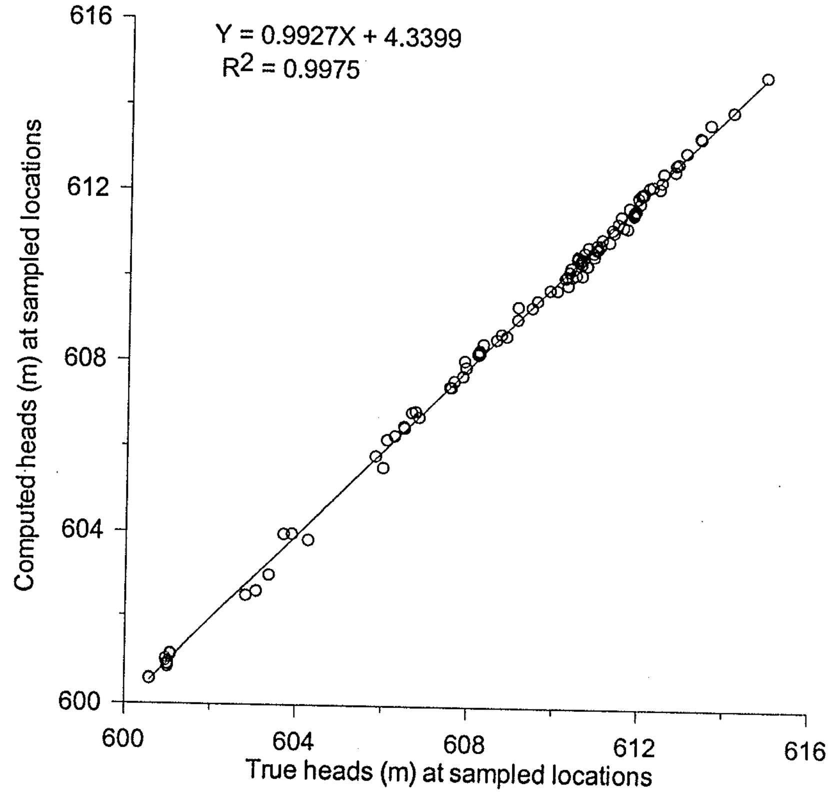

Figure 3-42 True heads versus computed heads based on ln (T) from 100 points of ln (T) and heads

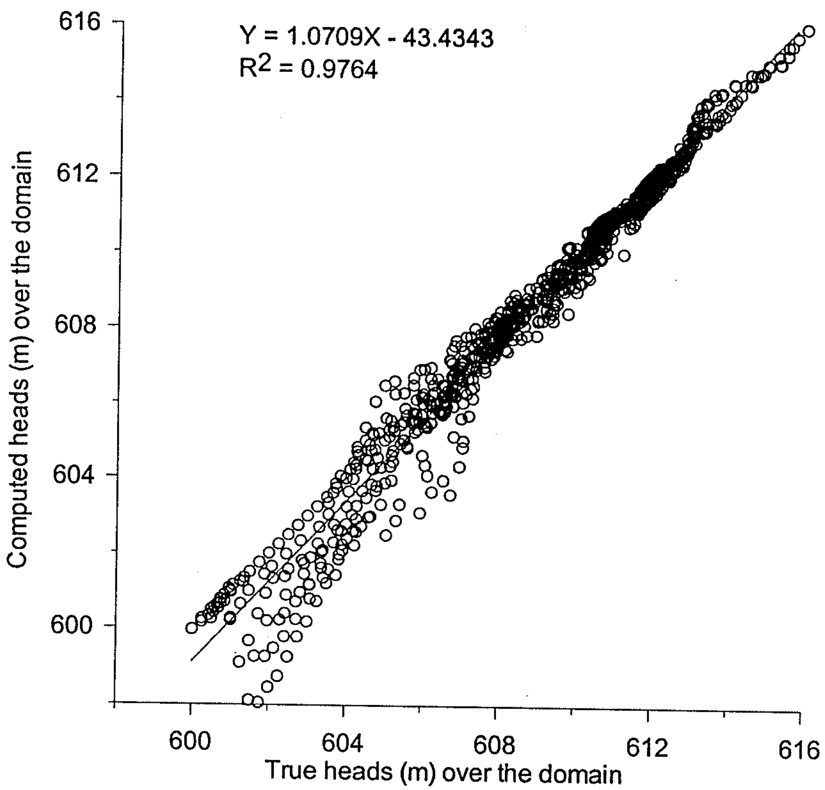

Figure 3-43 True heads versus computed heads based on updated ln (T) from 100 points of ln (T) (verification)

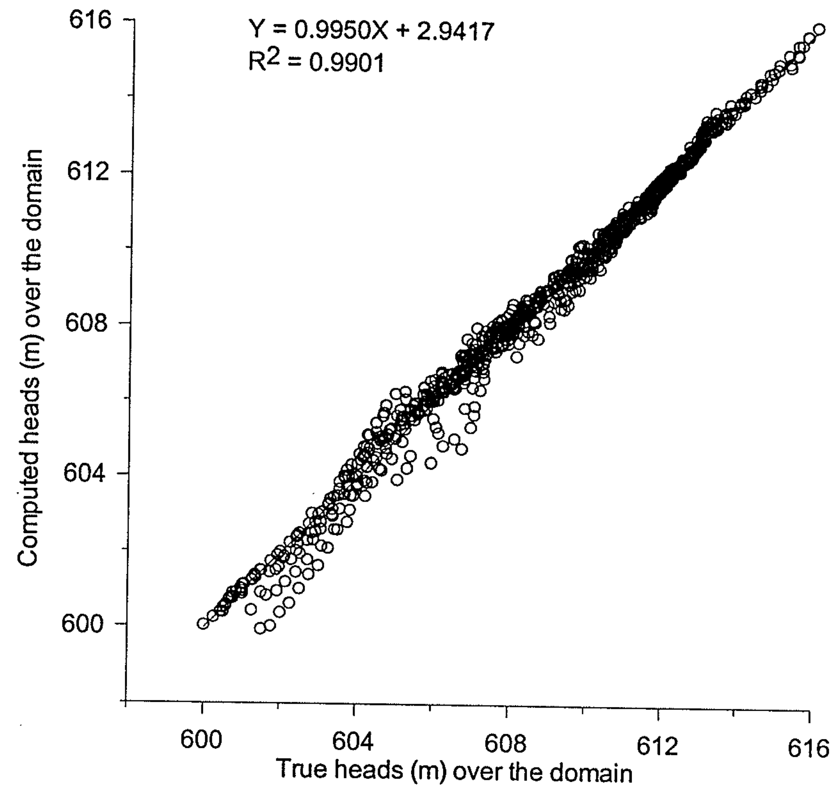

Figure 3-44 True heads versus computed heads based on updated ln (T) from 100 points of ln (T) and heads (verification)

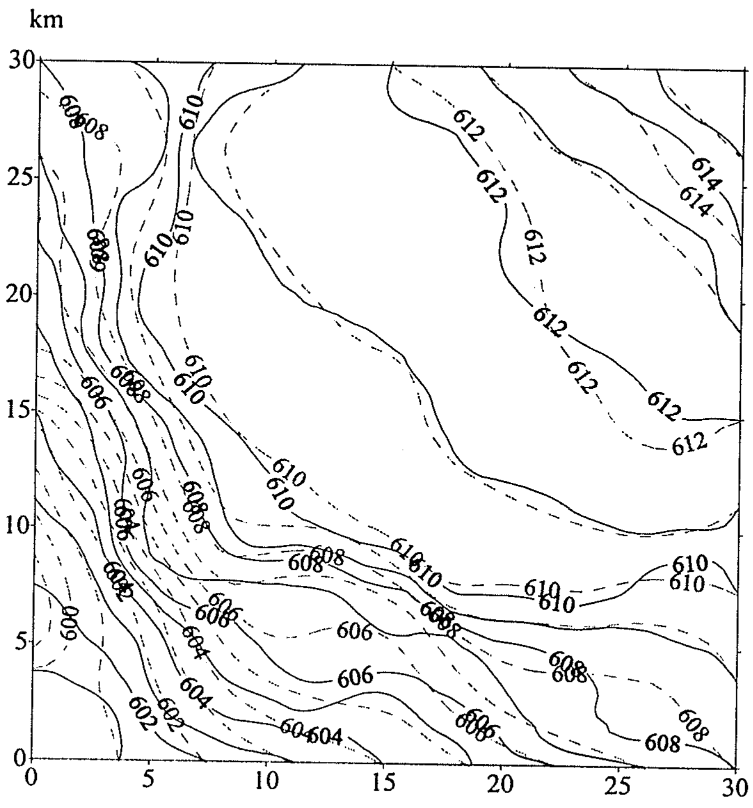

Figure 3-45 True head field (solid) versus computed head field (dash) based on updated ln (T) from 100 points of ln (T)

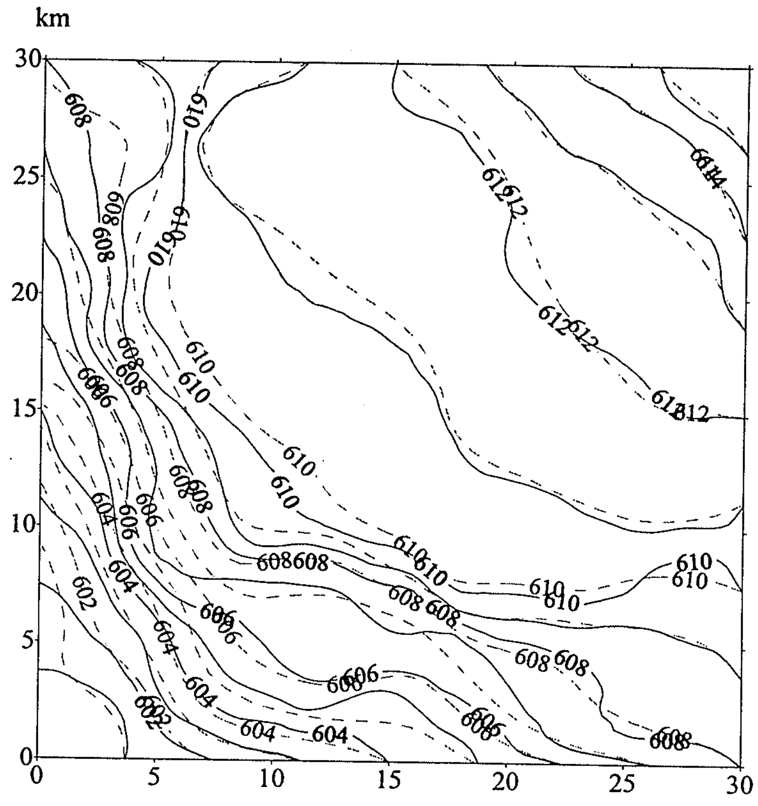

Figure 3-46 True head field (solid) versus computed head field (dash) based on updated ln (T) from 100 points of ln (T) and heads

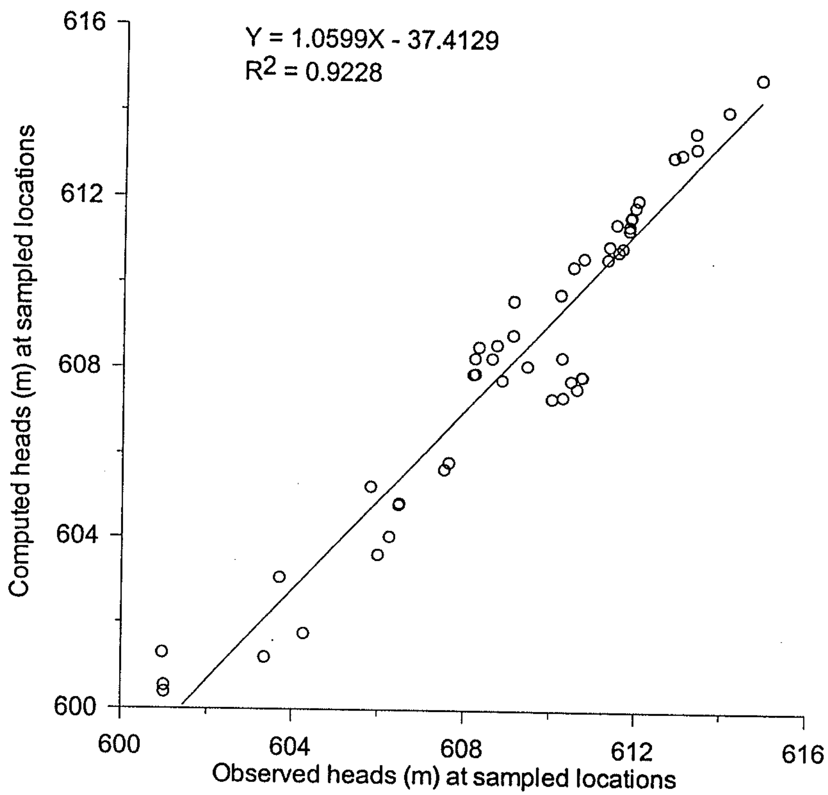

Figure 3-47 True heads versus computed heads based on updated ln (T) from 50 points of ln (T)

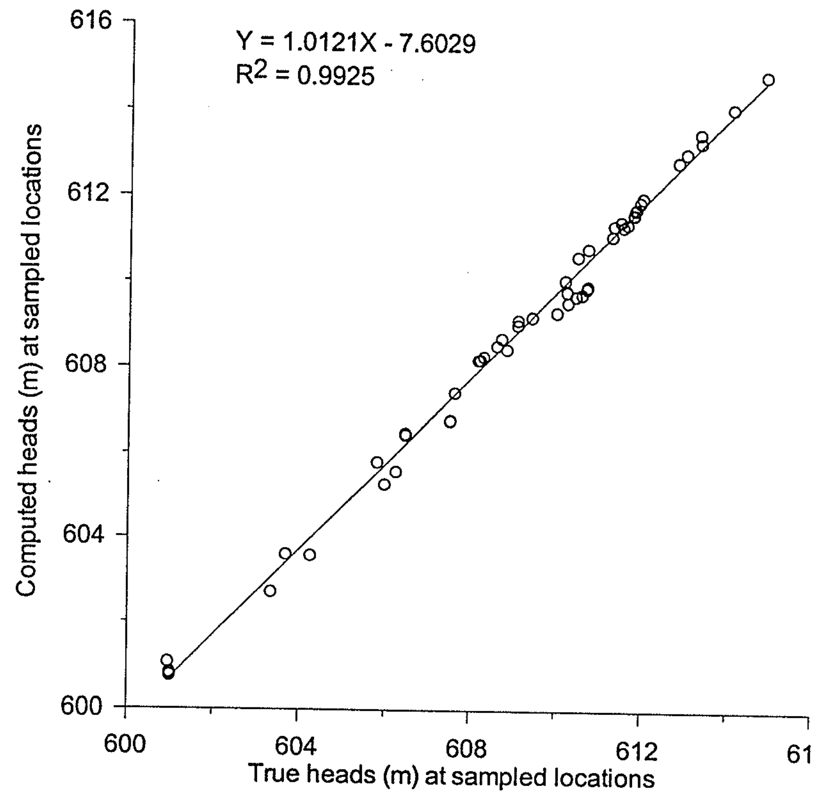

Figure 3-48 True heads versus computed heads based on updated ln (T) from 50 points of ln (T) and heads

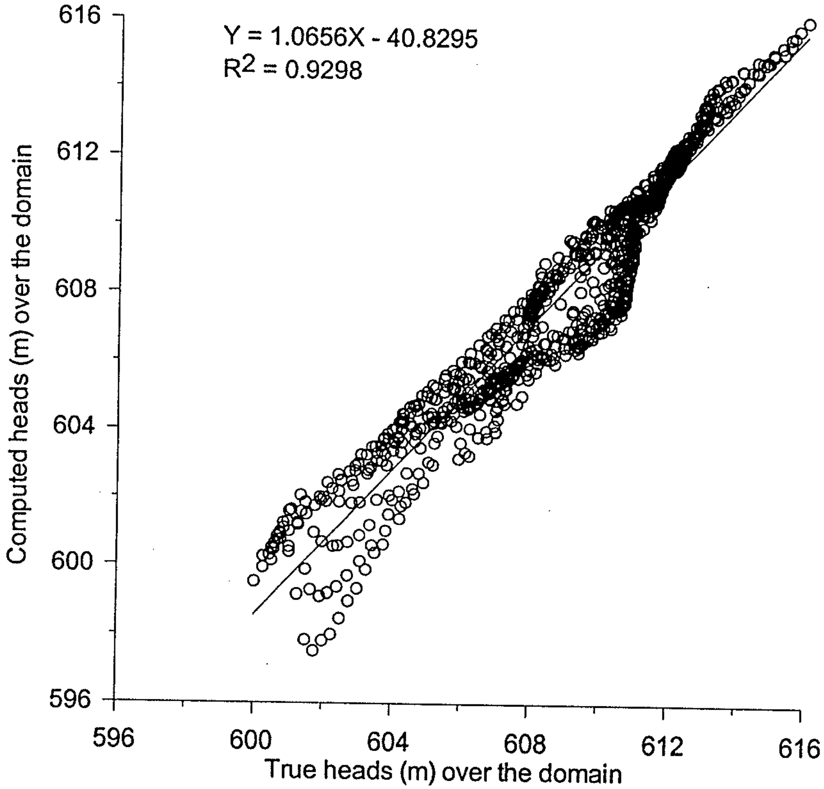

Figure 3-49 True heads versus computed heads based on updated ln (T) from 50 points of ln (T) (verification)

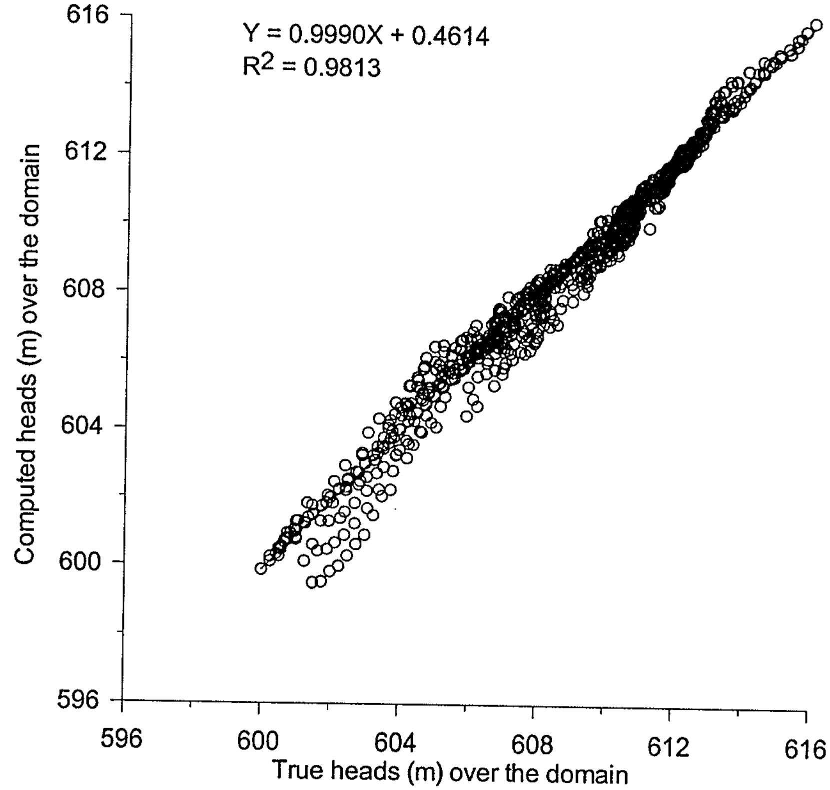

Figure 3-50 True heads versus computed heads based on updated ln (T) from 50 points of ln (T) and heads (verification)

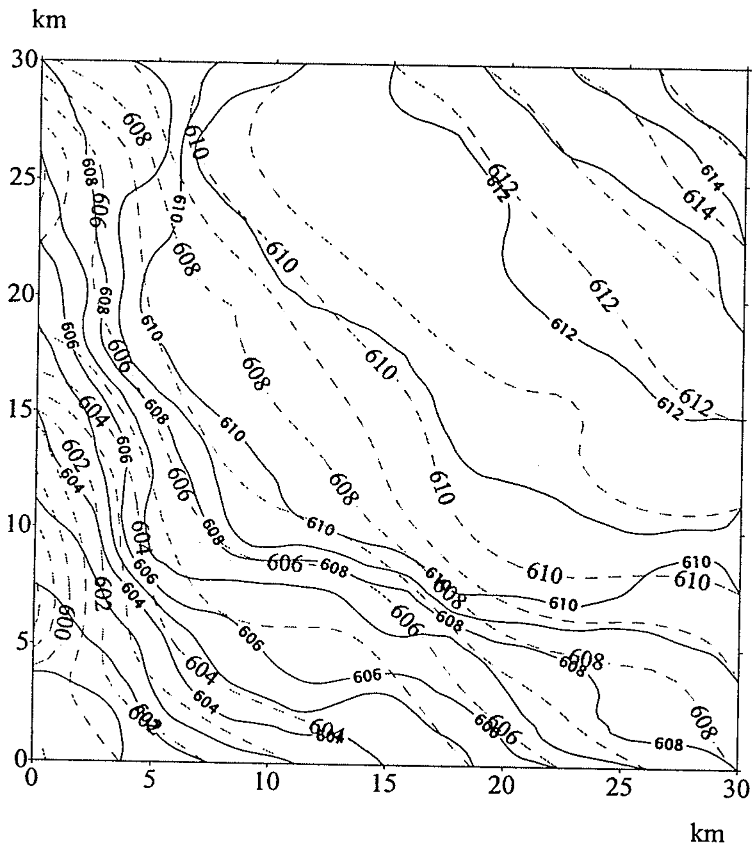

Figure 3-51 True head field (solid) versus computed head field (dash) based on updated ln (T) from 50 points of ln (T)

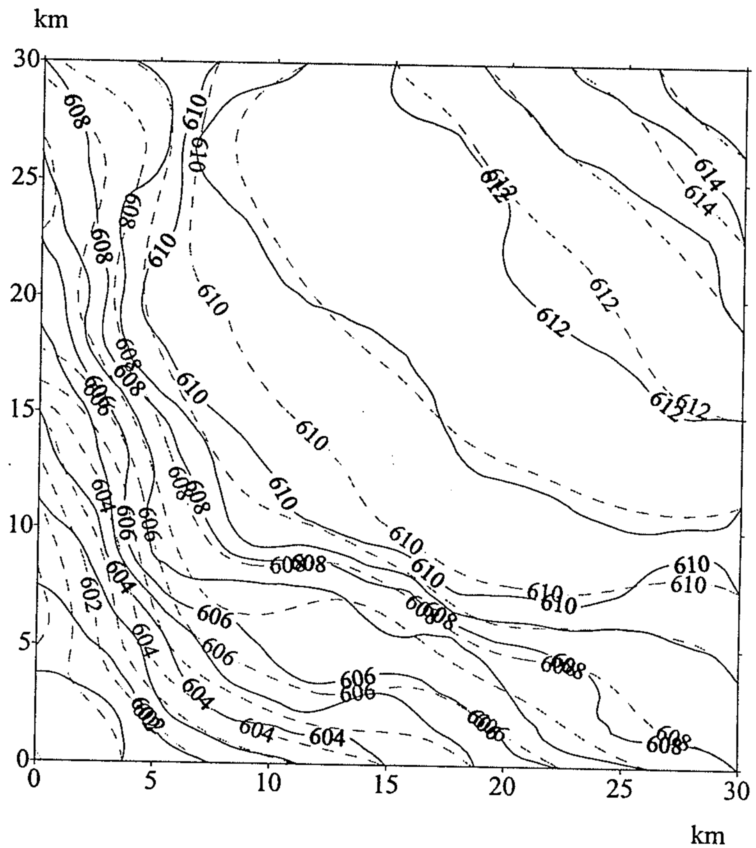

Figure 3-52 True head field (solid) versus computed head field (dash) based on updated ln (T) from 50 points of ln (T) and heads

Chapter 4

Application of Bayesian Approach to the Edwards Aquifer

4.1 Background

The United States Geologic Survey (USGS) is using the MODFLOW code to build a high-resolution two-dimensional groundwater flow model (Hereinafter known as the FD model) for the Edwards aquifer. The FD model consists of 87,890 active cells and the size of each rectangular cell is 402.25 by 402.25 m (0.25 by 0.25 miles). The carbonate aquifer is highly heterogeneous and hydraulic conductivities vary by more than 6 orders of magnitude through the study area. It has been estimated that the variances in logarithm hydraulic conductivity, ln (k), range from 6.4 to 9.7 (k in ft/d) and the integral scale ranges from 1200 to 5,000 and 15,000 meters for the confined and unconfined sections respectively (Personal communication with S. Painter, 2001). A classic parameter zoning approach is inappropriate for site characterization due to high heterogeneity and the large number of discretized cells involved in the MODFLOW grid. An upscaling/co-kriging procedure was instead utilized for this situation. The result of this upscaling/co-kriging procedure was then combined with maps of aquifer top and bottom to set the prior ln (T).

The finite difference (FD) MODFLOW model is to be calibrated against the steady state flow field corresponding to the years 1939 and 1946. More than one hundred hydraulic head measurements are to be honored. However, the MODFLOW model cannot reproduce the observed head measurements within specified error ranges based on the prior ln (T) field and it is impractical to calibrate the high-resolution FD model through a trial and error procedure. The new Bayesian algorithm discussed in Chapters 2 and 3 is employed to perform automatic calibration.

The prior conditional-expected ln (k) and covariance function together with the FD model data sets of boundary conditions and sinks or sources are provided by CNWRA. Boundary conditions and sinks or sources are assumed known for this work. Hydraulic head measurements taken over the flow domain are used to map the ln (T) field through Bayesian inversion. The inversion will produce a posterior ln (T) field of the Edwards aquifer conditioned on the hydraulic head and ln (k) measurements and upscaling, which will act as input to the USGS MODFLOW model. It is expected that the final model will reproduce the observed hydraulic heads within preconceived measurement and model errors and then the calibration task will automatically be accomplished.

4.2 The Edwards Aquifer

The Edwards aquifer extends about 290 km (180 miles) from a groundwater divide near Brackettville in Kninney County to another groundwater divide near Kyle in Hays County. The width of the aquifer ranges from about 6.4 km (4 miles) at the Colorado River at Austin to about 48 km (30 miles) in Median and Williamson Counties. It covers an area of about 10,360 km^2 (4,000 squares miles) (Figure 4-1). The aquifer provides water supply for about one million people.

The Edwards aquifer is a complex-faulted carbonate aquifer lying with the Balcones fault zone of south-central Texas. The aquifer consists of thin- to massive-bedded limestone and dolomite, most of which is in the form of mudstones and wackstones. Well-developed secondary porosity has formed in association with former erosional surfaces within the carbonate rocks and along inclined fractures. The aquifer is one of the most permeable and productive limestone aquifers in the United States. The aquifer is recharged mainly by stream flow losses in the outcrop area of the Edwards aquifer and is discharged by major springs located at considerable distances, as much as 240 km, from the areas of recharge and by wells (Maclay et al. 1988). During the years of 1939-1946, the flow was in steady state. The mean recharge was estimated at 6.9×10^7 ft^3/d. Pumping withdrawal was about 2.0×10^7 ft^3/d. A total quantity of 4.9×10^7 ft^3/d was discharged through the springs. The remaining flow (1.5×10^5 ft^3/d) was discharged through the rivers (Personal communication with S. Painter, 2001).

Both the Balcones fault and the 'Bad water line' on the south are assumed to be no flow boundaries and the springs and pumping wells are treated as sinks. The discharging rivers on the east are specified as prescribed head boundaries. The fluctuations of hydraulic heads are small compared to the vertical extension of the aquifer so that transmissivities for both of the unconfined and confined zones can be defined. The aquifer is then simplified as a two-dimensional, steady state, heterogeneous and isotropic system. The governing equation and boundary conditions for the groundwater flow takes the form of equations (3-1) to (3-3).

4.3 Computational Considerations

4.3.1 From FD Model to FE Model

It should be noted that the Bayesian algorithm is based on the finite element method and the finite difference version is not available so far. A finite element model compatible to the finite difference model has to be built for the calibration. The FE mesh is elaborately designed so that each FE node is located at the center of an active FD cell. This mesh is optimally renumbered so that the half-band width of the global stiffness matrix is limited to as small as 196. The total node number of this FE mesh, which is equal to the number of active cells in the FD grid, is 87,890. This compatible relation between the FD model and FE model allow the data of the FD model to be projected into the FE model.

4.3.2 Boundary Conditions

The boundary conditions and sinks or sources, which are assumed known in this work, are directly transferred or modified from the FD model. The springs are specified as constant head boundaries in the first phase simulation and then sinks in the second phase simulation. The pumping wells are simply considered as sinks. The rivers are viewed as specified head boundaries, which are slightly different from the drainage conditions dealt in the FD model. This modification will not influence the modeling results because the net river discharge accounts for a small portion of the total discharge. The cell-centered recharges are treated as inflow flux added at the related nodes.

4.3.3 Prior ln (k) and ln (T)

An Upscaling/co-kriging procedure was utilized to map the prior ln (T) field (Jiang et al., 2001). More than 1,000 hydraulic conductivities derived from well tests were upscaled to a 400.25 by 400.25 meters grid block scale and interpolated. Stochastic simulation (sequential indicator simulation) combined with numerical upscaling was used to determine the upscaled geostatistical model. Co-kriging was then used to interpolate the upscaled conductivities while honoring the well test measurements. This work was performed at CNWRA. The result of this upscaling/co-kriging procedure was then combined with maps of aquifer top and bottom to set the prior ln (T). With the thickness data the prior ln (T) can be computed as (Personal communication with S. Painter, 2001),

$$F_i = \ln(T)_i = \ln(k)_i + 0.5\sigma_i^2 + \ln(B_i) \tag{4-1}$$

Here F_i is the prior ln (T), i represents the i'th node, $\ln(k)_i$ and σ_i^2 are the upscaled logarithm hydraulic conductivity [denoted as ln (k)] and variance of ln (k), respectively and B_i is the aquifer thickness in feet.

A nested exponential correlation structure with integral scale between 1,200 and 5,000 meters and a 50% relative nugget effect was determined (for the confined portion, personal communication with S. Painter, 2001). The correlation function of prior ln (k) is written as,

$$C_p(k,l) = 0.25\sigma_k\sigma_l\left[\exp\left(-\frac{d}{1200}\right) + \exp\left(-\frac{d}{5000}\right)\right] + 0.5\delta(k,l)\sigma_k\sigma_l \qquad (4\text{-}2)$$

where σ is the standard deviation of ln (T), k and l refer to any two points in question, $d = \sqrt{(x_k - x_l)^2 + (y_k - y_l)^2}$ in meters and δ is the Kronecker number. $\delta = 1$, if k=l.

Note that covariance of ln (T) takes the same form of ln (k). This covariance function will be used as the prior covariance in the Bayesian algorithm. Equations (4-1) and (4-2) are used to estimate the prior model expectation and covariance.

The prior covariance matrix $\mathbf{C}_p$ has a dimension of 87,890 by 87,890. To save computer memory the covariance function for matrix operation is utilized instead of formally declaring this large matrix.

4.4 Simulations and Result Analysis

4.4.1 Simulation I

First a simulation with 108 head measurements is performed. Eight of the head measurements, which are located in the unconfined zone and have a different covariance function from that in the confined zone, are removed from the inversion. These points are presented on the head fit plot for verification (see Figure 4-5 and Figure 4-7). In this work the noise is fixed at two meters, which is determined from runs involving the fictitious aquifer. The boundary conditions for this simulation are slightly different from those detailed in next sections. Both the springs and the rivers on the east end of the aquifer are considered as first type boundaries. All pumping rates, which add up to 1.67×10^7 ft^3/d, are added at a single node. The recharge, totaling 7.55×10^7 ft^3/d, is assigned as sources distributed over the unconfined zone. Please note that these data provided by CNWRA are slightly different from those in simulation II, which will be detailed in next section. The Bayesian algorithm discussed in Chapter 2 and Chapter 3 is coded in Fortran 90 and termed BayesFe.f90. The code is parallelized and compiled using Visual Kap for OpenMp 3.9, and run on a Pentium III workstation with two 1.0 GHZ processors.

Comparison of the prior ln (T) field (Figure 4-2) and posterior ln (T) field (Figure 4-3) indicates the posterior ln (T) captures many major hydraulic properties that the prior field fails to. The high permeable streak from Uvalde to San Antonio and the low permeable barrier in the Knippa Gap are exactly mapped out. These are consistent with a qualitative inspection of the heads. One can see the fit between measured and computed heads based on the posterior ln (T) field (Figure 4-5) improves over that based on the prior ln (T) field (Figure 4-4). The RMS of calculated heads with the prior ln (T) field and measured heads is 123.3 feet, which accounts for 16% of the maximum head difference (1165-393=772) across the domain. The RMS of calculated heads with the posterior ln (T) and measured heads is 46 feet, which is only 4.75% of the maximum head difference (1379-400=978.5) across the domain. For verification an independent data set of head measurements, which is not used in this inversion and is used later, are plotted against the computed heads from the prior ln (T) field and posterior ln (T) field on Figure 4-6 and Figure 4-7 respectively. Figure 4-7 demonstrates that the calculated heads with the posterior ln (T) field not only match the measured heads used in the inversion but also those are not used in the inversion. These results verify that the FD model is successfully calibrated through the Bayesian inversion. The only problem is that the forward simulation with the posterior ln (T) field cannot reproduce the spring flow rate at each spring within an acceptable error limit. However, the total flow rates from all the springs are produced correctly.

4.4.2 Simulation II

An alternative data set of 158 head measurements together with new sinks/sources is analyzed. Most locations of the 158 measurements are different from those of the previous 108 measurements. The recharge rates and pumping rates were also modified with the FD model. The data on the Barton Springs, which are not available in simulation I, is available. It is noticed that the active cells in the new FD model are slightly different from those in the previous simulation. This modification leads to some of the FE nodes located at previously inactive FD cells and some active cells are not covered by the FE grid. The FE model yields less recharge than the new FD model because the FE grid misses some recharge cells. As it is infeasible to re-estimate a new prior ln (T) field and rebuild a FE grid following the new FD grid, to maintain mass balance the recharge rates overlaid by the FD grid and FE grid have to be scaled by a factor of 1.028. The mass balance is described in section 3. The previous prior ln (T) field and the FD gird are still valid from such treatment. The values of posterior ln (T) at those cells that are not covered by the FE grid will be evaluated using the nearest-neighboring approach.

In this simulation there are 1,098 wells and 6 springs, which are treated as sinks. Five head measurements, which are located in the unconfined zone, are removed. Given 153 head measurements plus 6 estimated heads at the springs, 87,731 unknown ln (T) values are to be determined from the inversion. The noise level is fixed at two meters. To check the how well the computed heads match the new data, both symmetrical (known as S) and unsymmetrical (known as U) forward problems with the prior ln (T) field and sinks at the springs are solved. Solution S and solution U refer to solutions of (3-1) and (3-4) respectively. It is found that solution U is systematically different than solution S except at the first type boundary nodes. It is anticipated that the approximation of transmissivity averaging over each element will result in some deviation between the two solutions, but not as high as hundreds feet. Adjusting the prior ln (T) around the downstream areas into more smooth values can largely reduce the deviation. Also the deviation can decline to a level derived from the transmissivity approximation if the springs are specified as constant heads. The prior ln (T) field is adjusted so that a smaller deviation between solution S and solution U can be achieved. The posterior ln (T) field (Figure 4-8) shows consistent results with qualitative analysis, but includes some extreme values. The grid Pelect number, which is defined as (4-3), is calculated to detect the problem.

$$Pe_x = \frac{\partial Y}{\partial x} \Delta x \tag{4-3}$$

where Pe_x is the Pelect number in x axis direction, and Δx is the spatial size of the grid in the x axis direction. Pe_y can be evaluated in the similar form of Pe_x.

The Peclet numbers of most elements are less than 2 and a few range from 3 to 5. These values indicate that numerical dispersion is unlikely to cause the large deviation between solution S and solution U as observed above and the inversion involves some undetected error. An alternative explanation is given below.

4.4.3 Model Error Investigation

An example is set up to investigate why introducing large sinks into the FE system leads to differences between solution S and solution U. The test system is a 3,000 by 3,000 m rectangular confined aquifer. The west and east ends of the aquifer are assigned as constant heads at 600 and 590 m respectively. At the middle of the north end exists a sink stress at a flow rate as high as 300,000 m^3/d. The rest sections of the boundary are impermeable. The aquifer is discretized into two grids. Grid one and grid two have spatial steps ($\Delta x = \Delta y$) at 200 and 100 meters respectively. The role the spatial step size plays in the mismatch can be assessed by using different spatial step grids. Ln (T) varies as a sin function across the domain, namely

$$Y_i = 7 + A\sin(\frac{x_i}{200}) \tag{4-4}$$

where Y_i is the ln (T) value at node i, A is the amplitude and x_i is the x coordinate at node i.

A typical ln (T) generation from this function can be illustrated on Figure 4-9. Note that using grid one and grid two generates the same distribution of ln (T). The amplitude, A, represents the variation magnitude of ln (T). Greater A values corresponds to greater variation. Using a different A, the same problem with different grid size is solved and the RMS between solution U and solution S against A is plotted on Figure 4-10. Next, replacing the sink with constant head, which is set at the value from solution S based on A=0.5, the forward problem with different grid size is solved again. The results are also plotted on Figure 4-10. For a homogeneous case (A=0) and a linear ln (T) distribution solution S and solution U are equivalent (RMS=0) regardless of what spatial step is applied. Figure 4-10 indicates that for a coarse grid the difference between solution S and solution U increases as the variation of ln (T) grows. This trend becomes more serious for the sink condition. As showed in Figure 4-10 for a fine grid RMS also increase as the amplitude rises, but the RMS values are within a much lower range compared to those of the coarse grid. There is no obvious difference between the RMS trends for constant head or sink condition is applied at the north discharging point. The RMS for the fine grid case is mostly derived from the approximation of ln (T) within each element and such trend and magnitude of RMS are reasonable. For the simulations performed the maximum RMS values of the coarse and fine grids account for 10.4% and 1.9% of maximum head difference across the domain respectively. The RMS values for the fine grid case can be considered (no strictly) as a deviation due to the approximation of ln (T) within each element. Subtracting these values from the RMS values for the coarse grid case, the remaining, which is still very large for high A, is resulted from a coarse spatial step size. In other words if the deviation due to the approximation of ln (T) over each element is negligible, solution U is also largely different than solution S for the configuration of coarse grid size, high variation of ln (T) and extremely high point stress. This error is introduced by FE approximation to the first order derivative terms in the unsymmetrical equations [See (3-7)-(3-8)]. It is noted that FE formulation for gradient is discontinuous and has first order accuracy (Huyakorn and Pinder, 1983). The configuration of coarse grid size, extremely high variation of ln (T) and extremely large point stress leads to poorer FE approximation to gradient evaluation. Smoothing ln (T) or refining FE grid may improve the accuracy of the approximation. A rough measurement to the accuracy is the RMS of solution S against solution U. A smaller RMS suggests a better approximation.

4.4.4 Simulation III

Given the original grid size of the FD model, the boundary conditions of simulation II and the upscaled prior ln (T) field the mean deviation between solution S and solution U is as high as 560 ft. The FE grid has to be refined or the prior ln (T) field has to be reset into a more smooth form if an accurate inversion is expected. It is noted that the prior ln (T) values around the Comal and San Marcos springs deviate from the real values so much that two large drawdown cones are established in the forward model. This fact suggests that there are reasons to systematically adjust the prior ln (T) in these regions, so that numerical error can be reduced to a minimum level in the inversion. The prior ln (T) field is modified so that solution U approximates solution S closely. This is fulfilled through adjusting the prior mean ln (T) around the spring zones. The modified prior ln (T) in the inversion is presented on Figure 4-11. Figure 4-14 shows the fit between measured heads and the calculated heads from this modified prior ln (T) field. Taking the estimated heads at the springs as data in the inversion is inappropriate. In the following simulation the calculated heads at the springs are not treated as known data. Therefore 153 head measurements are used and 87,737 ln (T) values are to be determined from the inversion.

The posterior ln (T) field is showed on Figure 4-12. Extremely low ln (T) zones on the west of Real and east of Hays are mapped out. Such low values are inconsistent with a qualitative analysis of the head measurements. This may be caused by the incompatibility of the observed data and covariance function or the coarse grid. Therefore the posterior ln (T) values in the two zones are recovered to the prior level. The measured heads are plotted against calculated heads from this posterior ln (T) field (Figure 4-13). From

Figure 4-14 and Figure 4-15 one can see that the fit based on the posterior ln (T) improves compared to that from the prior field. Major mismatches occur on the areas where prior ln (T) values are used. The deviations across the middle section (heads ranging from 550 to 1,000 feet) result from inversion errors, which are derived from coarse grid, high variation of ln (T) and extremely large stresses at the springs. The RMS of calculated heads with the prior ln (T) field and measured heads is 129.7 feet, which accounts for 12% of the maximum head difference (1284-226) across the domain. The RMS of calculated heads with the posterior ln (T) and measured heads is 62.9 feet, which account for 8% of the maximum head difference (1150-385) across the domain.

4.5 Summary and Discussion

The new Bayesian updating procedure is used to calibrate a high-resolution finite difference model of the Edwards aquifer. Utilizing cell-to-node discretion scheme a finite element model of the Edwards aquifer, which is compatible to the model, is successfully developed. The input data of the finite different model can be readily transferred into the finite element model and allow the finite-element-based Bayesian algorithm to be employed to calibrate the finite difference model. Two independent data sets are used in the inversion. First, 100 hydraulic head measurements are used to update the upscaled ln (T) field. The posterior ln (T) field is showed to capture some hydraulic properties that the prior field misses. The conditional-expected heads with the posterior ln (T) field match the observed heads very well. The problem that the forward simulation with the posterior ln (T) field cannot reproduce the spring flow rate at each spring within an acceptable error limit is totally derived from boundary assignments. Although simulation I encounters the same grid and magnitude of ln (T) variation as simulation II does, no node or element experiences as large as the spring flow rates as Comal springs and San Marcos springs in simulation I. This guarantees an accurate inversion, which generates an excellent fit between measured heads and calculated heads. This suggests that the Bayesian algorithm for two-dimensional steady state groundwater flow inverse problem can be applied to the estimation of transmissivity of extremely high heterogeneous aquifer with complicated boundary configuration.

Inverse simulations with an independent data set of 153 head measurements are performed. The springs are viewed as sinks with measured flow rates. The prior ln (T) values around the spring areas are adjusted that numerical error is reduced to a minimum level. Comparing the inverse results from simulation I and simulation III shows that the posterior ln (T) fields capture similar spatial distribution, though independent data sets are utilized. The differences between the two fields derive from different boundary configurations assigned in the inversions and data errors. This implies that the inverse algorithm is robust and the results are reliable. The posterior ln (T) yielded good fit between measured heads and calculated heads. Larger error derived from extremely high point stimulus attributes to the cause that fit from simulation III is not as good as that of simulation I. Refining the grid around the huge point stress areas may improve the inverse results. The spring flow rates are exactly reproduced because the springs acted as sinks in the forward modeling.

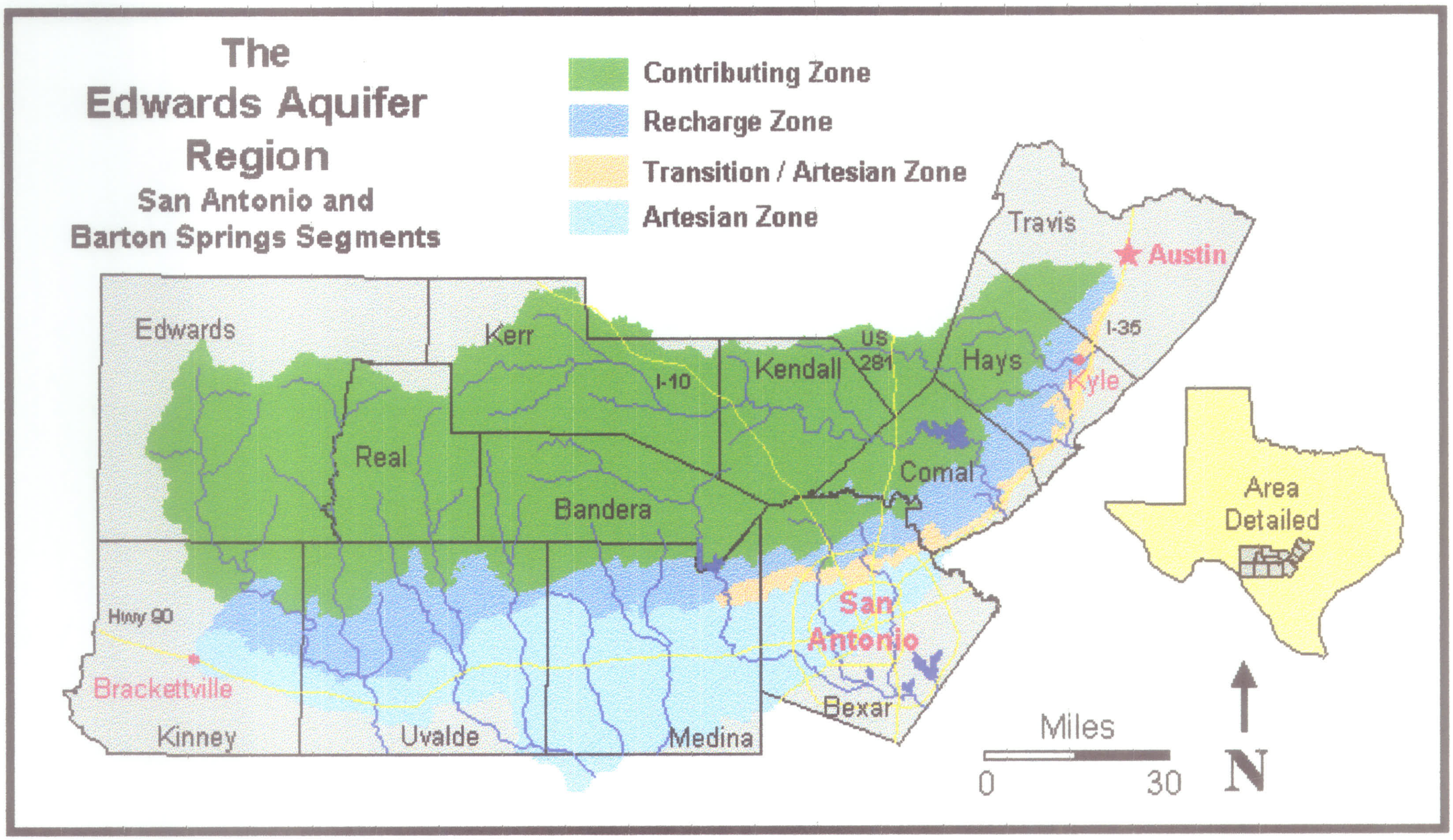

Figure 4-1 The Edwards Aquifer Region (Eckhardt, G.A., 1995~2002)

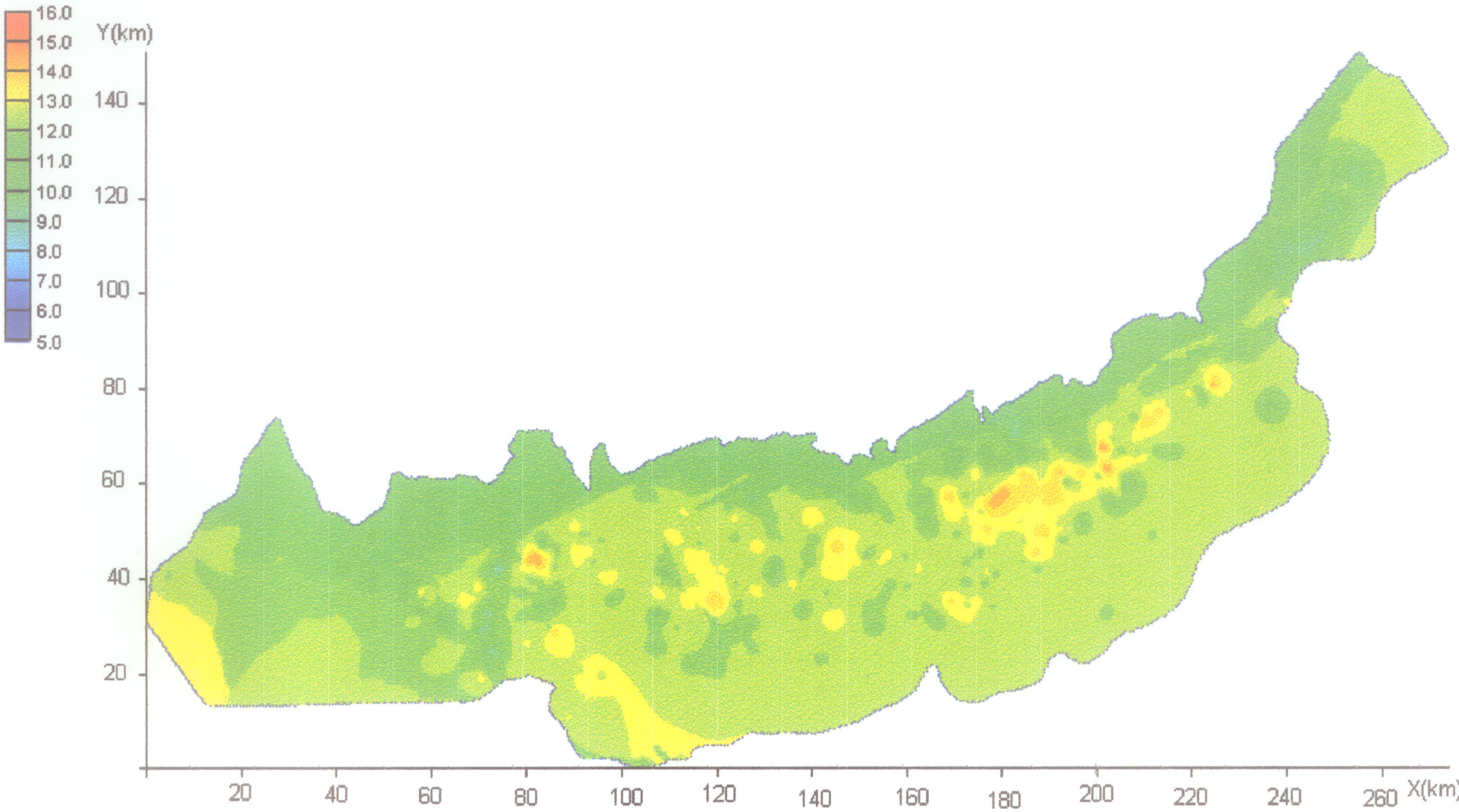

Figure 4-2 Prior ln (T) field of Edwards Aquifer determined by upscaling and co-kriging data from >1000 well tests

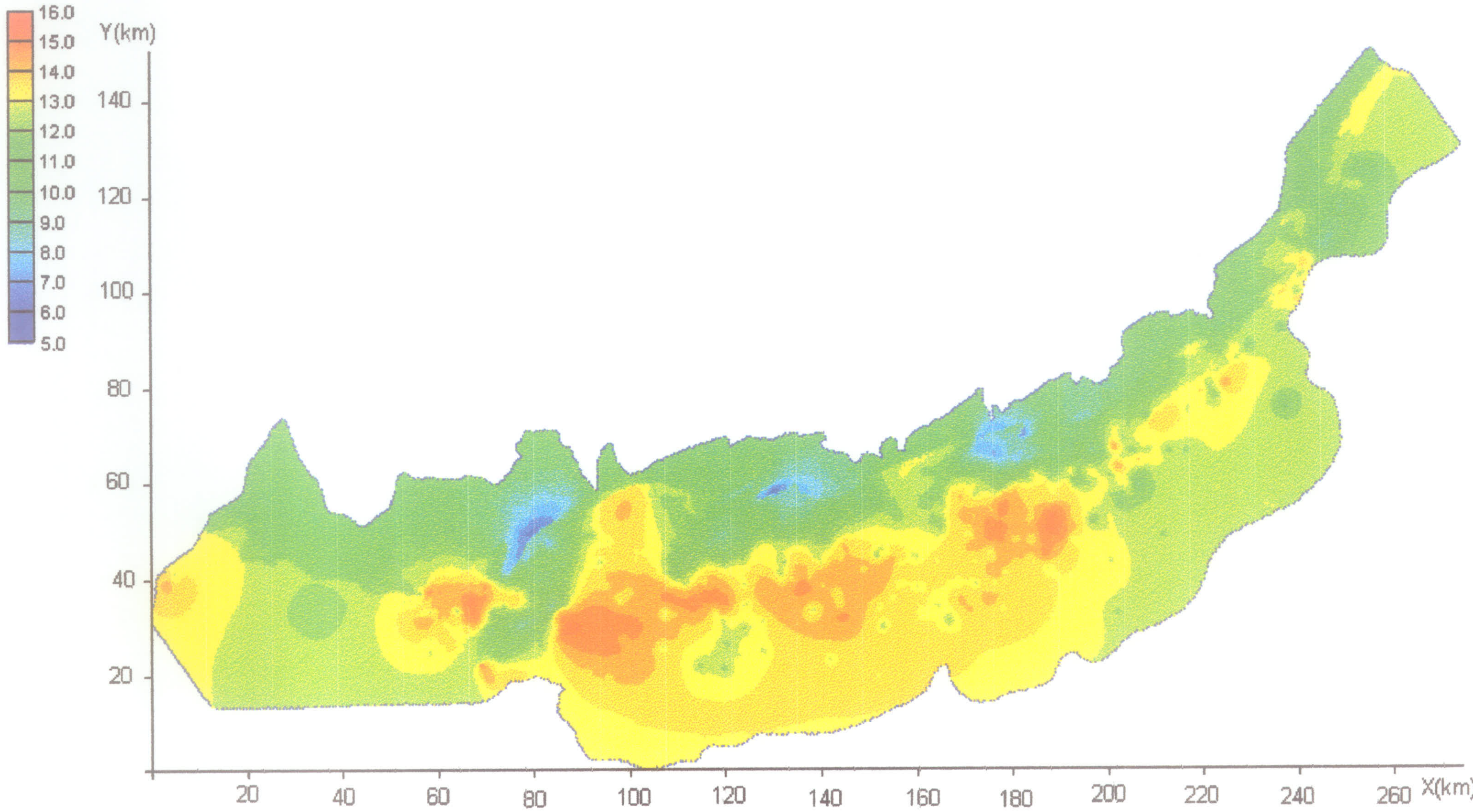

Figure 4-3 Bayesian updated ln (T) field of Edwards Aquifer determined from head measurements (note vastly undetermined problem with 100 data points and 87790 unknowns)

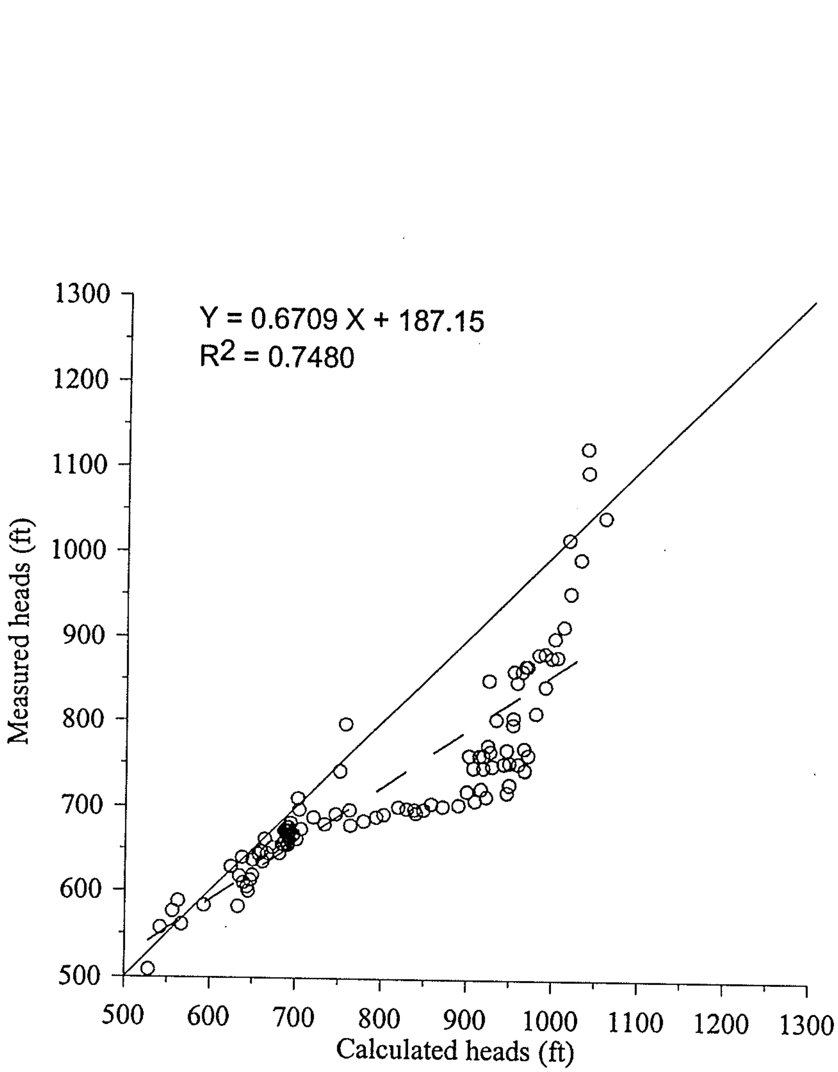

Figure 4-4 Measured heads (100 points) versus calculated heads with prior ln (T)

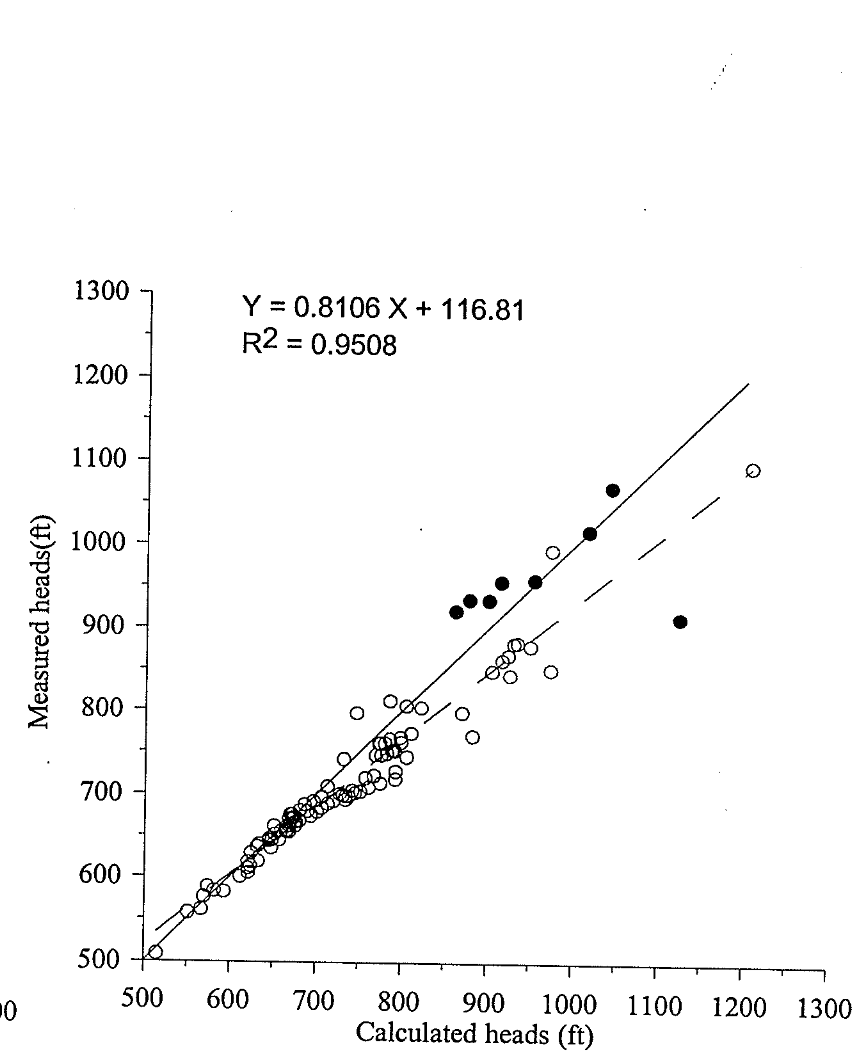

Figure 4-5 Measured heads versus calculated heads based on posterior ln (T) (The dot points are not used in the inversion)

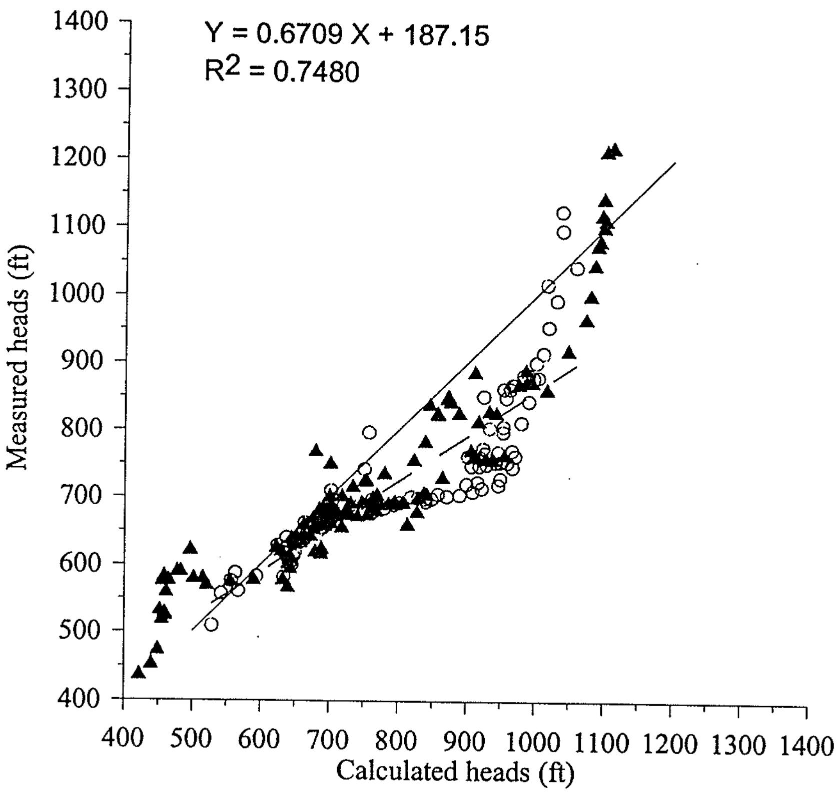

Figure 4-6 Measured heads (the triangle points are independent data) versus calculated heads with prior ln (T)

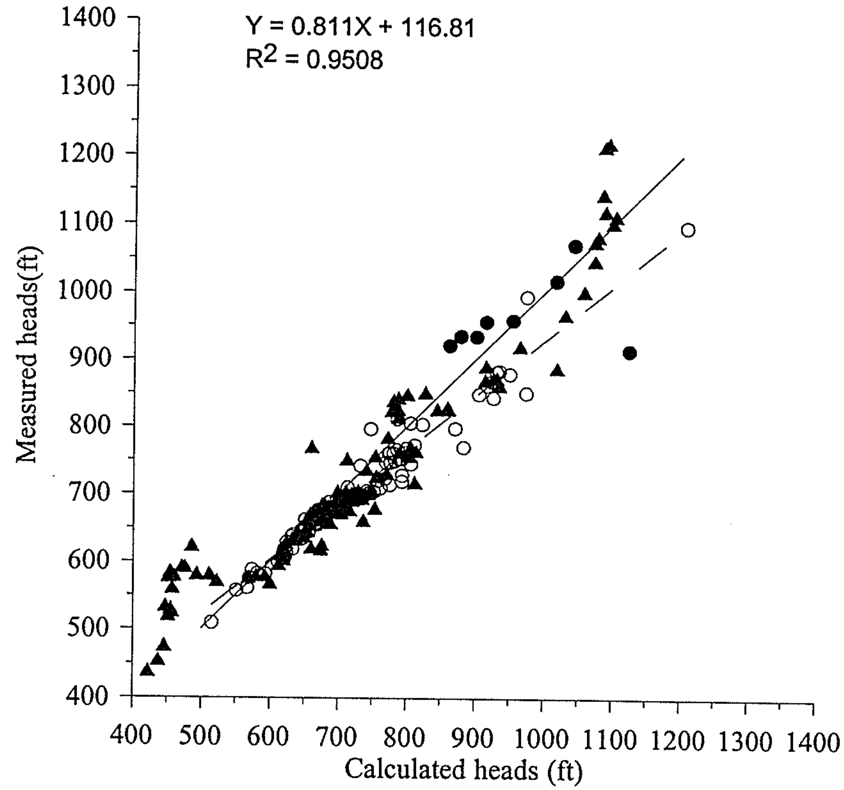

Figure 4-7 Measured heads (the triangle points are independent data, which are not used in this inversion) versus calculated heads based on posterior ln (T)

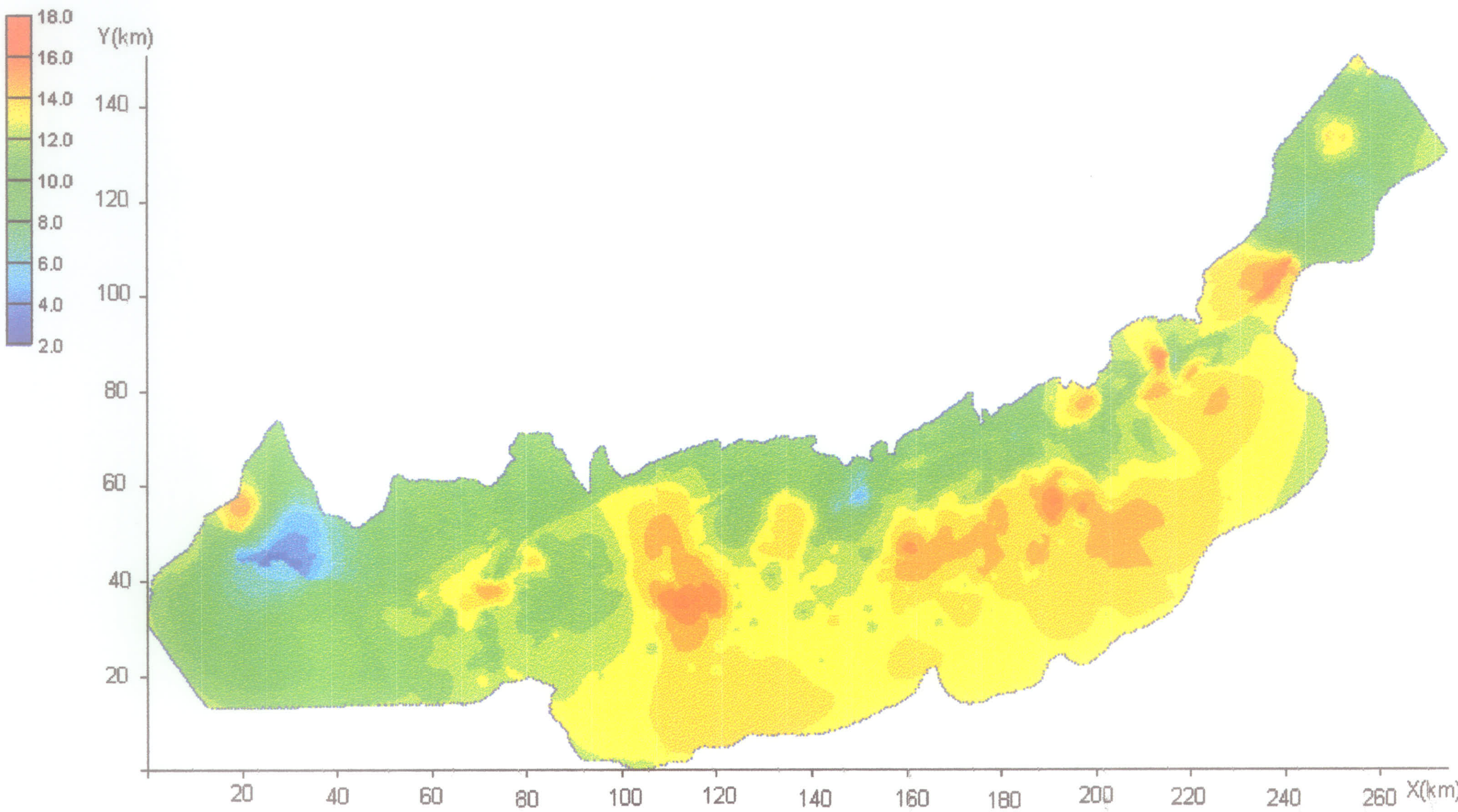

Figure 4-8 Bayesian updated (posterior mean) ln (T) field of Edwards Aquifer determined from head measurements (153 points)

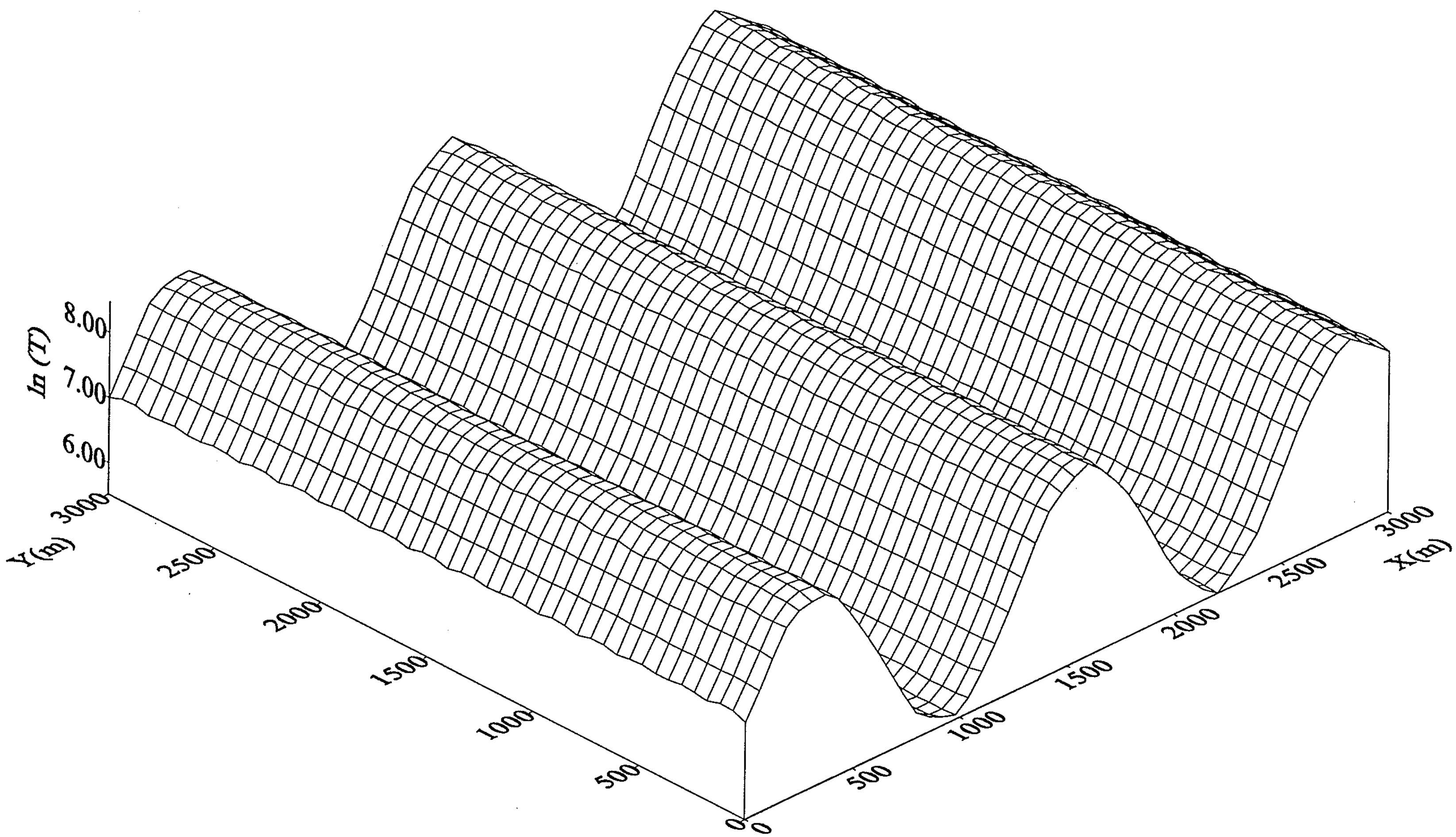

Figure 4-9 Typical generation of ln (T) field from sin function (A=1.5)

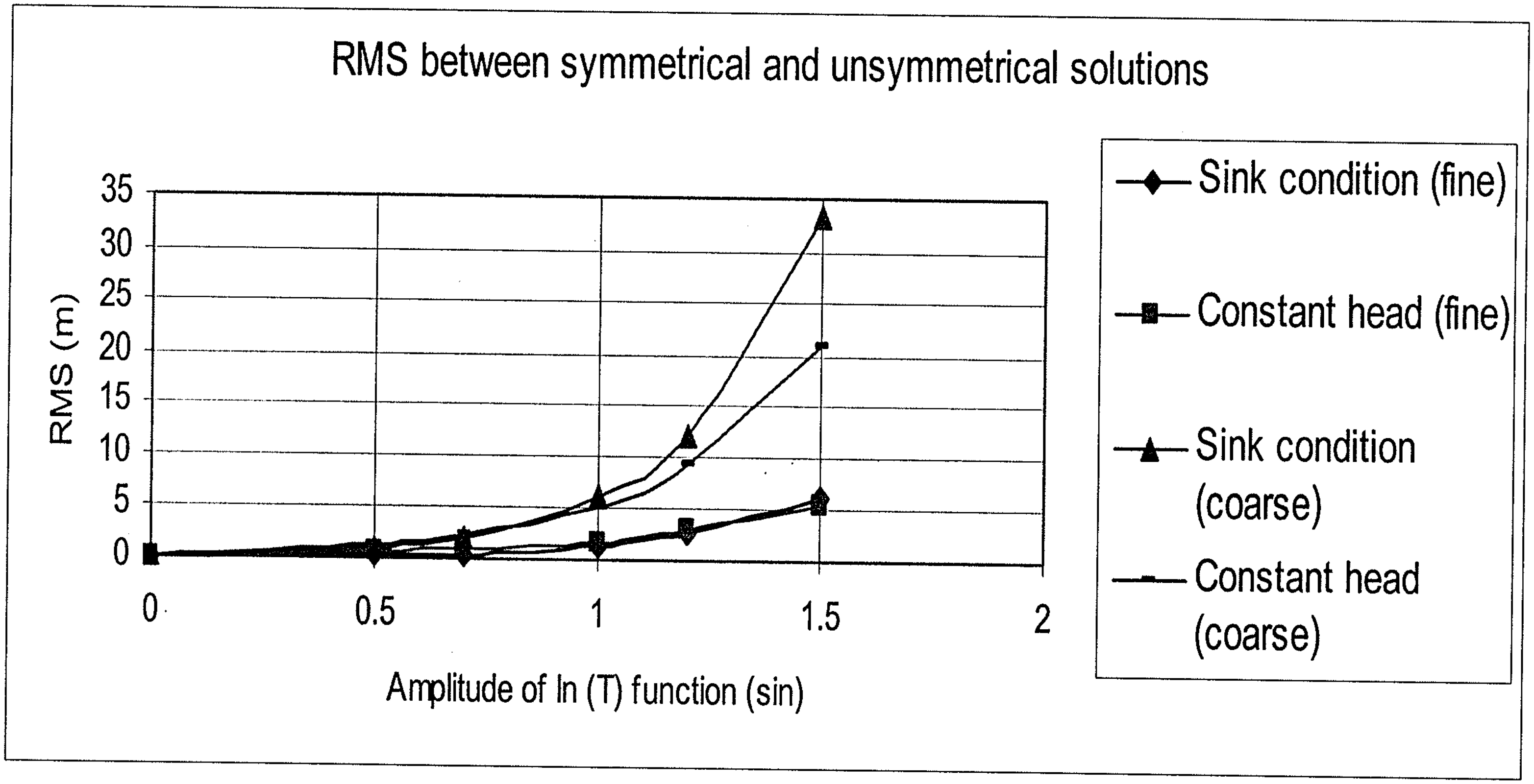

Figure 4-10 A comparison between symmetrical and unsymmetrical solutions with different FE grid sizes

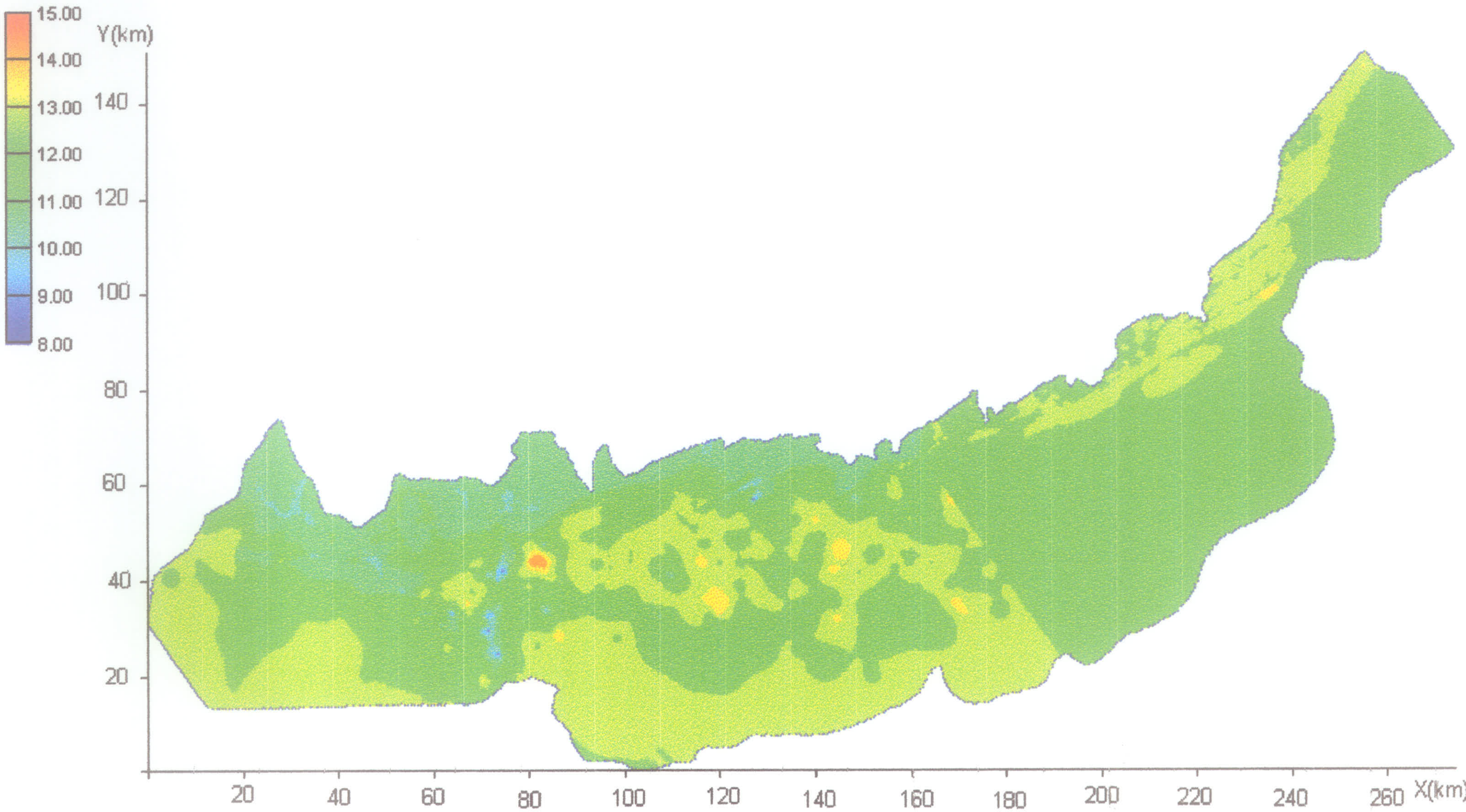

Figure 4-11 Modified prior ln (T) field of Edwards Aquifer determined by upscaling and co-kriging data from >1000 well tests

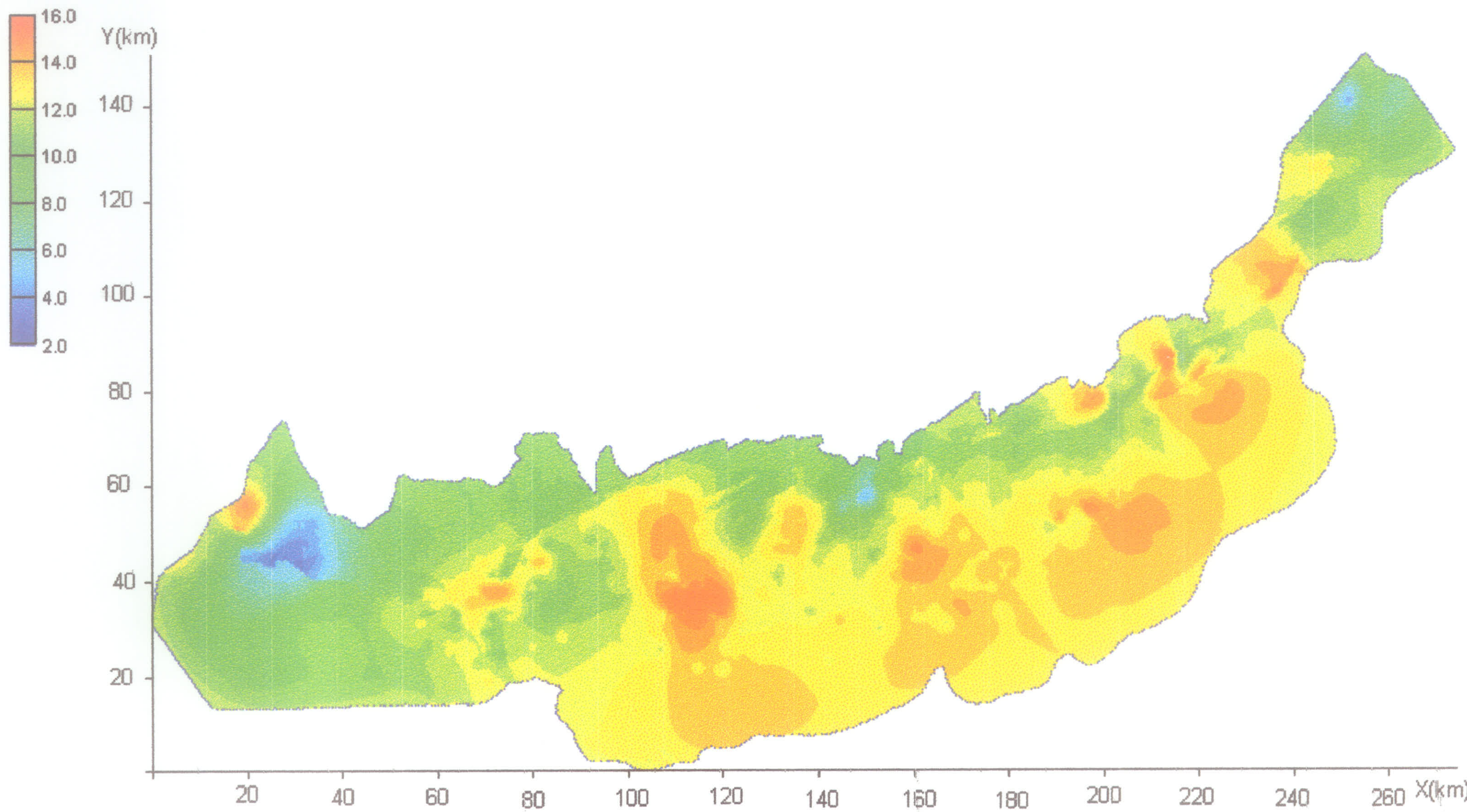

Figure 4-12 Bayesian updated ln (T) field of Edwards Aquifer determined from 153 head measurements (based on modified prior ln (T) field)

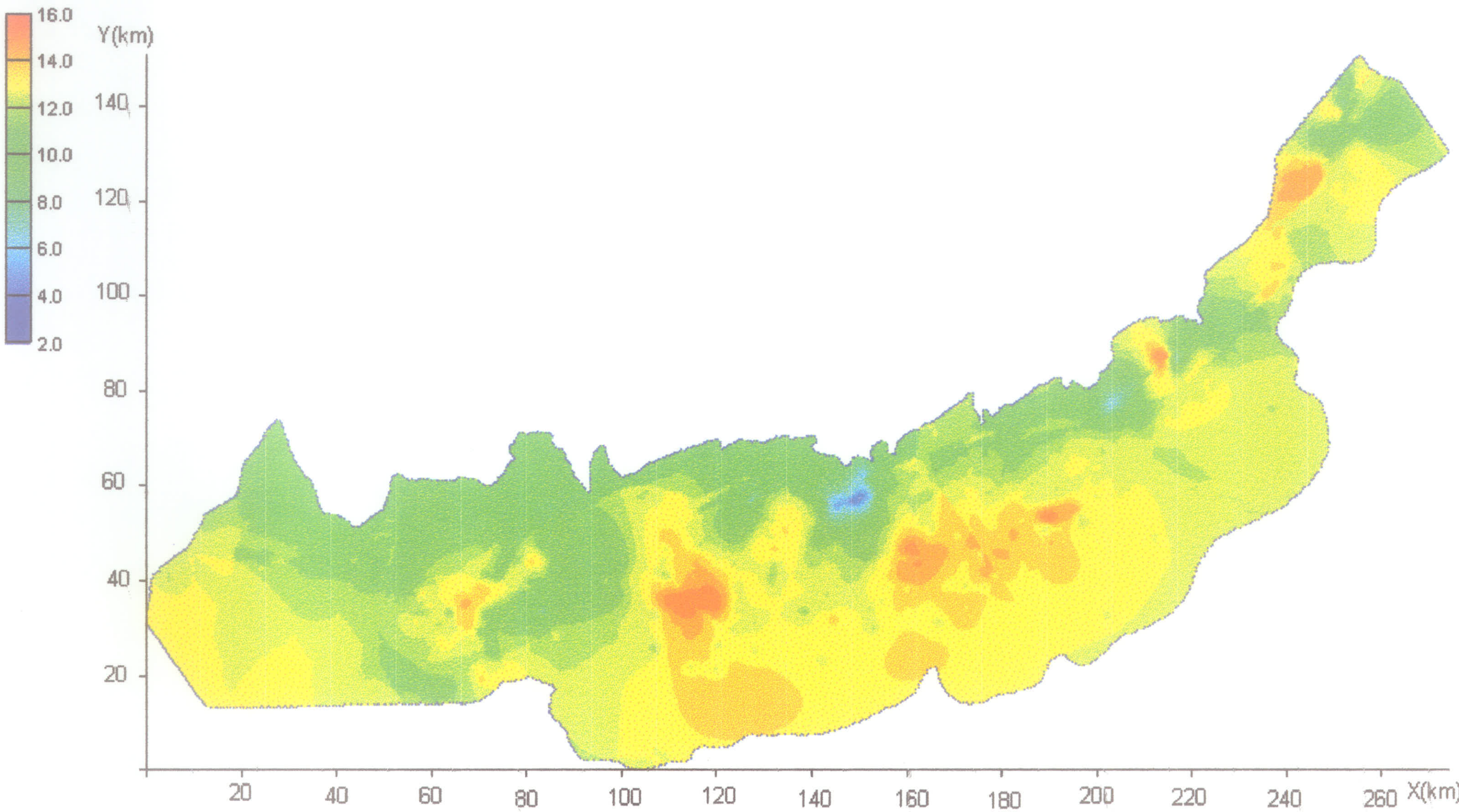

Figure 4-13 Bayesian updated ln (T) field of Edwards Aquifer determined from 153 head measurements [note extremely low ln (T) values at the far west and east (see Figure 4-12) are replaced with prior values]

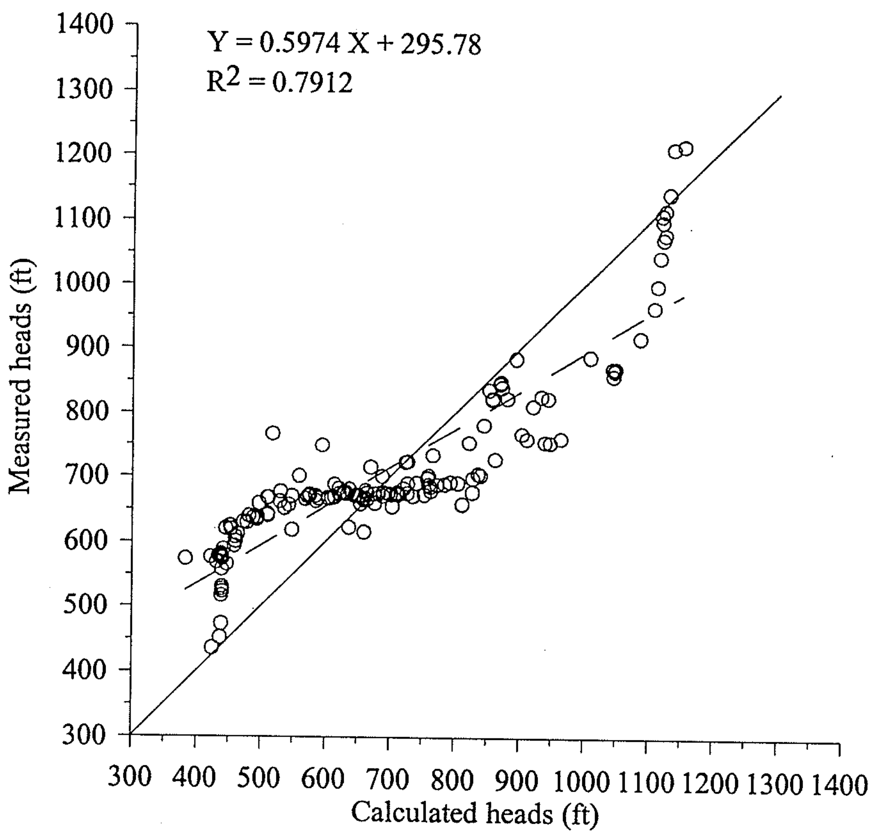

Figure 4-14 Measured heads (153 points) versus calculated heads with modified prior ln (T)

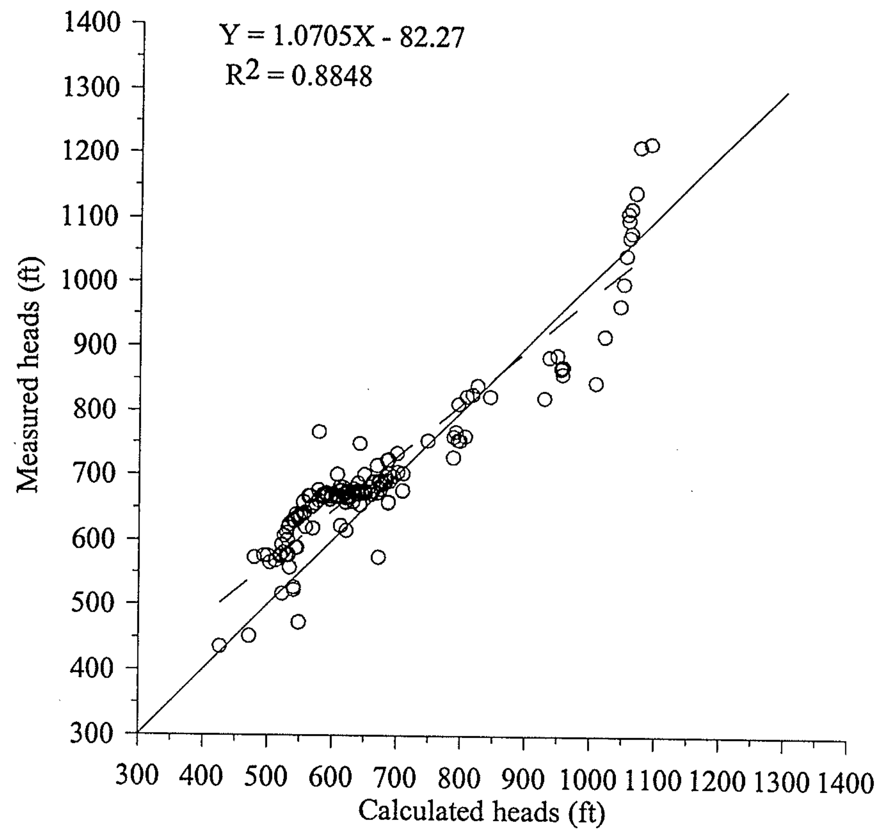

Figure 4-15 Measured heads (153 points) versus calculated heads based on posterior ln (T)

Chapter 5

A Full-Bayesian Approach to the Groundwater Inverse Problem for Steady State Heat Transport

The groundwater inverse problem is ill-posed, and this may be characterized by instability and non-uniqueness. The instability and nonuniqueness of solutions to the inverse problems can only be eliminated through introducing additional measurements and information (Carrera and Neuman, 1986). The challenge is to find inexpensive and reliable sources of information. The conjunctive use of temperature and hydrogeological data for site characterization has the potential to reduce these concerns. In this study the full-Bayesian approach is extended to the groundwater inverse problem for steady state groundwater heat transport. Using such approach appears beneficial for several reasons. First, addition of temperature data may further constraint the inverse problem and reduce the concern of non-uniqueness. Additionally, prior information is allowed and the uncertainty of the statistical properties associated with the first two moments in the probability density function (pdf) of the model can be removed through marginalization. A particularly appealing aspect of temperature inversion is the acquisition of temperature data is inexpensive and temperature measurements may be more accurate than hydraulic head data due to undetected improper piezometer instrumentation. In this chapter an algorithm of full-Bayesian approach to the groundwater inverse problem for steady state groundwater heat transport is developed and will be examined against a fictitious aquifer with Dirichlet conditions in terms of flow and heat transport.

5.1 Updating ln (T) Field by Steady State Groundwater Flow

The groundwater flow system discussed here is similar to that in Chapter 3 and only sources/sinks and Neumann conditions are excluded. The governing equation can be written as:

$$\frac{\partial}{\partial x}\left(T\frac{\partial \Phi}{\partial x}\right)+\frac{\partial}{\partial y}\left(T\frac{\partial \Phi}{\partial y}\right)=0 \tag{5-1}$$

where T is the transmissivity, Φ is the hydraulic head, x and y are Cartesian coordinates.

Applying the perturbation technique to (5-1) yields the following equations,

$$\frac{\partial^2 H}{\partial x^2}+\frac{\partial^2 H}{\partial y^2}+\frac{\partial F}{\partial x}\frac{\partial H}{\partial x}+\frac{\partial F}{\partial y}\frac{\partial H}{\partial y}=0 \tag{5-2}$$

$$\frac{\partial^2 h}{\partial^2 x}+\frac{\partial^2 h}{\partial^2 y}+\frac{\partial F}{\partial x}\frac{\partial h}{\partial x}+\frac{\partial F}{\partial y}\frac{\partial h}{\partial y}=-\frac{\partial f}{\partial x}\frac{\partial H}{\partial x}-\frac{\partial f}{\partial y}\frac{\partial H}{\partial y} \tag{5-3}$$

The notations in the equations are the same as those in (3-4) and (3-5).

(5-2) is of standard advection-dispersion equation, which can be solved by FEM. With the conditional-expected hydraulic heads and prior ln (T) known, applying FEM to (5-3) leads to,

$$\mathbf{Ah} = \mathbf{Bf} + \mathbf{Ch}_B \tag{5-4}$$

where **A**, **B** and **C** are constant matrices, **h** is a vector of non-boundary hydraulic head perturbations, $\mathbf{h}_B$ is a vector of boundary node head perturbations and **f** is a vector of ln (T) perturbations at the nodal points.

The boundary node perturbations are considered known and therefore are set to zero. Through some matrix operations on (5-4) following equation can be obtained,

$$\mathbf{D}\left(\mathbf{\Phi} - \mathbf{H} + \mathbf{A}^{-1}\mathbf{B}\mathbf{F}\right) = \mathbf{D}\left(\mathbf{A}^{-1}\mathbf{B}\right)\mathbf{Y} \tag{5-5}$$

(5-5) takes the form of $\mathbf{d}^* = \mathbf{Gm} + \boldsymbol{\nu}$ and can readily be employed to update the ln (T) field based on hydraulic head measurements following the Bayesian updating procedure detailed in Chapter 2.

5.2 Updating ln (T) Field by Steady State Heat Transport

A typical groundwater system redirects heat flows from the Earth's interior. Heat is transferred through the system by conduction, advection and radiation. Conductive transport occurs both in the solid medium and fluid, and is dominated by the properties of the porous medium and fluid, and the temperature gradient, while advective transfer occurs under the influence of moving groundwater. Within a system with high permeability, groundwater can redistribute heat, disturbing the conductive thermal regime. Subsurface temperature distribution and groundwater movement are interrelated and groundwater temperature can be used to infer hydraulic parameters (Woodbury and Smith, 1985).

The following assumptions will be adopted when groundwater heat transport equation is applied to the inverse problem. Both buoyancy effects, and heat dispersion due to groundwater velocity fluctuations are negligible. For the temperatures encountered in a shallow groundwater system, thermal properties of the medium can be considered independent of temperature. Viscous dissipation of energy is neglected due to low velocity. An isothermal state is reached instantaneously between the fluid and solid. Based on these assumptions, the two-dimensional steady state groundwater advection-conduction heat transport equation can be represented as (Bear 1972),

$$\frac{\partial}{\partial x}\left(\lambda_e \frac{\partial \theta}{\partial x}\right)+\frac{\partial}{\partial y}\left(\lambda_e \frac{\partial \theta}{\partial y}\right)-\rho_f c_f\left(q_x \frac{\partial \theta}{\partial x}+q_y \frac{\partial \theta}{\partial y}\right)=0 \tag{5-6}$$

where λ_e is the effective thermal conductivity, θ is the groundwater temperature, ρ_f is the groundwater density, c_f is the specific heat of groundwater, q_x and q_y are the specific discharge. λ_e is defined as (Bear, 1972),

$$\lambda_e = \omega\lambda_f + (1-\omega)\lambda_s \tag{5-7}$$

where f and s represent fluid and solid respectively, ω is the porosity.

It is further assumed the effective thermal conductivity and thermal boundary conditions are known and the hydraulic parameter ln (T) is to be estimated. Following the procedure similar to the treatment of the groundwater flow equation, groundwater temperature can be decomposed into a conditional-expected value (η) and perturbation (zero-mean) (ς) components. Temperature perturbation is mainly caused by groundwater velocity variations, which result from ln (T) fluctuations. Woodbury (1998) developed the linearized formulation between ln (T) and temperature perturbations and compared the linearized approximation to temperature with the true FE solution. His work is briefly repeated here. According to Darcy's Law, the components of specific discharge are formulated as,

$$q_x = -\frac{\exp(Y)}{B}\frac{\partial \Phi}{\partial x} \tag{5-8}$$

$$q_y = -\frac{\exp(Y)}{B}\frac{\partial \Phi}{\partial y} \tag{5-9}$$

where Y is the logarithm transmissivity, Φ is the hydraulic head and B is the thickness of the aquifer.

Because f is assumed small, the following approximation into the specific discharge expressions can be introduced,

$$\exp(Y) = \exp(F)\exp(f) \cong \exp(F)(1+f) \tag{5-10}$$

Note that,

$$\theta = \eta + \varsigma \tag{5-11}$$

Inserting (5-8)-(5-11) into (5-6) and taking expectations to both sides leads to,

$$\frac{\partial}{\partial x}\left(\lambda^{*}\frac{\partial \eta}{\partial x}\right)+\frac{\partial}{\partial y}\left(\lambda^{*}\frac{\partial \eta}{\partial y}\right)+C\left(\frac{\partial H}{\partial x}\frac{\partial \eta}{\partial x}+\frac{\partial H}{\partial y}\frac{\partial \eta}{\partial y}\right)=0 \tag{5-12}$$

where $C = \rho_f c_f$ and $\lambda^{*} = \dfrac{\lambda_e B}{\exp(F)}$.

Inserting (5-12) back into (5-6) and dropping the products of perturbations gives

$$\frac{\partial}{\partial x}\left(\frac{\lambda^{*}}{C}\frac{\partial \varsigma}{\partial x}\right)+\frac{\partial}{\partial y}\left(\frac{\lambda^{*}}{C}\frac{\partial \varsigma}{\partial y}\right)+\left(\frac{\partial H}{\partial x}\frac{\partial \varsigma}{\partial x}+\frac{\partial H}{\partial y}\frac{\partial \varsigma}{\partial y}\right)=-\left(\frac{\partial h}{\partial x}\frac{\partial \eta}{\partial x}+\frac{\partial h}{\partial y}\frac{\partial \eta}{\partial y}\right)-f\left(\frac{\partial H}{\partial x}\frac{\partial \eta}{\partial x}+\frac{\partial H}{\partial y}\frac{\partial \eta}{\partial y}\right)$$

(5-13)

Applying FEM to (5-12) yields the conditional-expected temperature field. Using FEM to the perturbation equation (5-13) produces,

$$\mathbf{M}\boldsymbol{\varsigma} = \mathbf{N}\mathbf{h} + \mathbf{O}\mathbf{f} \tag{5-14}$$

where **M** is a global stiffness matrix, **N** is a constant matrix related to conditional-expected temperature, **O** is a constant matrix related to mean head and mean temperature,

ς, **h** and **f** are vectors of perturbation heads, perturbation temperatures and perturbation ln (T) respectively.

Substituting (5-4) into the Woodbury linearization formulation (5-14) and performing some matrix operations leads to,

$$\mathbf{D}\{\theta - \eta + \mathbf{M}^{-1}(\mathbf{NA}^{-1}\mathbf{B} + \mathbf{O})\mathbf{F}\} = \mathbf{D}\{\mathbf{M}^{-1}(\mathbf{NA}^{-1}\mathbf{B} + \mathbf{O})\}\mathbf{Y} \tag{5-15}$$

where **D** is a simple Boolean matrix. (5-15) takes the form of $\mathbf{d}^* = \mathbf{Gm} + \nu$. By analogy this formulation can be employed to update the ln (T) field based on temperature measurements.

It is noted that one can update the ln (T) field by taking **F** as the conditioned ln (T) field from measurements of ln (T) and head or directly taking **F** as the conditioned ln (T) field from ln (T) measurements alone, following this temperature inversion formulation.

5.3 Case Study

5.3.1 Fictitious Aquifer

The two-dimensional numerical application of the full-Bayesian approach to the inverse problem will be examined through simulations in this section. The aquifer test case is square with each side being 3 km long. The heads and temperatures are prescribed on the east and west sides. Its north side, south side, top and base are impermeably and adiabatically bounded. The thickness and the porosity of this confined aquifer are constantly assigned at 100 m and 0.1 respectively. The effective thermal conductivity of the aquifer is 75 kcal/m·d·°C, which is similar to the values used by Parsons (1970), Smith and Chapman (1983), and Woodbury and Smith et al. (1988). The aquifer is discretized into 256 nodes and 450 triangular elements. Next an ln (T) field along with its associated hydraulic head field and temperature field is generated using a multivariate random number generator with known statistical parameters. An exponential correlation structure is assumed for the ln (T) field. The statistical properties of ln (T) are mean value=2, standard deviation=0.5, and integral scales in x and y equal to 1000 m. The generated fields are analogous to the true fields. The two-dimensional steady state hydraulic head field and temperature field are solved by FEM. Following this step random samples of the ln (T) values, computed hydraulic heads and temperatures are taken from the fictitious system. The sampling data are analogous to field or laboratory measurements and the task of this exercise is to reconstruct the true ln (T) field conditioned on the sampling data. The full-Bayesian approach to the groundwater inverse problem for steady state flow has been verified (see previous chapters). Next the inverse algorithm for steady state heat transport will be tested.

5.3.2 True Solution and Linearized Approximation to Temperature

The first test of the numerical procedure is to check if the linearized solution to the heat transport equation produces a reasonably accurate temperature field. The ln (T) field is shown in Figure 5-1 and the temperature field is shown in Figure 5-2. Notice that the linearized solution reproduces the true solution very well. The standard deviation error RMS (Root Mean Square) of the true field against the linearized solution is 0.048, which is less than 1% of the maximum temperature difference across the aquifer. Other tests, though not showed, indicate that linearized solution to temperature approximates the true temperature solution very well for this example when unconditional standard deviation of ln (T) is less than 1.

5.3.3 Bayesian Updating From ln (T), Head and Temperature Measurements

In the following simulations the hyperparameters (s, σ_Y, σ_d and λ) are treated as unknown. In other words, they are also treated as random variables and their pdfs are determined from minimum relative entropy (MRE) considerations (See Chapter 2). The effects of the hyperparameters on ln (T) interpolation are removed through 500 Monte Carlo simulations.

It is also assumed the data of heads and temperatures include noise, which may derive from measurement or modeling errors. The noise variances are unknown and are distributed as Jeffreys pdfs (Woodbury and Ulrych, 2000). The posterior pdfs of noise variances are again determined from MRE. The lower bound, mean and upper bound for the noise are 0.05, 0.1 and 0.2, and 0.005, 0.01 and 0.02 for head and temperature respectively. Five hundred Monte Carlo simulations are performed to evaluate the effects of data noises on the inversion.

The results of the ln (T) update for 20 and 50-point samples are showed on Figure 5-3 to Figure 5-8. Comparing these figures with the true ln (T) field (Figure 5-1), one can see that the resolution of the reconstructed ln (T) field gradually improves as the incorporations of ln (T), head and temperature measurements into the updating procedure. A glance at the results from a sparse data set, one can see that the ln (T) field is well recovered from 20-point samples of ln (T), head and temperature measurements through the Bayesian updating procedure. The addition of temperature greatly refines the ln (T) estimation. This can also be confirmed by examining the RMS values in Table 5-1.

Table 5-1. Square root of the mean squared difference between the interpolated field and the 'true' field

	B2	B2H2	B2H2θ2	B5	B5H5	B5H5θ5	B2θ2	B5θ5	B2θ5	B5θ2
RMS	0.345	0.285	0.269	0.270	0.228	0.214	0.353	0.265	0.350	0.256

Note: RMS refers to the square root of the mean squared difference between the updated field and the 'true' field. 2 and 5 represent 20 and 50 points of sample respectively. B refers to a Bayesian update from ln (T) measurements (i.e. spatial interpolation); BH refers to the ln (T) field updated from the ln (T) and hydraulic head measurements; BHθ refers to the ln (T) field updated from ln (T), hydraulic head and the temperature measurements; Bθ refers to the ln (T) field updated from the ln (T) and temperature measurements.

5.3.4 Bayesian Updating From ln (T) and Temperature Measurements

The algorithm is examined in situations that ln (T) measurements and temperature measurements are the data sets available but head measurements are unavailable or assumed unreliable. Figures 5-9 to 5-12 show the updated ln (T) fields for the cases that the ln (T) and temperatures are used but head measurements are not. Taking the interpolated field from 20 ln (T) measurements as a prior input, the ln (T) fields (Figures 5-9 and 5-11) conditioned on temperature measurements approximate the shapes of the true ln (T) field well. However, the RMS values do not decrease compared to the interpolated ln (T) field, for either 20-point or 50-point temperatures. If the interpolated field from 50 ln (T) measurements is used as prior input, as shown in Table 5-1, Figure 5-10 and Figure 5-12, the posterior ln (T) approximates the true ln (T) well in every aspect. This implies that the accuracy of the update from temperature measurements relies on the accuracy of the prior ln (T) estimation. It is interesting to note that the decreased value of RMS (B5θ5) resulted from the addition of temperature data is less than that (B5H5) caused by the addition of the same number of head data.

5.4 Limitation of Temperature Application to the Inverse Problem and Requirements for Further Study

The Peclet number (P_e) is a measure of the ration of advection to diffusion and is defined as (Domenic et al. 1998),

$$P_e = \frac{\rho_f c_f q^*}{\lambda_e B / L^*} \tag{5-16}$$

where q^* is the flow rate per unit aquifer width; L^* is the length of the flow field, and B is the thickness of the aquifer. The temperature inversion algorithm applies to the cases with an appropriate global Peclet number. This implies that there is a range for which the numerical scheme for temperature inversion should show increased sensitivity of the model parameters to subsurface temperature.

Woodbury and Smith (1988) showed that for values of P_e much less than 1, the thermal regime is dominated by conductive effects; for the values of P_e approaching 1, the thermal regime enters a transition and isotherms are distorted from conductive configuration; for P_e greater than 5, the thermal field tends to be near isothermal, with temperatures on the fluid inflow boundary propagating across much of the flow domain. This suggests that the inverse algorithm for steady state heat transport apply to the situation of P_e ranging from 1 to 5. In the example section above P_e is 4.92.

The performance of the temperature algorithm needs to be investigated against high-variance ln (T) cases. Further work is required to extend the code for the case of sources or sinks.

5.5 Summary

The methodology for the spatial inversion of transmissivity for the steady state two-dimensional groundwater heat transport is developed, based on a full-Bayesian approach. This approach assumes that the ln (T) field is multivariate Gaussian and the parameters governing the stochastic process are treated as hyperparameters whose effects on the parameter estimation can be removed by marginalization. A spatially interpolated ln (T) field can be produced following the full-Bayesian framework.

Two linearized partial differential equations, one relating hydraulic head to ln (T) and the other relating temperature to ln (T), are developed and employed to update the interpolated ln (T) field. The updates can be performed jointly using head and temperature measurements or temperature alone. The head and temperature measurements are assumed noisy and these effects are again removed by marginalization.

The combined Bayesian update produce conditional-expected values of ln (T) over the aquifer, and estimated errors.

The procedure is applied to a series of test cases in which the actual values of ln (T), hydraulic head and temperature are generated with known values of stochastic parameters. Sparse data (20 and 50 points) are randomly taken from the fictitious aquifer. Basic statistics of the sampled data are used to derive pdfs of the hyperparameters. The use of temperature data is showed to improve the ln (T) estimates, in comparison to the updated ln (T) field conditioned on sparse ln (T) and head data. Also the addition of temperature data in absence of head data to the update aids refinement of the ln (T) field compared to simply interpolating the sparse ln (T) data alone. These results suggest that low-cost temperature measurements are a promising data source for site characterization.

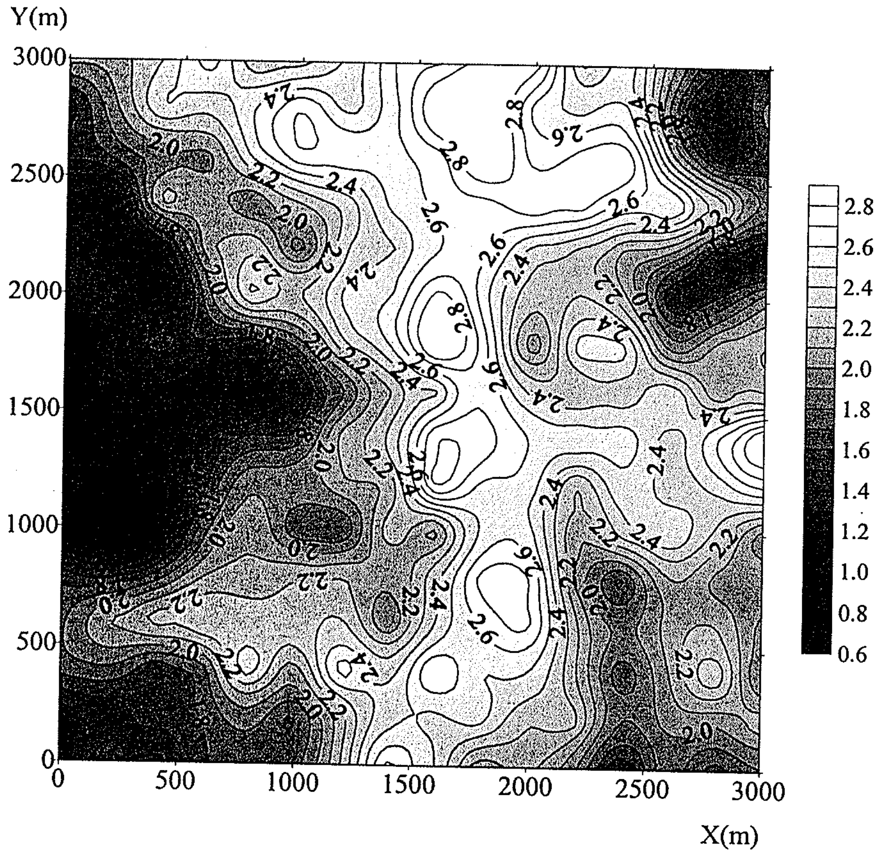

Figure 5-1 ln (T) field generated by multivariate random number generator (specified statistics: mean=2, standard deviation=0.5, integral scale=1000 m)

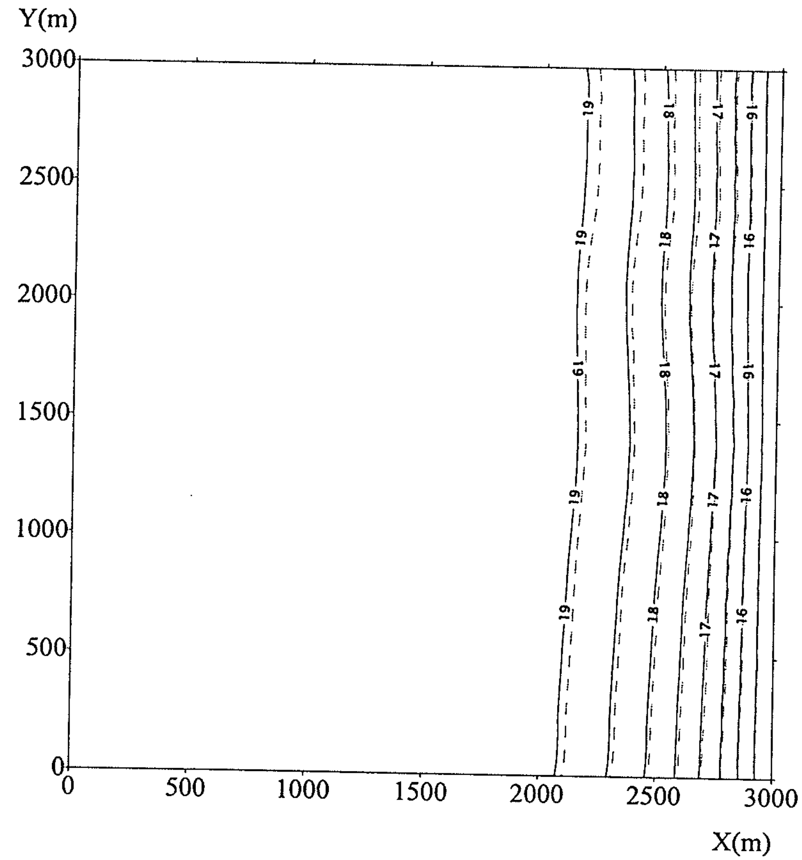

Figure 5-2 True temperature (solid) versus linearized approximation (dash) for ln (T) variance=0.5

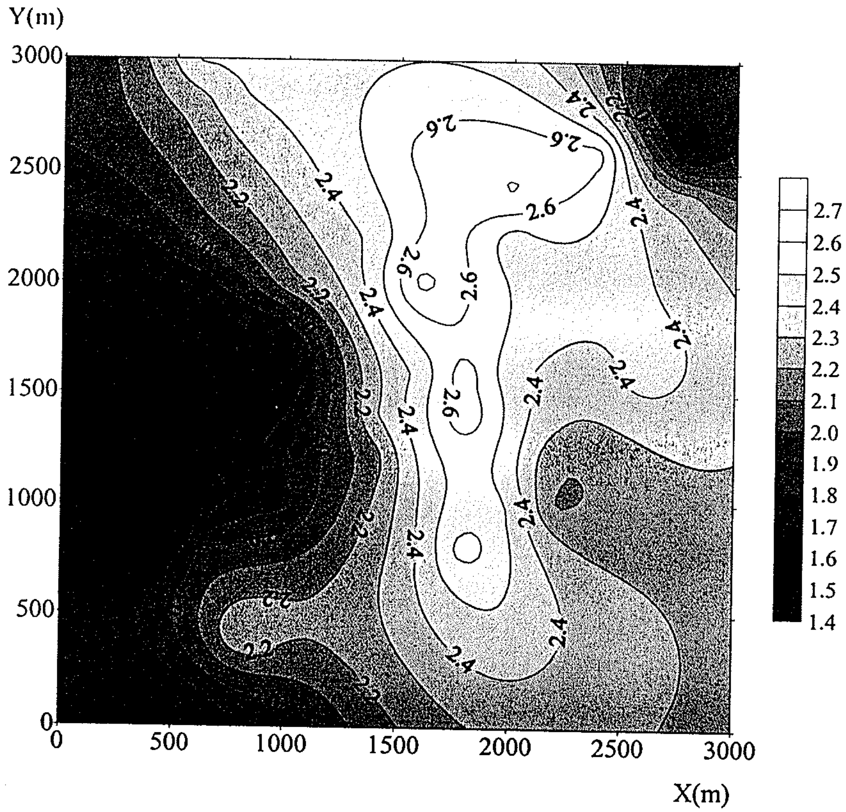

Figure 5-3 Bayesian updated ln (T) field from 50 points of ln (T)

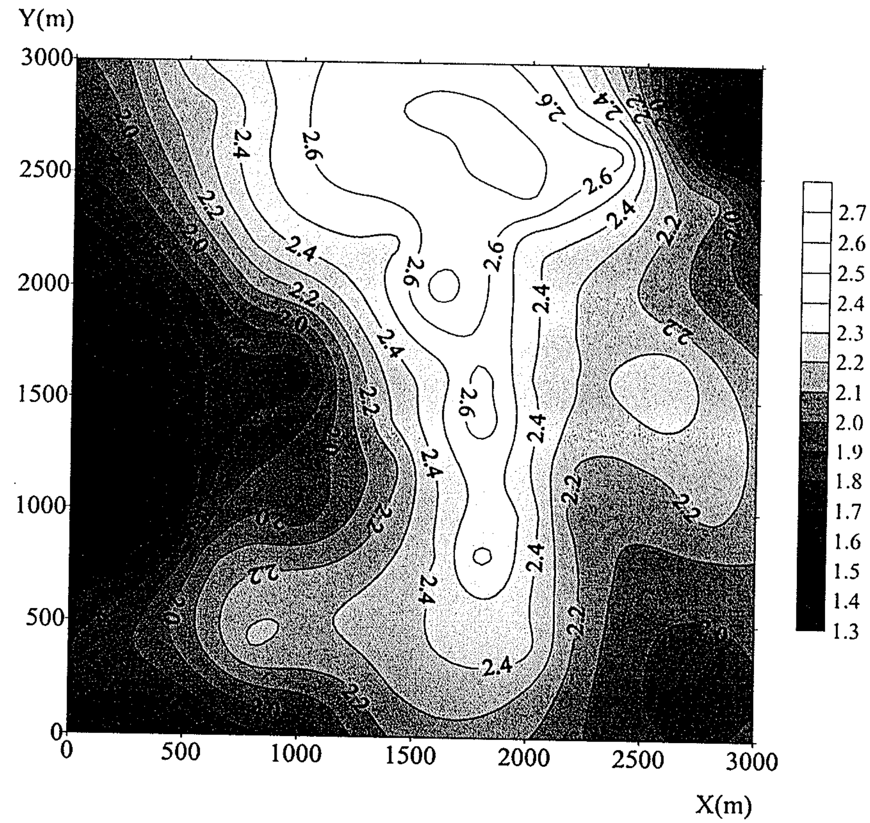

Figure 5-4 Bayesian updated ln (T) field from 50 points of ln (T) and heads

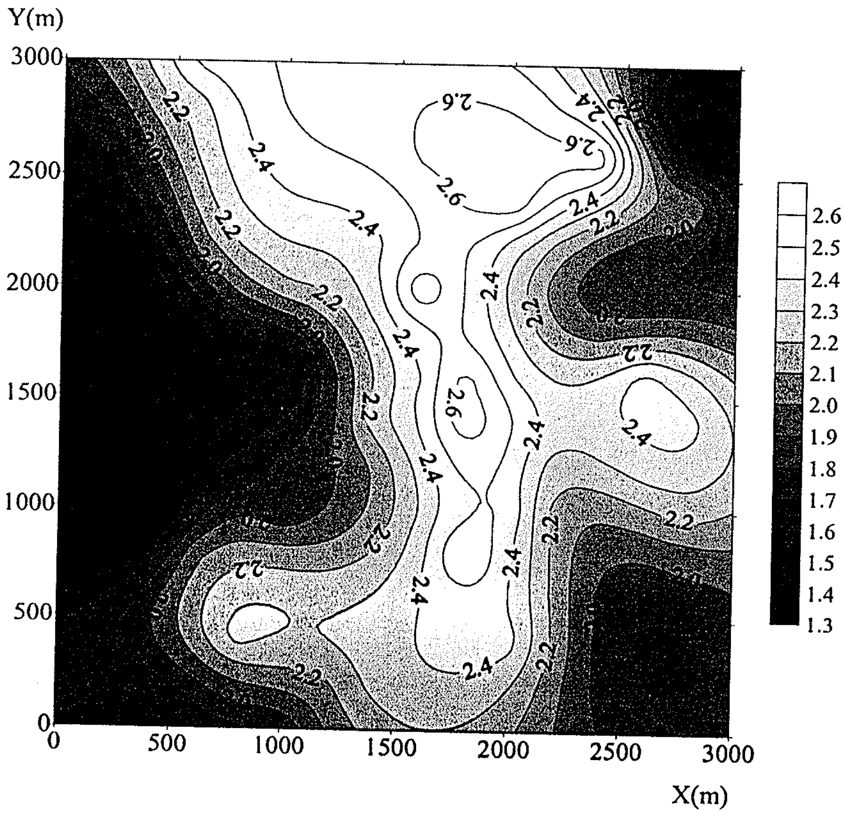

Figure 5-5 Bayesian updated ln (T) field from 50 points of ln (T), heads and temperatures

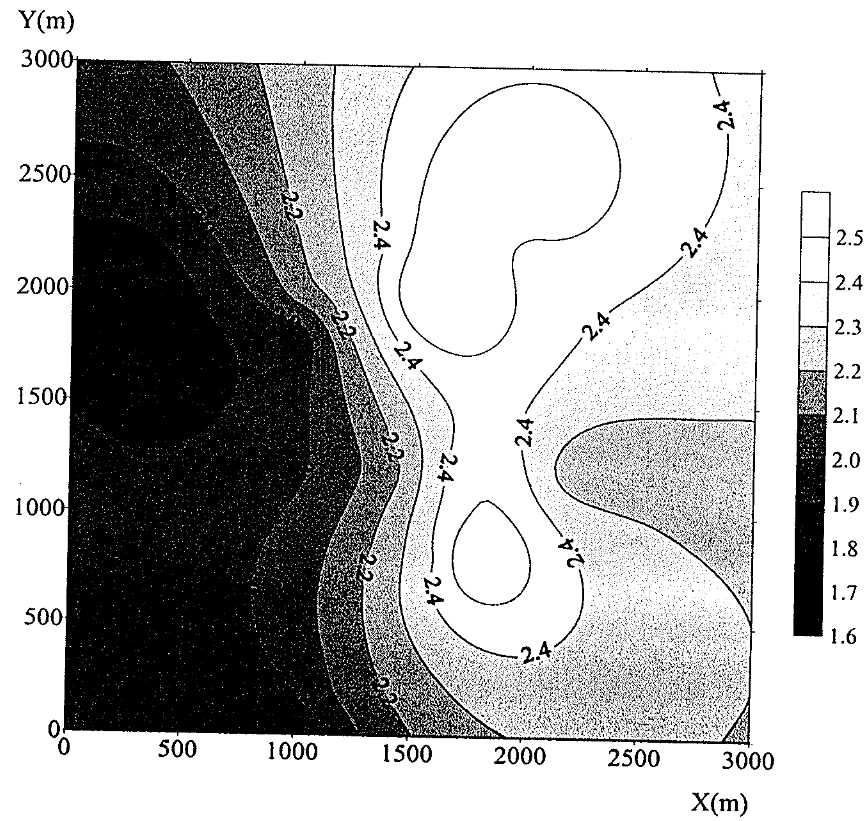

Figure 5-6 Bayesian updated ln (T) field from 20 points of ln (T)

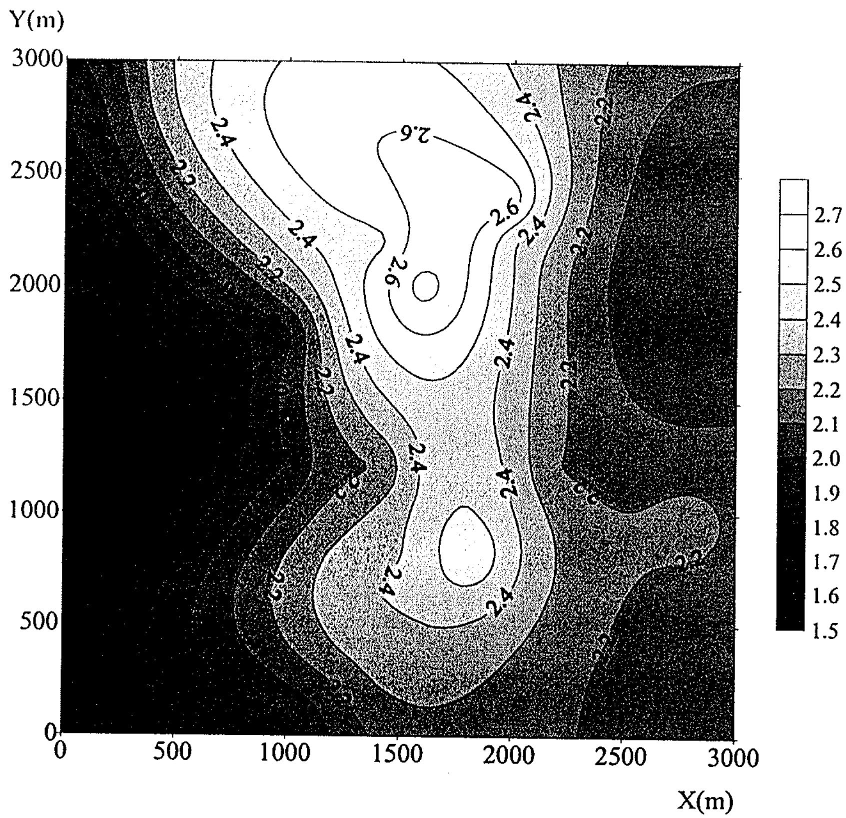

Figure 5-7 Bayesian updated ln (T) field from 20 points of ln (T) and heads

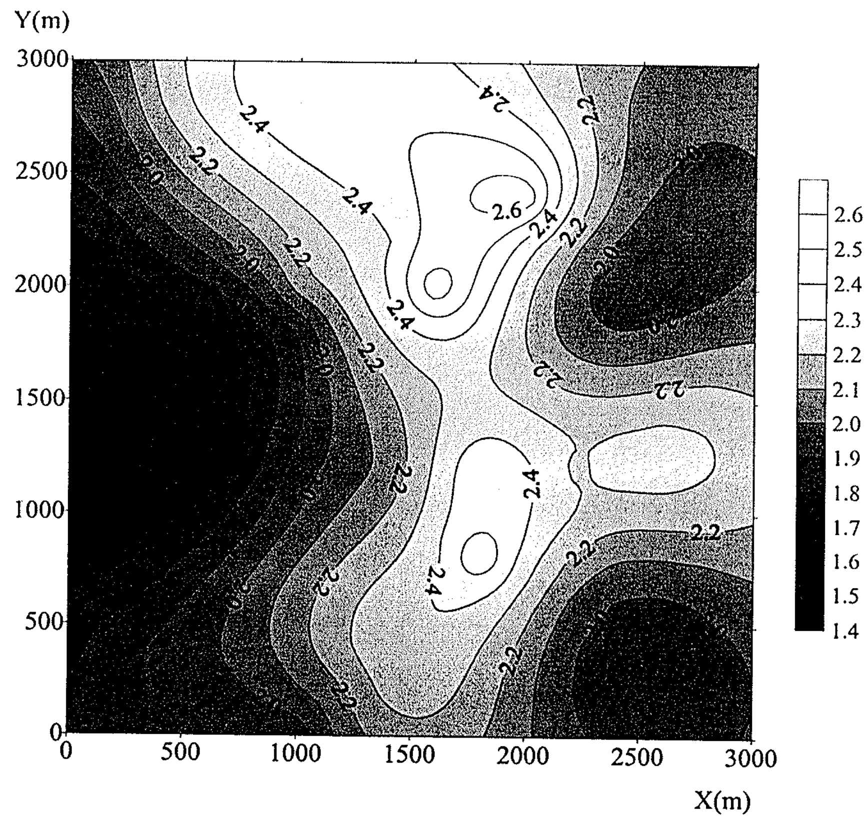

Figure 5-8 Bayesian updated ln (T) field from 20 points of ln (T), heads and temperatures

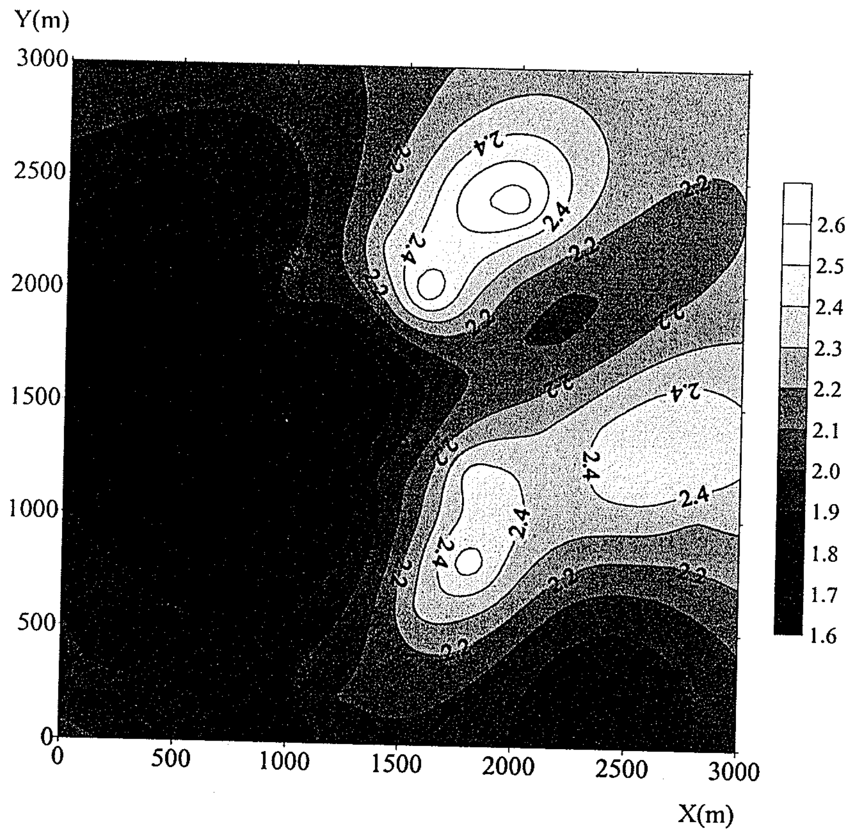

Figure 5-9 Bayesian updated ln (T) field from 20 points of ln (T) and temperatures

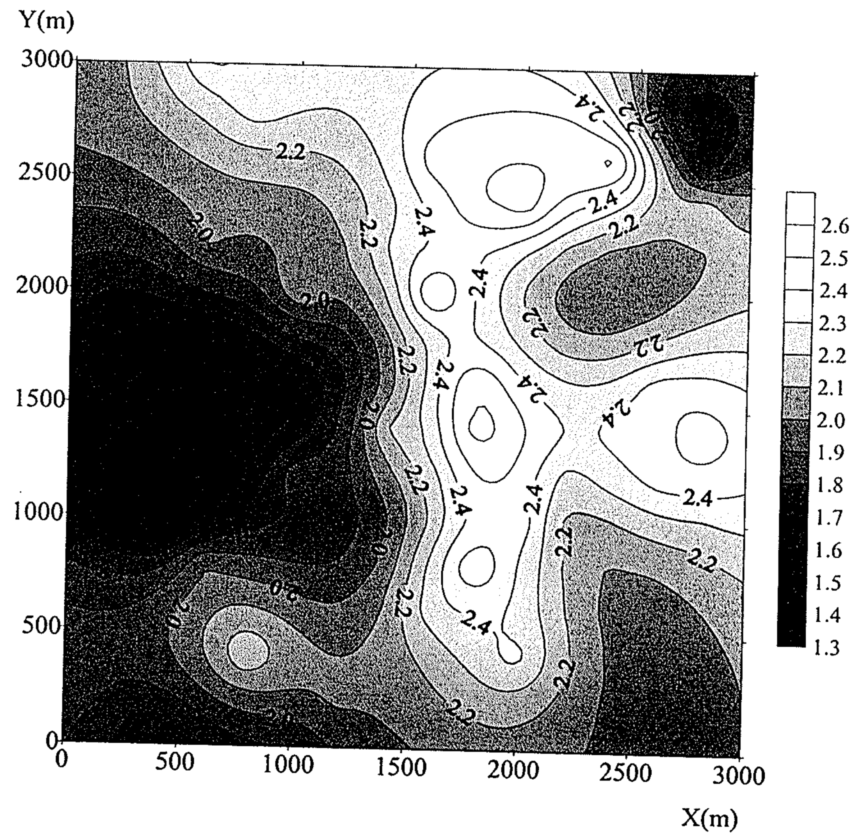

Figure 5-10 Bayesian updated ln (T) field from 50 points of ln (T) and temperature

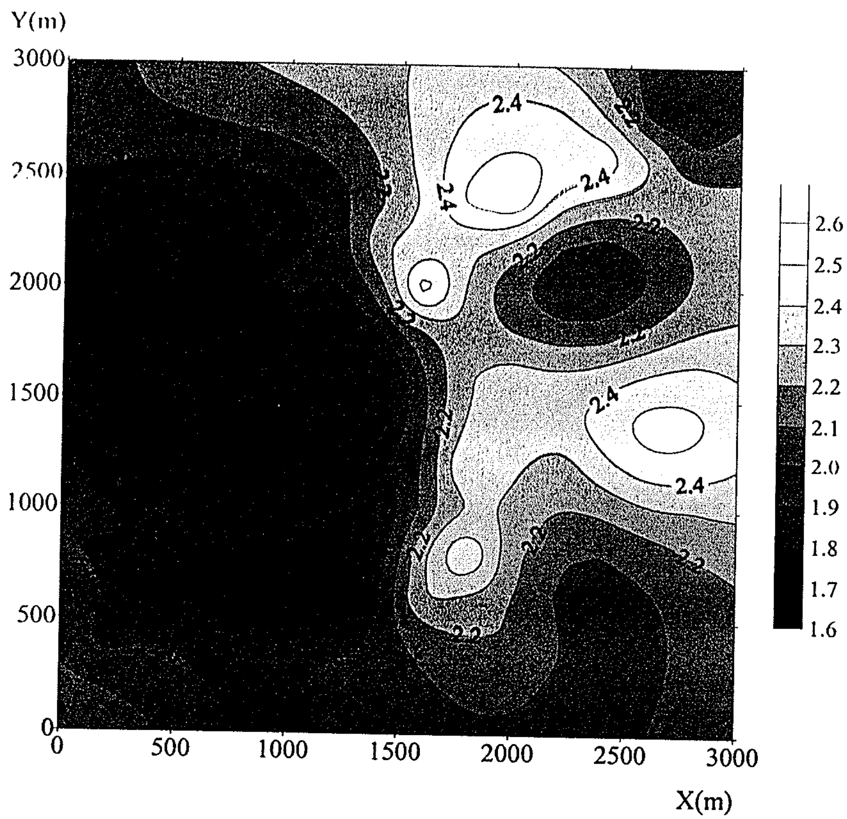

Figure 5-11 Bayesian updated ln (T) field from 20 points of ln (T) and 50 points of temperature

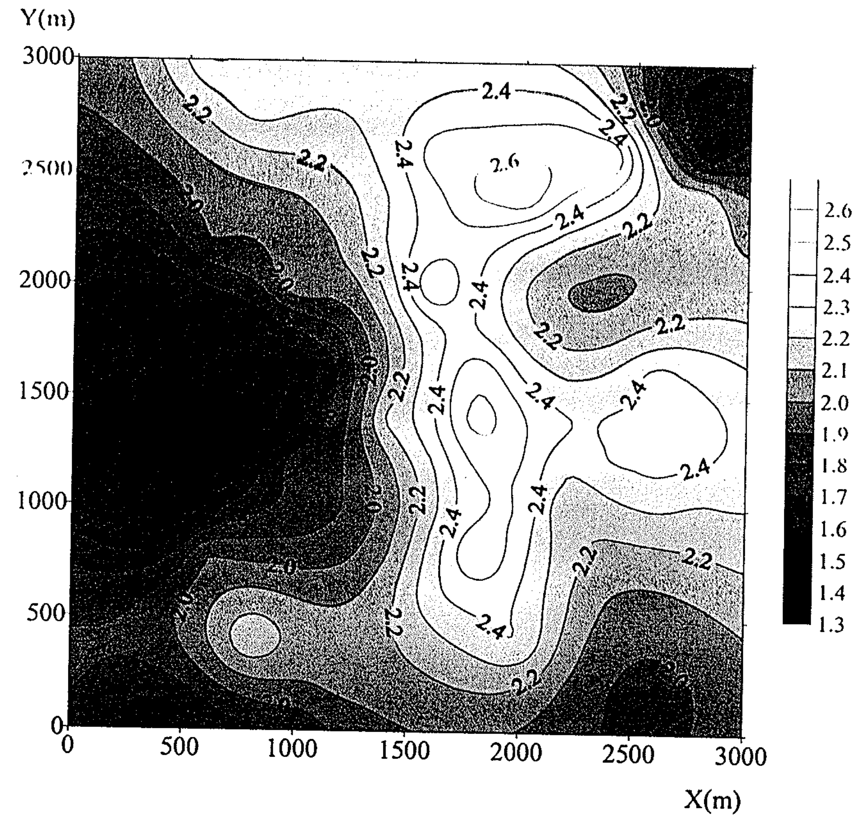

Figure 5-12 Bayesian updated ln (T) field from 50 points of ln (T) and 20 points of temperature

Chapter 6

Summary and Conclusions

Numerical models are now widely employed to simulate the responses of groundwater systems. One well-known obstacle for groundwater model applications is to obtain sufficient and reliable hydrogeological parameters for model input. Groundwater systems are often highly heterogeneous and there is often insufficient measurement of hydraulic parameters for a comprehensive, detailed characterization. A large portion of the model input may be determined through solving the inverse problem. The full inverse problem is ill-posed, and this is characterized by instability and non-uniqueness. The problem cannot be eliminated unless additional measurements and information are introduced. This topic has attracted many research efforts over the past thirty years and numerous solution approaches have been developed. But, no panacea has been available.

In this thesis a Bayesian approach is employed to the groundwater inverse problem. In this approach the estimated parameter is described as a stochastic field, which is believed to better represent the spatial variation of geological materials. The essential point is to take advantage of data from different sources and cast the problem in a probability framework. Any knowledge of the identified system can constraint the inverse problem and reduce the concern of nonuniqueness. The uncertainty with the data can be well described as probability distribution. A new Bayesian algorithm to the estimation of transmissivity field of aquifers with high-variance ln (T) and Neumann condition and sources/sinks is developed. The algorithm is examined against a fictitious aquifer with high-variance and extremely high-variance ln (T) configurations respectively. The code is employed to calibrate a high-resolution finite difference model of the Edwards aquifer. The methodology for the spatial inversion of transmissivity for two-dimensional steady state groundwater heat transport is developed based on the full-Bayesian approach. The temperature inversion code is checked against a series of test cases. This work can be summarized as follows:

(1) The physics of groundwater flow, which consists of linearized aquifer flow equation and a first-order approximation of Taylor's series for the exponential terms introduced by sinks and sources or Neumann condition, yields acceptable head approximation for ln (T) variance up to 9 in the test case. The accuracy of the linearized approximation depends on the unconditional variance of the ln (T) field. Smaller ln (T) variances yield a better approximation. The approximation can be improved through grid refinement.

(2) The linearized formulation between hydraulic head and ln (T) perturbations is applied to the Bayesian update of ln (T) field by incorporation of head measurements for an extremely high-variance aquifer. Forward solutions with the conditional-expected ln (T) field show that the conditional heads match the true heads better than the unconditional linearized approximation does. This suggests that the Bayesian approach can be applied not only to problems in which linearized approximation is valid but also to the cases that linearized approximation may not be strictly satisfactory. That is due to the configuration of prior ln (T) field and if spatial step size of the grid is favorable for solving conditional head equation.

(3) The addition of hydraulic head measurements aids in the refinement of ln (T) estimation. For a high- or extremely-high variance ln (T) configuration the more head data are utilized the better the updated ln (T) approximates the true field. This is especially true for the extremely high-variance case. The joint use of sparse ln (T) and head measurements can yield equivalent estimation from dense ln (T) measurements alone. This implies the Bayesian approach can take advantage of the multi-source data sets, as may reduce the concern of nonuniqueness of the inverse problem and potentially reduce the cost for site characterization.

(4) Utilizing a cell-to-node discretion scheme the finite element based Bayesian code is employed to calibrate a high-resolution finite difference model of the Edwards aquifer.

First, 100 heads are utilized to map the ln (T) field with the springs as constant heads. Forward modeling based on the posterior ln (T) field match the measurements, including both those used in the inversion and another independent data set, much better than those from the prior ln (T). Another data set, which consists of 153 head measurements, is employed to update the upscaled ln (T) field given the springs as sinks. Forward modeling using the prior ln (T) demonstrates that the unsymmetrical solution used in the inversion does not correspond to the symmetrical solution within an acceptable deviation given the springs as sinks. An example is set up to investigate the error and numerical stability with the new Bayesian algorithm. It is concluded that numerical errors are mainly derived from numerical approximation to the gradient of conditional-expected ln (T) field. The configuration of extremely high stresses, extremely high ln (T) variation and coarse grid attributes to the misfit between the symmetrical and unsymmetrical solutions. Refining the grid and adjusting prior estimation improves the posterior estimation. Adjusting the prior ln (T) values around the springs area allows the inversion code produce a posterior ln (T) from the 153 head measurements. This updated ln (T) improves the fit between the measured heads and computed heads, but shows a larger mismatch than the case of setting the springs as constant heads.

(5) A full-Bayesian code for joint use of transmissivity, head and temperature measurements is developed. Temperature measurements can be utilized to further update the ln (T) field by adopting linearized approximation to the steady state heat transport equation. The procedure is examined against a series of test cases. The use of temperature data improves the ln (T) estimates, in comparison to the updated ln (T) field conditioned on sparse ln (T) and head data. Also, the addition of temperature data in absence of head data to the update aids refinement of the ln (T) field compared to simply interpolating the sparse ln (T) data alone. These results suggest that low-cost temperature measurements are a promising data source for site characterization.

References

Bear, J., Dynamics of fluids in porous media, Elsevier, Amsterdam-New York, 1972, pp.641-663

Bear, J. and M.Y. Corapcioglu, A mathematical model for consolidation in a thermo elastic aquifer due to hot water injection or pumping, Water Resources Research, 1981, 17(3): 723-736

Bredehoeft, J. and I.S. Papadopulos, Rates of vertical groundwater movement estimated from the earth's thermal profile, Water Resources Research, 1965, 1(2): 325-328

Brott, C.A., D.D. Blackwell and J.P. Ziagos, Thermal and tectonic implications of heat flow in the eastern Snake River plain, Idaho, Journal of Geophysical Research, 1981, 86(B12): 11709-11734

Carrera, J., and S.P. Neuman, Estimation of aquifer parameters under transient and steady state conditions, 1, Maximum likelihood method incorporating prior information. Water Resources Research, 1986, 22(2): 199-210

Clifton, P.M. and S.P. Neuman, Effects of Kriging and inverse modeling on conditional simulation of the Avra Valley aquifer in Southern Arizona, Water Resources Research, 1982, 18(4): 1215-1234

Cooley, R.L., A method of estimation parameters and assessing reliability for models of steady state ground flow, 1, Theory and numerical properties, Water Resources Research, 1977, 13(2): 318-324

Dagan, G., Stochastic models of groundwater flow by unconditional and conditional probabilities: The inverse problem, Water Resources Research, 1985, 21(1): 65-72

David, M., Geostatistical ore reserve estimation, Elsevier scientific publishing company, 1977, pp. 237-273

De Marsily, Spatial variability of properties in porous media: a stochastic approach, in: Fundamental of transport phenomena in porous media, ed. by J. Bear and M.Y. Corapciglu, NATO ASI series 1984, pp.721-769

Domenico, P.A. and V.V. Palciauskas, Theoretical analysis of forced convective heat transfer in regional groundwater flow, Geological Society of America Bulletin, 1973 (84): 3803-3814

Domenico P.A. and F.W. Schwartz, Physical and chemical hydrogeology (2nd edition), John Wiley and Sons, Inc., 1998, pp.191-214

Dwyer, T.E., and Y. Eckstein, Finite element simulation of low-temperature, heat-pump-coupled, aquifer thermal energy storage, Journal of Hydrology, 1987, 95: 19-38

Eckhardt, G.A., http://www.edwardsaquifer.net/, 1995-2002

Forster, C.B. and L. Smith, Groundwater flow systems in mountainous terrain: 1, Numerical modeling technique, Water Resources Research, 1988, 24 (7): 999-1010

Forster, C.B. and L. Smith, The influence of groundwater flow on thermal regimes in mountainous terrain; a model study, Journal of Geophysical Research, Solid Earth and Planets, 1989, 94 (B7): 9439-9451

Freeze, R.A., A stochastic-conceptual analysis of one-dimensional groundwater flow in nonuniform homogeneous media, Water Resources Research, 1975, 11(5): 725-741

Freeze, R.A., Hydrogeological decision analysis: 1. A framework, Ground water, 1990, 28(5): 738-766

Garabedian, S.P., Hydrology and digital simulation of the regional aquifer system, Eastern Snake River Plain, Idaho, U.S. Geological Survey Professional Paper 1480-F, 1992

Griffiths, D.V. and G.A. Fenton, Seepage beneath water retaining structures founded on spatially random soil, Geotechnique, 1993, 43(4): 577-587

Gui, S., R. Zhang, J.P. Turner and X. Xue, Probabilistic slope stability analysis with stochastic soil hydraulic conductivity, Journal of Geotechnical and Geoenvironmental Engineering, 2000, 126(1): 1-9

Hachich, W. and E.H. Vanmarcke, Probabilistic updating of pore pressure fields, Journal of Geotechnical engineering, 1983, 109 (3): 373-387

Hefez, E., V. Shamir, and J. Bear, Identifying the parameters of an aquifer cell model, Water Resources Research, 1975, 11(6): 993-1004

Hoeksema, R.J. and P. Kitanidis, An application of the geostatistical approach to the inverse problem in two-dimensional groundwater modeling, Water Resources Research, 1984, 20(7): 1003-1020

Huyakorn, P. and G. Pinder, Computational methods in subsurface flow, Academy Press, 1983

Jiang, Y., A. Woodbury and S. Painter, A full-Bayesian approach to the estimation of aquifer parameters in highly heterogeneous aquifers, Eos Trans. AGU, 82(47), H12D-0326

Jiang, Y., and X. Zhang, An integrated model formulation of stream-aquifer interaction system and its application, ACTA Geographica Sinica, 1999, 54(6): 526-533

Kitanidis, P.K., On the geostatistical approach to the inverse problem, Advances in Water Resources, 1996, 19 (6): 333-342

Kitanidis, P.K. and E. Vomvoris, A geostatistical approach to the inverse problem in groundwater modeling (steady state) and one-dimensional simulations, Water Resources Research, 1983, 19 (3): 677-690

Kitanidis, P.K., Parameter uncertainty in estimation of spatial functions: Bayesian analysis, Water Resources Research, 1986, 22(4): 499-507

Kleinecke, D., Use of linear programming for estimating geohydrological parameters of groundwater basins, Water Resources Research, 1971, 7(2): 367-375

Kley, W., and W. Heekmann, Waste heat balance in aquifers calculated by a computer program, Ground Water, 1981, 19(2): 144-48

Kukkonen, I.T., V. Cermak and J. Safanda, Subsurface temperature-depth profiles, anomalies due to climatic ground surface temperature changes or groundwater flow effects, Global and Planetary Change, 1994, 9: 221-232

Lindholm, G.F., Summary of the Snake River Plain Regional Aquifer-System Analysis in Idaho and Eastern Oregon, U.S. Geological Survey Professional Paper 1408, 1996

Mansure, A.J., and M. Reiter, A vertical groundwater movement correction for heat flow, Journal of Geophysical Research, 1979 (84): 3490-3496

Mao, S., J. Wang and X. Pu, Advanced mathematical statistics, China Higher Education Press Beijing and Springer-Verlag Berlin Heidelberg, 1998, pp.302-389

Massmann, J. and R.A. Freeze, Updating random hydraulic conductivity fields: a two-step procedure, Water Resources Research, 1989, 25 (7): 1763-1765

Massmann, J. and R. A. Freeze, Groundwater contamination from waste management sites: the interaction between risk-based engineering design and regulatory policy: 1. Methodology, Water Resources Research, 1987, 23 (2): 351-367

McLaughlin, D. and L.R. Townley, A reassessment of the groundwater inverse problem, Water Resources Research, 1996, 32(5): 1131-1161

Menke, W., Geophysical data analysis: discrete inverse theory, Academic Press, New York, 1984

Molson, J. W., E. O. Frind, and C. D. Palmer, Thermal energy storage in an unconfined aquifer: 2. Model development, validation, and application, Water Resources Research, 1992, 28(10): 2857-2867

Molz, F.J., A.D. Parr, P.F. Anderson, V.D. Lucido, and J.C. Warman, Thermal energy storage in a confined aquifer: Experimental results, Water Resources Research, 1979, 15(6): 1509-1514

Molz, F.J., A.D. Parr, and P.F. Anderson, Thermal energy storage in a confined aquifer: Second cycle, Water Resources Research, 1981, 17(3): 641-646

Neuman, S.P., Calibration of distributed parameter groundwater flow models viewed as a multi-objective decision process under uncertainty, Water Resources Research, 1973, 9(4): 1006-1021

Neuman, S.P. and S. Yakowitz, A statistical approach to the inverse problem of aquifer hydrology, 1, Theory, Water Resources Research, 1979, 15(4): 845-860

Neuman, S.P., Statistical characterization of aquifer heterogeneities: An overview, Geological Society of America special paper 189, 1982, pp. 81-102

Papadopulos, S.S., and S.P. Larson, Aquifer storage of heated water: II. Numerical simulation of field results, Groundwater, 1978, 16(4): 242-248

Parr, A.D., F.J. Molz, and J.G. Melville, Field determination of aquifer thermal energy storage parameters, Ground Water, 1983, 21(1): 22-35

Parsons, M.L., Groundwater thermal regime in a glacial complex, Water Resources Research, 1970, 6(6): 1701-1720

Press, S.J., Bayesian statistics: principles, models, and applications, Wiley Series in Probability and mathematical statistics, 1989

Rae, J., P.C. Robinson, and L.M. Wickens, Coupled heat and groundwater flow in porous rock, Edited by Lewis, R.W., K. Morgan and B.A. Schrefler, Numerical methods in thermal problems: proceedings of the fourth international conference held in Swansea, U.K. on 15th-18th July 1985

Roth, C., J. Chiles and C. Fouguet, Combining geostatistics and flow simulators to identify transmissivity, Advances in Water Resources, 1998, 21: 555-565

Smith, J.L., Numerical Simulation techniques for modeling advectively-distributed thermal regimes, Hydrogeological regimes and their subsurface thermal effects, edited by Alan E. Beck, 1989, pp.107-118

Smith, J.L. and D.S. Chapman, On the thermal effects of groundwater flow: 1. Regional scale systems, Journal of Geophysical Research, 1983, 88(B): 593-608

Smith, J.L., C.B. Forster, and A.D. Woodbury, Numerical simulation techniques for modeling advectively disturbed thermal problems, Hydrogeologic Regimes and Their Subsurface Thermal Effects, 1989, pp.1-6

Smith, M., and J. M. Konrad, Influence of seepage on the temperature distribution in a zoned earth dam, 1989

Sun, N., Mathematical modeling of groundwater pollution, Springer, 1996: pp. 193-196

Sobol I.M., The Monte Carlo Method, The University of Chicago Press, 1974

Sykes, J.F., R.B. Lantz, S.B. Pahwa, and D.S. Ward, Numerical simulation of thermal energy storage experiment conducted by Auburn University, Ground Water, 1982, 20(5): 569-576

Tarantola, A., Inverse Problem Theory (Methods for data fitting and model parameter estimation), Elsevier, 1987, pp.52-99

Tsang, C.F., T. Buscheck, and C. Doughty, Aquifer thermal energy storage: A numerical simulation of Auburn University field experiments, Water Resources Research, 1981, 17(3): 647-658

Ulrych, T. J., M. D. Sacchi, and A. Woodbury, A Bayes tour of inversion: A tutorial: Geophysics, 2001, (66): 55-69

Wang, K., P. Shen and A.E. Beck, A solution to the inverse problem of coupled hydrological and thermal regimes, Hydrogeological regimes and their subsurface thermal effects, edited by Alan E. Beck, 1989, pp.107-118

Wiberg, N.E., Heat storage in aquifers analyzed by the finite element method, Ground Water, 1984, 22(1): 6-12

Woodbury, A.D. and L. Smith, On the thermal effects of three dimensional groundwater flow, Journal of Geophysical Research, 1985, 90(B1): 759-767

Woodbury, A.D., Bayesian updating revisited, Mathematical Geology, 1989, 21(3): 285-308

Woodbury, A.D., Simultaneous inversion of thermal and hydrological data: Where do we go from here? Eos Trans., AGU, 1999, 80(46), F337

Woodbury, A.D. and J.L. Smith, Application of finite element techniques to heat flow investigations within sedimentary basins, Proc. 5th, Int. Conf. Finite Elements in Water Resources, Editors J.P. Laible, C.A. Brebbia, W. Gray, G. Pinder, Springer-Verlag, 1984, pp. 701-713

Woodbury, A.D., and J.L. Smith, On the thermal effects of three dimensional groundwater flow, Journal of Geophysical Research, 1985, 90(B1): 759-767

Woodbury, A.D., J. L. Smith, and W.S. Dunbar, Simultaneous inversion of temperature and hydraulic head data: 1. Theory and application using hydraulic head data, Water Resources Research, 1987, 23(8): 1586-1606

Woodbury, A.D., and J.L. Smith, Simultaneous inversion of temperature and hydraulic head data: 2. Application with thermal data, Water Resources Research, 1988, 24(3): 356-372

Woodbury, A.D., B. Narod and B. Chandra et al., Temperature measurement in Geotechnical studies using low-noise, high-resolution digital techniques, Journal of Canadian Geotechnical, 1991, 28: 639-649

Woodbury, A.D., F.W. Render and T.J. Ulrych, Practical probabilistic groundwater modeling, Groundwater, 1995, 33(4): 532-538

Woodbury, A.D. and Y. Rubin, A full-Bayesian approach to parameter inference from tracer travel-time moments, Water Resources Research, 2000, 36(1): 159-171

Woodbury, A.D. and T.J. Ulrych, Minimum relative entropy and probabilistic inversion in groundwater hydrology, Stochastic Hydrology and Hydraulics, 1998, 12: 317-358

Woodbury, A.D. and T. J. Ulrych, A Full-Bayesian approach to the groundwater inverse problem for steady state flow, Water Resources Research, 2000, 36(8): 2081-2093

Xue, Y., C. Xie, and Q. Li, Aquifer thermal energy storage: A numerical simulation of field experiments in China, Water Resources Research, 1990, 26(10): 2365-2375

Yeh, T.-C. J., M. Jin and S. Hanna, An iterative stochastic inverse method: conditional effective transmissivity and hydraulic head fields, Water Resources Research, 1996, 32(1): 85-92

Yeh, W. W.-G., Review of parameter identification procedures in groundwater hydrology: the inverse problem, Water Resources Research, 1986, 22(2): 95-108

Yeh, W. W.-G. and Y.S. Yoon, Parameter identification with optimum dimension in parameterization, Water Resources Research, 1981, 17(3): 664-672

Zhang, H., A comparative study of numerical solution of PDE in Geosciences, ACTA Geologica Sinica, 1993, 67(3): 266-275

Zhang, J. and T.-C. Jim Yeh, An iterative geostatistical inverse method for steady flow in the vadose zone, Water Resources Research, 1997, 33(1): 63-71

Zhang, K., A. D. Woodbury, and W. S. Dunbar, Application of the Lanczos algorithm to the simulation of groundwater flow in dual-porosity media, Advances in Water Resources, 2000, 23: 579-598